VECTORS FOR ALGERNON

Receptor-Targeted Lentiviral and Adeno-Associated Vectors in Syngeneic Mouse Models of *In Vivo* Gene Therapy

Dissertation zur Erlangung des Grades

Doctor rerum naturalium
(Dr. rer. nat.)

von

Alexander Michels

Genehmigt vom Fachbereich Biologie der
Technischen Universität Darmstadt

Erstgutachterin   Prof. Dr. Ulrike Nuber
Fachbereich Biologie
Technische Universität Darmstadt

Zweitgutachter   Prof. Dr. Christian J. Buchholz
Molekulare Biotechnologie und Gentherapie
Paul-Ehrlich-Institut

Darmstadt 2023
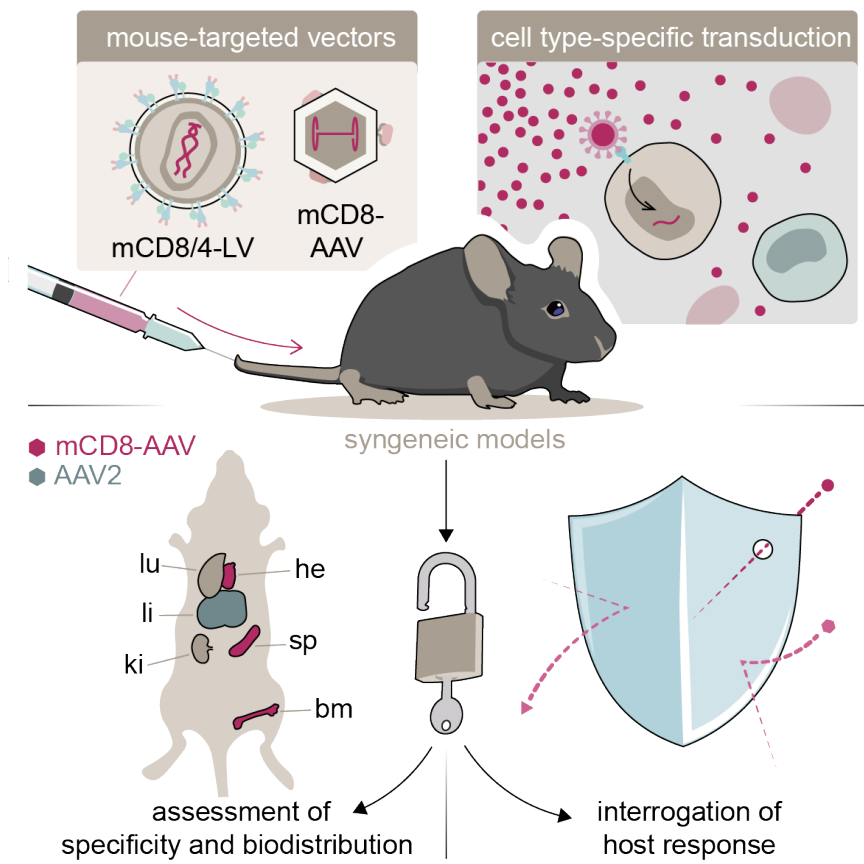
Für Doro.

Für Gregor, Marianne und Matthias.

Für Antonia.

Für Markus, der hiermit eine Wette gewinnt.

It's time to move on, it's time to get going
What lies ahead, I have no way of knowing
But under my feet, baby, grass is growing
It's time to move on, time to get going

— **Tom Petty**

mouse-targeted vectors

mCD8/4-LV

mCD8-
AAV

cell type-specific transduction

mCD8-AAV
AAV2

syngeneic models

lu

he

li

ki

sp

bm

assessment of
specificity and biodistribution

interrogation of
host response

Summary

Driven by recent leaps in receptor targeting technology, advanced vector platforms are currently reshaping gene therapeutic strategy, promising to enable a new generation of accessible, safe and unprecedentedly effective products. Their transformative potential has been impressively demonstrated by recent preclinical reports describing the *in vivo* generation of chimeric antigen receptor (CAR) T cells in short-term mouse models. Beyond proof-of-principle, however, important questions remain, many of them motivated by an insufficient understanding of the host immune response to vector administration, which will likely critically impact the products' real-world safety and efficacy.

Toward a better understanding of the host response, syngeneic mouse models - capable of recapitulating the response of a complete, complex mammalian immune system to vector administration - can helpfully complement the existing body of work on humanized models and enable the thorough preclinical examination of vector-host interplay which is warranted by the tumultuous history of clinical gene therapy research. Such models require surrogate reagents, which have so far been unavailable for certain classes of receptor-targeted vectors, especially viral vectors. This thesis describes the generation and characterization of such mouse-compatible viral vectors, as well as their use in the syngeneic mouse models of *in vivo* gene therapy they enable.

Lentiviral vectors targeted to CD8+ and CD4+ murine lymphocytes (mCD8- & mCD4-LVs) were generated by insertion of anti-mCD8α MSE10 designed ankyrin repeat protein (DARPin) and anti-mCD4 GK1.5 single chain variable fragment, respectively, into the blinded measles virus pseudotype pioneered by the host laboratory. Crucially, in spite of the well-documented, multicausal inability of LVs' infamous parent virus HIV-1 to productively infect murine cells, the introduction of mouse receptor-targeted binders was sufficient to confer mouse-compatibility to the particles, which displayed transducing titers on primary mouse splenocytes similar to those observed for hCD8- and hCD4-LVs on human T cell lines. Additionally, binder insertion rendered mCD4- and mCD8-LV highly selective for cells expressing their cognate receptor: Five days after vector addition, >98% of GFP+ lymphocytes extracted from whole mouse blood treated with mCD8-LV were found to be CD8+. The subtype-specific presence of tagged viral glycoproteins on T cells only two hours after addition of mCD4- and mCD8-LV to whole mouse blood observed on closer examination suggest that the vectors' selectivity is achieved at the stage of cell binding.

Interestingly, receptor incompatibility is a principal barrier not only for the efficient transduction of murine cells with lentiviral, but also with adeno-associated

vectors (AAVs). When the mCD8α-specific MSE10 DARPin was inserted into the GH2/GH3 loop of VP1 of the AAV2 capsid, the resulting DARPin-targeted (DART) mCD8-AAV displayed near-absolute selectivity for CD8+ primary murine lymphocytes and transducing titers six- to sevenfold higher than those of regular AAV2.

When mCD8- and mCD4-LV were used for GFP transfer in BALB/c mice, protein and genome level transfer signals were close to the lower limit of detection, but were strongest in the tissues with the highest T cell content. Notably, pronounced remodeling of the lymphoid compartment, i.e. decreases in the relative frequency and increases in size and granularity of CD3+ cells in spleen and blood, were observed, indicating an immune response to vector administration.

Host response was minimal when a mix of phagocytosis-shielded CD47^{hi} mCD8- and mCD4-LVs was systemically injected into BALB/c mice to generate αmCD19-CAR T cells directly *in vivo*, as no signs of immune activation were observed and no CAR-related changes in peripheral blood were found within 43 days post injection. On final analysis, qPCR identified splenic vector integration only in treated mice, and flow cytometric analysis yielded a shift of the CD3+/CD19+ composition in spleens of vector-treated animals.

Data highlighting the considerable influence of receptor targeting on vector biodistribution was obtained when mCD8-AAV was tested in Ai9 mice. In this reporter-tolerant system, infusion of mCD8-AAV resulted in >87% specific transduction of mCD8+ cells and overall transduction rates in blood, spleen and bone marrow approximately 4-100 fold higher than for unmodified AAV2. Additionally, targeting of AAVs by MSE10 was found to reduce liver transduction, assessed by measuring whole organ surface fluorescence, twentyfold.

The observed utility of receptor targeting in the context of two molecularly distinct vector platforms well-illustrates its crucial role in the maturation of gene therapy, enabling pivotal vector platforms as well as their detailed preclinical examination. Indeed, the syngeneic mouse models enabled here through the generation of mouse-compatible viral vectors well-summarized current concerns in the field, as they confirmed both the challenge *in vivo* gene therapy faces from restrictive host responses – stressing the urgent need for the evaluation and implementation of immune-modulatory strategies to enable productive *in vivo* transduction in immunocompetent systems – and the key role of receptor targeting technology in profoundly improving genetic treatment, e.g. by decreasing liver burden for a vector class whose liver toxicity upon systemic administration is an emerging issue.

Zusammenfassung

Durchbrüche in genetischer Vektortechnologie schicken sich an, das noch junge Feld der Gentherapie grundlegend zu verändern, indem sie die Entwicklung breit anwendbarer, verträglicher Produkte nie vorher da gewesener Wirksamkeit ermöglichen. Eine Schlüsseltechnologie ist dabei die Rezeptortargetierung von Vektorpartikeln, deren transformatives Potenzial von kürzlich erschienenen präklinischen Berichten zur Generierung von mit chimären Antigenrezeptoren (CARs) ausgestatteten T-Zellen direkt *in vivo* eindrucksvoll veranschaulicht wurde.

Wichtige Fragen jenseits solcher Machbarkeitsdemonstrationen sind jedoch bisher unbeantwortet geblieben, vor allem solche, die die Auswirkung einer durch Vektorgabe ausgelösten Immunantwort auf die Wirksamkeit und das Nebenwirkungsprofil der Therapie betreffen. Zur Beantwortung solcher Fragestellungen können syngene Mausmodelle, welche in der Lage sind, die Reaktionen eines kompletten Säugerimmunsystems auf Vektorinjektion wiederzugeben, Erkenntnisse aus humanisierten Mausmodellen hilfreich ergänzen und so die gründliche Untersuchung der Interaktion von Vektor und Wirt ermöglichen, die in Anbetracht der turbulenten Geschichte klinischer Forschung in der Gentherapie angemessen erscheint.

Voraussetzung für solche Modelle ist das Vorhandensein mauskompatibler Ersatzreagenzien, welche im Fall rezeptortargetierter viraler Vektoren bisher nicht verfügbar waren. Diese Thesis beschreibt die Generierung und Charakterisierung solcher mausverträglicher viraler Vektoren und ihren Einsatz zur syngenen Modellierung der *in vivo* Gentherapie.

Gegen murines CD4 bzw. CD8 gerichtete lentivirale Vektoren (mCD4- und mCD8-LVs) wurden durch Insertion des anti-mCD8α MSE10 *designed ankyrin repeat protein* (DARPin) bzw. des anti-mCD4 Einzelkettenantikörperfragments GK1.5 in den Masernviruspseudotyp geschaffen, für dessen Entwicklung das gastgebende Labor dieser Doktorarbeit maßgebliche Arbeit geleistet hat. Durch die Insertion mausrezeptorgerichteter Binder wurden die lentiviralen Partikel mauskompatibel, d.h. auf primären murinen Splenozyten wurden ähnliche Gentransferaktivitäten beobachtet wie für gegen menschliches CD4 und CD8 gerichtete LVs auf menschlichen T-Zelllinien. Zusätzlich waren die Vektoren auch in komplexeren Zellgemischen sehr selektiv für Zellen, die den entsprechend kognaten Rezeptor exprimierten: So waren fünf Tage nach Vektorzugabe mehr als 98% der aus vektorbehandeltem Vollblut isolierten GFP-positiven Lymphozyten CD8-positiv. Bei näherer Untersuchung der Bindungseigenschaften wurde die subtypspezifische (d.h. CD4- oder CD8-spezifische) Präsenz viraler Glykoproteine auf T-Zellen aus Vollblut bereits zwei Stunden nach Zugabe von mCD4- und mCD8-LV festgestellt, was nahelegt, dass die hohe Selektivität im Zuge der Zellbindung zustande kommt.

Bemerkenswerterweise scheint Rezeptorinkompatibilität nicht nur ein Hindernis für die effiziente Transduktion von Mauslymphozyten durch LVs zu sein, sondern auch durch die lentiviralen Vektoren molekular recht unähnlichen adenoassoziierten Vektoren (AAVs). Durch Insertion des MSE10 DARPin in die GH2/GH3-Schleife von VP1 des AAV2-Kapsids wurden sogenannte "DARPin-targetierte" (DART) mCD8-AAVs generiert, die sich auf primären murinen Splenozyten durch fast vollständige Selektivität für mCD8 und unerwarteterweise durch gegenüber unmodifizierten AAV2-Partikeln sechs- bis siebenfach höhere Transduktionstiter auszeichneten.

Bei der Verwendung von mCD4- und mCD8-LV zum Transfer von GFP in BALB/c Mäusen lagen Transfersignale auf Protein- und Genomebene jeweils nah an der unteren Detektionsgrenze, waren jedoch in denjenigen untersuchten Geweben am ausgeprägtesten, die den höchsten Anteil von T-Zellen aufwiesen. Gleichzeitig fand in Folge der Vektorinjektion in Blut und Milz eine Restrukturierung der lymphoiden Zellnische hin zu niedrigeren relativen Konzentrationen, höherer Granularität und grösserem Durchmesser von CD3-positiven Zellen statt, welche auf eine Immunantwort gegenüber der Vektorgabe hindeutet.

In einem ebenfalls in BALB/c Mäusen durchgeführten Folgeexperiment kamen vor Phagozytose durch Überexpression des menschlichen Phagozytoseinhibitors CD47 in Produktionszellen geschützte, gegen murines CD19 gerichtete CAR transferierende mCD4- und mCD8-LVs zum Einsatz. Hier wurden keine Anzeichen einer Immunmobilisierung beobachtet, und es gab über einen Zeitraum von dreiundvierzig Tagen nach Vektorgabe keine messbaren Veränderungen im peripheren Blut der Tiere. Im Zuge der finalen Analyse fünfzig Tage nach Vektorinjektion wurde splenische Integration des Vektorgenoms nur in vektorbehandelten Mäusen festgestellt. Zusätzlich wurde in vektorbehandelten Tieren eine Verschiebung des Verhältnisses von CD3+ zu CD19+ Zellen zugunsten ersteren Typs beobachtet.

Den beträchtlichen Einfluss von Rezeptortargetierung auf die Biodistribution von Vektoren aufzeigende Daten konnten in einem anderen experimentellen System gesammelt werden: In reportertoleranten Ai9 Mäusen resultierte die Infusion von Cre-transferierenden mCD8-AAV in mehr als 87% spezifischer Transduktion von CD8-positiven Zellen in Blut, Milz und Knochenmark und im Erreichen von vier- bis hundertfach höheren Transduktionsraten als durch die Gabe der gleichen Vektorgenomdosis AAV2. Zusätzlich war das durch mCD8-AAV hervorgerufene Leberoberflächenfluoreszenzsignal etwa zwanzigmal niedriger als das von AAV2 hervorgerufene.

Die scheinbar zentrale Rolle der Rezeptortargetierung in der Nutzbarmachung zweier molekular distinkter Vektorplattformen für den murinen Kontext verdeutlicht die Wichtigkeit der Technologie in der weiteren Entwicklung der Gentherapie, in der sie nicht nur richtungsweisenden Vektorplattformen zugrundeliegt, sondern auch

die gründliche präklinische Testung selbiger ermöglicht. Tatsächlich unterstreichen die beschriebenen Mausexperimente nicht nur die Bedeutung der im Fachdiskurs an Brisanz gewinnenden Herausforderung der Wirtsimmunität für *in vivo* Gentherapie und die dringende Notwendigkeit zur Evaluierung und Implementierung immunmodulatorischer Maßnahmen zur Ermöglichung produktiver *in vivo* Gentherapie in immunkompetenten Systemen: Die beobachtete Verringerung der hepatischen Belastung bei einer für das Risiko von Lebertoxizität nach systemischer Anwendung unter Beobachtung stehenden Vektorklasse veranschaulicht die Schlüsselrolle der Rezeptortargetierung in der Realisierung substanziell verbesserter, breiter zugänglicher Gentherapien.

Contents

INTRODUCTION

The Past, Present and Future of Gene Therapy

In Daniel Keyes' *Flowers for Algernon* [Keyes, 2004], a man gains superhuman cognitive abilities through an experimental surgery. As his manifold powers develop, he learns that the health of the now supermurinely intelligent mouse on which the treatment was first tested, the novel's namesake, Algernon, is starting to deteriorate. So warned, the protagonist starts researching his and the mouse's condition, hoping to prevent his own fall, but to no avail: Before long, he, too, succumbs to the treatment's long-term adverse effects.

Although this – regrettably – is not a dissertation on 20th century science fiction, the relationship of Keyes' genre classic to the subject matter of this thesis is remarkable in two ways: The first is that the story was initially published in 1959, directly before reports of gene transfer into mammalian cells would start to emerge, prompting researchers to discuss the possibility of genetic treatment of human disease and its implications, events that would mark the birth of the field of gene therapy [Friedmann, 1992].

The second is that, now, more than sixty years later, when some aspects of the story may appear out-of-date to many readers, the assessment of the value of mouse models contained in the novel's plot could not be more relevant or timely: Not only can mouse models supply proof-of-principle for experimental treatments prior to human trials, they also provide valuable medium- and long-term safety and efficacy data that should inform the treatment of humans and is ignored at the clinical researchers' and, more importantly, their patients', peril.

Written decades after (and inspired by) Algernon's death, this thesis lacks the literary qualities of Keyes' novel[1]. Still, readers may appreciate the mouse models it describes and the timely insights they provide now that gene therapies have arrived in the clinics to stay.

---

[1]Also, any orthographic or grammatical errors left in this thesis are not deliberately used stylistic devices, as they are in the novel. They are simply overlooked mistakes.

1.1 Gene Therapy in the Clinics

Almost exactly thirty years after Friedmann recounted the beginnings of the field [Friedmann, 1992] and despite early – and more recent – setbacks (p. 16), gene therapies have established a foothold in the clinics. Especially the last decade has seen over a dozen European marketing authorizations for gene therapy products usher in a new era of medical treatment [Schüßler-Lenz et al., 2022]. The gene therapies marketed at the time of this writing (see Table 1.1) represent the culmination of decades of basic and applied research into molecular medicine, genomics and immunology, and - in some cases for the first time - present sufferers of debilitating disease with viable therapeutic options. They also represent the current state-of-the-art of gene therapy, demonstrating both its great potential and current limitations, which become apparent when the products are categorized by indication and by type of gene transfer. At this time, the marketed therapies comprise products for the treatment of genetic disease as well as products addressing cancer.

1.1.1 Congenital Disease

Notably, less than half (six of fourteen) of the currently marketed gene therapies rely on *in vivo* gene transfer, i.e. the direct administration of vector to the patient. Most of these *in vivo* therapies address rare genetic disorders, which either drastically shorten life expectancy or reduce quality of life from a young age. Consequently, they are indicated for use in children or adolescents, with Zolgensma, an AAV9-based product for the treatment of spinal muscular atrophy, even being indicated for use in children below the age of two. Similarly, AAV2-based Upstaza and the autologus cell product Libmeldy are used to mitigate the neurodevelopmental impact of aromatic L-amino acid decarboxylase and arylsulfatase A deficiency, respectively. Also based on AAV2, Luxturna is used to combat vision loss in patients with congenital retinal dystrophy caused by a mutation in the *RPE65* gene. Finally, AAV5-based Roctavian and Hemgenix, as well as the cell product Strimvelis, address congenital hematological disorders, namely haemophilias A, B and severe-combined immunodeficiency caused by adenosine deaminase deficiency (ADA-SCID), respectively.

1.1.2 Cancer & CAR T Cell Therapy

Crucially, and perhaps somewhat counterintuitively, seven of the fourteen currently marketed gene therapies are not indicated for the treatment of congenital disease but

for treatment of cancer, a set of complex, acquired conditions. Except for one product of oncolytic herpes virus, all of these are chimeric antigen receptor (CAR) T cell therapies, which make up the majority of marketed autologous adoptive therapies. In these, cells are extracted from patients, genetically modified *ex vivo*, i.e. outside of the body, and then re-administered. Making up the largest class among marketed gene therapies, CAR products signify a major new direction in the field of gene therapy, which is no longer 'just' occupied with replacing or repairing mutated genes for the treatment of monogenetic, congenital diseases but aims to tackle complex acquired illnesses like cancer by delivering therapeutically active, often artificial proteins on the genetic level.

CAR T cell therapy is a form of adoptive T cell therapy, in which cancer patients receive tumor-specific T cells that were genetically altered and expanded *ex vivo*. Chimeric antigen receptors are composed of an extracellular antigen-binding domain, connected via a hinge region and a transmembrane domain to one or more intracellular signalling domains. Upon binding to their targets, CARs induce intracellular signalling that results in antigen-specific killing of the target cell and simultaneous proliferation of the CAR T cell [June and Sadelain, 2018; Sadelain, 2017]. Thus, CAR T cells can be regarded as living drugs that amplify in patients when they encounter target cancer cells.

In recent years, this therapeutic concept has boosted research worldwide, with six products having been granted marketing authorization in Europe. Initial authorizations were granted to Yescarta and Kymriah, both targeting lymphoma cells via the B cell marker CD19. Besides lymphoma cells, healthy B lymphocytes are eliminated by these products, resulting in B cell depletion as prominent side-effect in treated patients [Maude et al., 2018]. Recently, four more products, Tecartus, Breyanzi, Abecma and Carvykti, have received regulatory approval, the latter two extending indications for CAR therapy to multiple myeloma via B cell maturation antigen (BCMA) [EMA, 2021a; EMA, 2022b]. The approval of the first CAR cell product not directed to CD19 marks an important step in this new field in cancer immunotherapy.

The unprecedented responses achieved through the use of CAR T cell products in the treatment of hematological cancers are a major driving force behind a current worldwide research momentum of hundreds of ongoing clinical trials aiming to harness gene therapy's full potential by improving upon the vector technology underlying (and limiting) the marketed products.

1.2 The Vectors Behind the Products

TABLE 1.1: Gene therapies currently marketed in the European Union. Based [Schüßler-Lenz et al., 2022].

Trademark (INN)	Indicated for treatment of	Type (mode of application)	Administered product (modified by)	Transgene	Reference
Carvykti® (Ciltacabtagene autoleucel)	multiple myeloma	ex vivo (infusion)	autologous CAR T cells (LV)	anti-BMCA-CAR	[EMA, 2022b]
Breyanzi® (Lisocabtagene maraleucel)	B cell lymphoma	ex vivo (infusion)	autologous CAR T cells (LV)	anti-CD19-CAR	[EMA, 2022a]
Abecma® (Idecabtagene vicleucel)	multiple myeloma	ex vivo (infusion)	autologous CAR T cells (LV)	anti-BMCA-CAR	[EMA, 2021a]
Tecartus® (Brexucabtagene autoleucel)	mantle cell lymphoma	ex vivo (infusion)	autologous CAR T cells (RV[a])	anti-CD19-CAR	[EMA, 2021f]
Kymriah® (Tisagenlecleucel)	acute lymphatic leukemia, B cell lymphoma	ex vivo (infusion)	autologous CAR T cells (LV)	anti-CD19-CAR	[EMA, 2021b]
Yescarta® (Axicabtagene ciloleucel)	B cell lymphoma	ex vivo (infusion)	autologous CAR T cells (RV)	anti-CD19-CAR	[EMA, 2021g]
Libmeldy® (Atidarsagene autotemcel)	metachromatic leukodystrophy	ex vivo (infusion)	autologous CD34+ -enriched cells (LV)	ARSA	[EMA, 2022e]
Strimvelis®	severe combined immunodeficiency due to adenosine deaminase deficiency	ex vivo (infusion)	autologous CD34+ -enriched cells (RV)	ADA	[EMA, 2022h]
Luxturna® (Voretigene neparvovec)	retinal dystrophy	in vivo (subretinal injection)	AAV, serotype 2	hRPE65	[EMA, 2021c]
Zolgensma® (Onasemnogene abeparvovec)	spinal muscular atrophy	in vivo (infusion)	AAV, serotype 9	SMN	[EMA, 2021h]
Upstaza® (Eladocagene exuparvovec)	aromatic L-amino acid decarboxylase deficiency	in vivo (intracranial injection)	AAV, serotype 2	DDC	[EMA, 2022I]
Roctavian® (Valoctocogene roxaparvovec)	haemophilia A	in vivo (infusion)	AAV, serotype 5	hFVIII-SQ	[EMA, 2022g]
Hemgenix® (Etranacogene dezaparvovec)	haemophilia B	in vivo (infusion)	AAV, serotype 5	hFIX-Padua	[EMA, 2023]
Imlygic® (Talimogene laherparepvec)	melanoma	in vivo (intratumoral injection)	attenuated HSV-1	GM-CSF	[EMA, 2022d]

[a] γ-retroviral vector.

4

1.2.1 Common Vector Platforms

Vectors – molecular means of gene delivery to cells – are central to gene therapy. Only once safe and effective vectors are available can molecular insights into disease be translated from basic research into treatment. To understand the limitations of vectors in marketed products, it is important to understand the basic characteristics of the gene delivery platforms used in them.
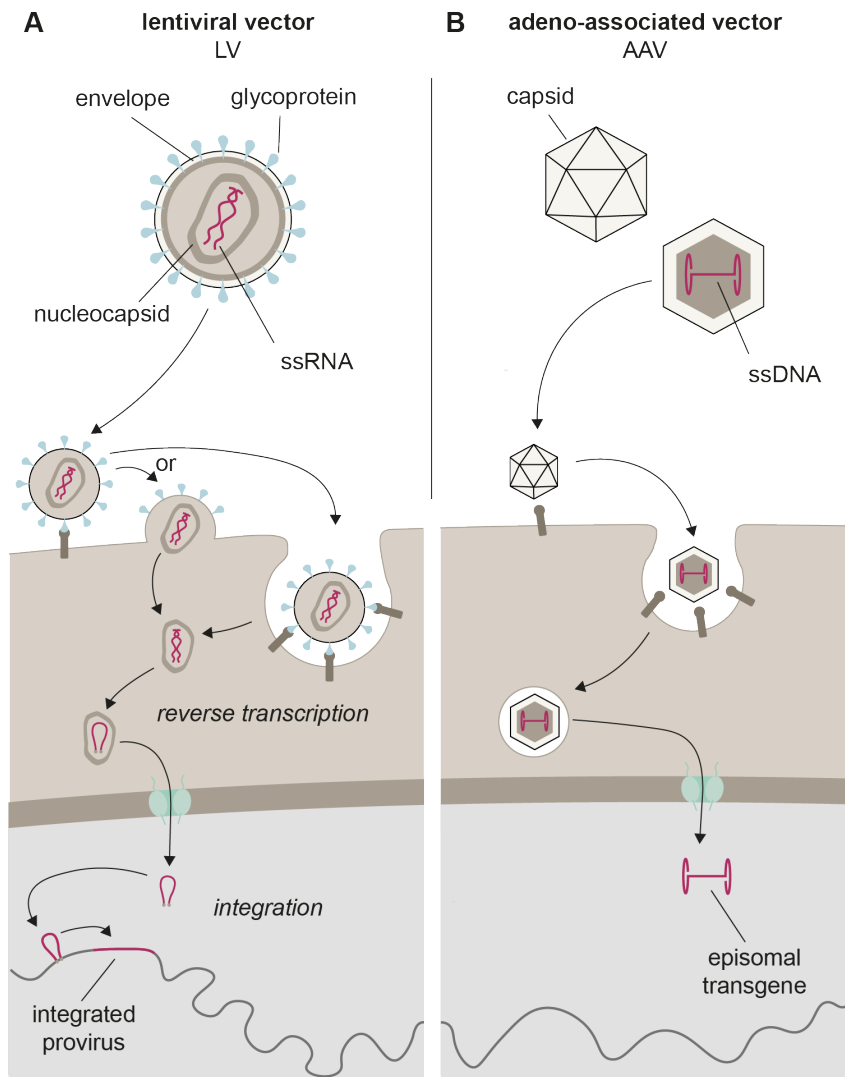
1.2.1.1 Lentiviral Vectors

Lentiviral vectors (LVs) are enveloped particles relying on reverse-transcription of their RNA genomes. After binding to the host cell via the viral glycoproteins on the vector envelope, LVs fuse with the host cell membrane, releasing the nucleocapsid containing the RNA genome into the cytoplasm. The RNA is then reverse-transcribed and the resulting proviral genome is integrated into the host cell chromosomes by vector proteins (**Figure 1.1a**). First described in 1996 [Naldini et al., 1996], LVs are based on the lentivirus human immunodeficiency virus 1 (HIV-1). Improving upon previously described retroviral vectors such as those based on murine leukemia virus (MLV), LVs are capable of transducing non-dividing cells. This is mediated by interactions of virion proteins with the nuclear import machinery [Milone and O'Doherty, 2018].

Like their γ-retrovirus-derived cousins, LVs stably integrate their genetic payload into host chromatin. Stable integration is crucial for long-term gene expression and ensures that the progeny of a transduced cell carries the transgene. Integration of HIV-1 is not random, favoring sites in actively transcribed genes [Gil-Farina and Schmidt, 2016]. LVs can accommodate large transgenes: The genome of HIV-1 is approximately 9 kb long and measurable titers were described for LVs with transgenes over 18 kb long, with vector titer decreasing semi-logarithmically with RNA length [Canté-Barrett et al., 2016; Kumar et al., 2001].

In light of the notoriety of the parent virus, considerable effort has gone into ensuring the safety of LVs. Vectors are commonly produced in a multiday-process by 293T producer cells via three- to four-plasmid systems which contain only three to four of the nine genes of HIV-1; crucial virulence factors have been removed. No HIV-1-derived genes are packaged into vector particles, as only the transfer vector plasmid contains the necessary packaging signal (ψ) and the flanking long terminal repeats (LTRs) required for genomic integration.

Lentiviral vectors are usually outfitted, or pseudotyped, with the glycoprotein G of vesicular stomatitis virus (VSV) resulting in particles 120-150 nm in diameter. VSV G mediates cell entry via the low density lipoprotein receptor (LDLR) and

A   lentiviral vector   **B**   adeno-associated vector
           LV   AAV

envelope   glycoprotein   capsid

nucleocapsid

ssRNA   ssDNA

or

reverse transcription

integration

integrated   episomal
provirus   transgene

FIGURE 1.1: Vector platforms used in marketed gene therapy products
The vector particles' main features (genetic information shown in red) and their cell entry modes, including nuclear entry and potential genomic integration, are depicted from top to bottom, respectively. **A** LVs are enveloped particles containing one or more viral glycoproteins (blue) and two copies of a ss-RNA genome packaged in a nucleocapsid. Depending on the glycoprotein, cell entry occurs directly at the cell membrane or is dependent on endocytosis. The transferred gene is reverse transcribed, shuttled into the nucleus, and integrated into the host genome. **B** AAVs consist of a ssDNA genome packaged into an icosahedral protein capsid. Cellular uptake by endocytosis is followed by release of the transferred gene into the nucleus, where it resides episomally, separate from host chromatin. Adapted from [Michels et al., 2022].

its family members, which are expressed on many cell types [Finkelshtein et al., 2013]. Accordingly, VSV G-pseudotyped LVs have a broad tropism and achieve high transduction efficiencies on different human cell types.

The stable integration of the transgene and the considerable packaging capacity of LVs make them ideally suited for CAR delivery. In fact, conventional CAR therapy mostly relies on either lentiviral or γ-retroviral vectors for *ex vivo* transduction. LVs are used to generate CAR cells for four of the six CAR products authorized by the European Medicines Agency (EMA), Breyanzi, Carvykti, Kymriah and Abecma; the other two products, Yescarta and Tecartus, are being manufactured using retroviral vectors (see TABLE 1.1). In 2018, 54% of clinical studies in the United States used LVs for CAR T cell generation [Vormittag et al., 2018]. Beyond that, over 100 registered clinical trials are ongoing, mostly using LVs in the context of immunological and hematological disorders and cancer [L. A. Kohn and D. B. Kohn, 2021; clinicaltrials.gov, 2022[2]].

1.2.1.2 Adeno-Associated Vectors

Adeno-associated vectors (AAVs) are - in many ways - polar opposites to LVs. AAVs consist of non-enveloped protein capsids containing a single-stranded (ss) DNA genome. Where LVs insert their transgene stably into host chromatin, genetic modification by AAVs is usually transient, especially in proliferating cells. After interaction with their entry receptor, clathrin-mediated endocytosis and intracellular trafficking – the specifics of these processes being determined by the serotype of the capsid used – vectors enter the nucleus and release a single-stranded transgene which, after synthesis of the second strand, is available for transcription [Li and Samulski, 2020] (FIGURE 1.1B). Some genomic integration of AAV transgenes does occur, but its extent is a matter of ongoing discussion (frequencies of up to 1-3% have been reported) [Dalwadi et al., 2021]. While transgene expression is quickly lost in rapidly dividing tissues such as activated lymphocytes [Michels et al., 2021], long-term gene expression over several years in the clinical setting has been reported for post-mitotic cells in skeletal muscle, liver, and the eye [Herzog, 2020].

Just 25 nm in diameter, the icosahedric AAV particles are the smallest gene transfer vehicles. Accordingly, they are capable of efficient tissue penetration but are limited in their packaging capacity. Wild-type adeno-associated virus 2 has a 4.7 kb genome, of which approximately 300 nt are inverted terminal repeats. Functional vectors were described for transgenes >6 kb, with vector titer decreasing with transgene length [Grieger and Samulski, 2005]. A critical bottleneck in AAV-

---

[2]status: recruiting, not yet recruiting, active not recruiting, enrolling by invitation; intervention: lentiviral vector

mediated transduction is the complementation of the ssDNA genome to form dsDNA. To achieve higher transduction efficiencies and faster expression kinetics, AAVs can be outfitted with self-complementary (sc) genomes. When using the sc configuration, packaging capacity of the vectors is halved [McCarty, 2008].

Like LVs, AAVs are produced by co-transfection of plasmids into production cells, with only the transgene plasmids containing the inverted terminal repeats (ITRs) required for packaging. The packaging plasmids encode helper virus proteins as well as the AAV capsid and replicase proteins [Castle, 2019].

Because of their differences in vector biology, LVs and AAVs are complementary tools for gene therapy, with one or the other being favorable depending on the specific therapeutic setting. Accordingly, over 60 registered trials are currently ongoing, investigating AAVs as interventions mostly for metabolic, blood coagulation, nervous system and eye diseases [clinicaltrials.gov, 2022[3]]. Five AAV-based gene therapy products are currently marketed in the EU (see TABLE 1.1).

1.2.2 Technical Challenges

While the products discussed in CHAPTER 1.1 are an important spearhead, they are still far from being widely administered and available. At this time, the marketed therapies are used either for the treatment of rare congenital disorders or in cancer patients with late-stage, multiply relapsed or refractory disease. Additionally, they are prohibitively expensive, with annual treatment costs often being in the order of several hundred thousand euros per patient. These realities reflect logistical complexities and technical difficulties which presently stand in the way of gene therapy products such as CAR T cells being made available to more patients who would benefit from them. Many of these limitations relate to the shortcomings of the vector systems currently in clinical use.

A case in point are autologous CAR T cell products: Here, the tedious, unscalable [Parayath and Stephan, 2021] and error prone [Vormittag et al., 2018] *ex vivo* production process - which entails the stringent isolation of cells from the blood of unhealthy donors, their genetic modification outside of the patient's body and their readministration - is mandated not only by HLA barriers but also by the indiscriminate tropism of the lenti- or γ-retroviral vectors used for genetic modification, which necessitates thorough sorting of the cell product before administration (see FIGURE 1.3). Transfer of the CAR to off-target cells, especially to cancer cells, can be fatal for the patient, as was infamously demonstrated when a leukemic clone transduced with anti-CD19-CAR was inadvertently infused into a patient together with the CAR T

---

[3]status: recruiting, not yet recruiting, active not recruiting, enrolling by invitation; intervention: adeno-associated vector

cell product, causing tumor relapse and death [Ruella et al., 2018]. Thankfully, this incident, through the stringent sorting and quality control procedures employed for the production of CAR T cells, remains an unfortunate anecdote. Still, it highlights the risk associated with off-target transduction.

Even when the low toxicity of the transgene warrants systemic administration of vector, as is the case for two currently marketed AAV-based products, the broad tropism of the AAV serotypes used impacts the treatments' efficacy and safety. When an organ other than the liver is the intended target, high doses of vectors are required, since only a small fraction of the administered particles reaches the therapy-relevant cell type, as was impressively shown by human biodistribution data from two deceased children treated with Zolgensma [Thomsen et al., 2021]. Treatment is further complicated by potentially dose-limiting toxicities, which have become apparent in human trials of *in vivo* gene therapy. These include thrombotic microangiopathies, myocarditis, neurotoxicity and hepatotoxicity [Food and Drug Administration, 2021; Ertl, 2022]. Regrettably, in a trial investigating treatment of X-linked myotubular myopathy with AAV8, three patients receiving the higher dose of 3E14 vector genomes/kg experienced severe hepatotoxicity; all died [Wilson and Flotte, 2020; Philippidis, 2020].

Vectors that preferentially (or even exclusively) transduce the therapy-relevant cell type upon systemic administration would meet the express need for more effective platforms [Ertl, 2022; Philippidis, 2020], reducing the dose required for effective therapy and decreasing dose-associated toxicities [Buchholz et al., 2015]. Additionally, vectors targeted at the stage of cell entry will likely help constrain the distribution of transgene and prohibit transduction of undesirable cells. Indeed, substantial progress in vector targeting has been made in the past years, reshaping gene therapeutic strategy.

1.3 Selective Transduction Reshapes Therapeutic Strategy

1.3.1 Choosing Wisely: Rational Design and the Holy Grail of Gene Therapy

Looking back at the beginnings of the still young field of gene therapy in 1992, Theodore Friedmann identified 'direct, targeted *in vivo* gene delivery' as the holy grail of gene therapy, and accurately predicted the importance of, i.a., new viral vector platforms for obtaining it [Friedmann, 1992]. Thirty years later, increasingly

mature advanced vector systems capable of selectively transducing cell types of interest directly *in vivo* are challenging the status quo in gene therapy. They are a product of receptor-targeting, an approach of rational design in which high-affinity binders like single chain variable fragments (scFvs), nanobodies or designed ankyrin repeat proteins (DARPins) are incorporated into the particles' entry machinery.

Although these vectors were rationally engineered, they were not conceived *de novo*. Instead, their design is based on insights from complementary processes of directed evolution. In these high-throughput processes, candidates from diversified libraries are selected for properties-of-interest, e.g. in binding or transduction assays. This diverse family of approaches includes those in which vectors are selected from a combinatorial space of AAV capsid variants [Becker et al., 2022] or chemical compositions of nanoparticles [Paunovska et al., 2019; Liu et al., 2021]. Such strategies have yielded vectors with improved tissue-tropism, such as the AAV-PHP.B capsid family, capable of transducing brain cells across the blood brain barrier [Deverman et al., 2016; Huang et al., 2022; Chan et al., 2017]; additionally, they are capable of providing crucial insights into the structure-function relationships underlying vector tropism [Becker et al., 2022]. Finally, ligand screening processes like ribosome display [Plückthun, 2015; Frank et al., 2020b; Michels et al., 2021; Hartmann et al., 2018] supply novel high-affinity binders, e.g. DARPins, for receptors-of-interest (FIGURE 1.2A).

Integrating these key insights through rational design, receptor-targeting achieves true cell type selectivity: *In vivo*, some receptor-targeted vectors displayed selectivities exceeding 95%. Accordingly, cell type-selective viral vectors should be appreciated as the culmination of decades of advances in molecular virology and protein engineering and present a potential solution to major roadblocks to clinical gene therapy.

1.3.2 Receptor Targeting of Viral Vectors

1.3.2.1 Lentiviral Vectors

Engineering of envelope proteins for receptor targeting of LVs is a two-step process which entails i) the ablation of natural receptor usage and ii) the insertion of a proteinaceous binder selective for the receptor-of-interest. Since VSV G protein mediates both receptor-binding and membrane fusion, altering its receptor usage is challenging [Anastasov et al., 2016]. While the recent identification of the residues by which it contacts its natural receptor LDLR [Nikolic et al., 2018] may help accelerate ongoing efforts to alter the tropism of G protein without compromising
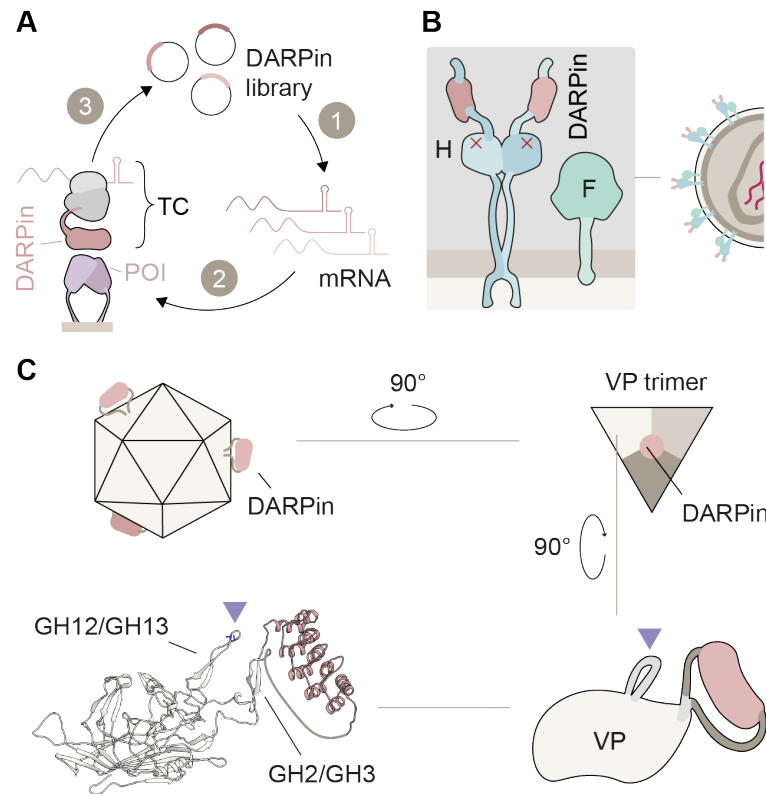
FIGURE 1.2: Receptor-targeting of viral vectors
The receptor-targeting process for viral vectors entails the selection of high-affinity binders such as DARPins and their insertion into the vectors' entry machinery. **A** Workflow of ribosome display for DARPin selection. An mRNA library is generated from the DNA DARPin library (1) and then translated in a combined reaction that yields polypeptide bound to ribosomes arrested on the mRNA (2). These ternary complexes (TC) are then subjected to pre-selection before being bound to immobilized proten-of-interest (POI) and washed stringently. After washing, ternary complexes are eluted, RNA is reverse-transcribed and amplified by reverse transcriptase PCR, and adapters are ligated before another round of screening is initiated (3). **B** LVs are pseudotyped with paramyxoviral glycoproteins. The receptor-binding measles virus H protein is shown in complex with the membrane fusion proteins F. Ablation of natural receptor binding by point mutations is indicated by red crosses. Target receptor binding is mediated through DARPins C-terminally fused to H protein by flexible linkers. **C** An AAV particle displaying DARPins (red) at its 3-fold symmetry axis is shown. Zooming in to a single VP, the DARPin is shown inserted into the GH2/GH3 loop. Residues in the GH12-GH13 loop mutated to ablate binding to the attachment receptor heparan-sulfate proteoglycan are labeled by the triangle. The ribbon structure was generated using ColabFold [Mirdita et al., 2021]. Linker length was adapted manually to improve clarity. Based on [Michels et al., 2022].

its membrane fusion capacity, targeting approaches for VSV G-pseudotyped LVs are not yet as advanced as those utilizing glycoproteins from paramyxoviruses, which use separate envelope proteins for binding and fusion [Buchholz et al., 2009].

The paramyxoviral targeting platform (Figure 1.2b) was first established in the context of oncolytic viruses by mutating the receptor binding site in the measles virus (MV) hemagglutinin (H) and fusing it to a tumor antigen-specific scFv [Nakamura et al., 2005]. This approach was transferred to the lentiviral context in this thesis' host laboratory by cytoplasmatic truncation of the receptor-targeted H and the fusion protein (F) of MV by 18 and 30 amino acids (AA), respectively, which facilitates incorporation into LV particles [Funke et al., 2008]. A similar approach was later described using the envelope proteins of Nipah virus (NiV). Because of the specifics of NiV envelope protein architecture, use of NiV-pseudotyped receptor-targeted particles can result in higher vector titers relative to MV-pseudotyped LVs when membrane-proximal receptor domains are targeted. Additionally, NiV-pseudotyped particles, likely because of the relatively low prevalence of NiV, were found to be at least tenthousandfold less sensitive to neutralization by pooled human serum antibodies than LVs pseudotyped with the glycoproteins of MV, against which vaccination programs are in place [Bender et al., 2016]. For both approaches, DARPins, which can be conveniently selected *in vitro* from large combinatorial libraries by ribosome display [Plückthun, 2015], may be used instead of scFvs [Michels et al., 2021; Frank et al., 2020a; Frank and Buchholz, 2018].

Using both pseudotypes and classes of binders, the host laboratory has described LVs specific for more than a dozen different cell surface proteins which, in addition to surface markers of tumor cells, neuronal subtypes and endothelial cells [Anliker et al., 2010], include markers of immune and hematopoietic cells with high relevance for *in vivo* CAR gene delivery [Frank and Buchholz, 2018]. Recent studies on vectors targeted to these latter classes of markers have highlighted the considerable selectivity of receptor-targeted paramyxoviral pseudotypes, observing transcript-level on-target rates upwards of 99% for hCD8-targeted NiV-LVs on PBMCs [Charitidis et al., 2021], as well as their ability to modulate target cell behaviour through interaction with their target receptor, e.g. to increase cytolytic activity of T cells in CD8-LV-mediated transfer of T cell receptors [Q. Zhou et al., 2012], downmodulate CD4 expression upon vector addition to primary cell culture [Q. Zhou et al., 2015] or enable efficient and selective transduction of T cells from PBMCs in cell culture without the aid of activating antibodies and even direct gene transfer in unprocessed blood through the use of agonistic scFvs derived from αhCD3 antibodies, combining T cell activation and targeting [Frank et al., 2020b].

1.3.2.2 Adeno-Associated Vectors

AAV particles' lack of a membranous envelope requires incorporation of the binder into their rigid capsid for receptor-targeting. To this challenge of vector design, effective solutions have only recently emerged.

AAV capsids are icosahedral, with 60 viral proteins (VPs) making up the structure. These are arranged into 20 facets; each facet consists of a trimer of VPs. Three different VPs – VP1 through VP3 – have been described. VP1-3 share the VP3 common region and differ in their flexible N-terminal tail, with VP3 having the shortest and VP2 and VP1 having increasingly longer tails. The VP1/VP2 common region includes a nuclear localization signal. Mass spectrometry aided by computer simulations found that AAV capsids produced from plasmids assemble stochastically following a random draw principle, with virtually every capsid in a given preparation having a unique stochio-spatial configuration of VPs [Wörner et al., 2021].

Similarly, binding and cellular uptake of AAVs is a complex and serotype-dependent process. AAVs often use glycans – heparan sulfate proteoglycan (HSPG) in the case of AAV2 – as attachment factors. Additionally, dozens of cellular proteins are implicated in AAV uptake, among them the transmembrane AAV receptor (AAVR), which was shown to be crucial for transduction by most serotypes [Meyer and Chapman, 2021; Riyad and Weber, 2021].

Accordingly, to target AAVs through rational design, binding of the AAV2 capsid to HSPG was abrogated by mutating two relevant arginine residues to alanine (**Figure 1.2c**) before a DARPin directed against the tumor marker Her2/neu was fused the N-terminus of VP2. Notably, targeting reduced the accumulation of intravenously administered vector to the liver substantially [Münch et al., 2013]. Following this proof-of-principle, N-terminally-modified AAVs were generated for the specific transduction of GluA4-, CD105-, EpCAM- and CD4-positive cells; all were used successfully in mouse models and/or human blood [Münch et al., 2015; Hartmann et al., 2019; Hartmann et al., 2018].

In addition to the examples recounted above, the proven N-terminal insertion site was exploited for more advanced targeting approaches, such as the non-genetic covalent coupling of DARPins and scFvs to the capsid of a universal AAV through protein splicing [Muik et al., 2017] and a light-inducible transduction system in which phytochrome-interacting factor 6 is N-terminally linked to AAV2 VP2. Interestingly, transduction efficiency using the latter system was found to improve with prolonged incubation of the vector stock at 65°C prior to transduction [Hörner et al., 2021], indicating that not all of the N-terminally fused binders are located outside of the capsid. An alternative, surface-exposed insertion site in the GH2/GH3 loop of the VP3 common region capable of accommodating larger proteins was identified by

13

screening of a random insertion library for clones capable of transgene delivery and capsid assembly despite insertion of mCherry [Judd et al., 2012]. Utilizing this site, Eichhoff et al. constructed vectors targeted to CD38, ARTC2.2 and P2X7 by means of nanobodies inserted into VP1 of AAV2 [Eichhoff et al., 2019]. Expanding on their approach, AAVs targeted to murine CD8 by means of a DARPin in the VP1 GH2/GH3 loop are described in this thesis and in [Michels et al., 2021] (Figure 1.2c).
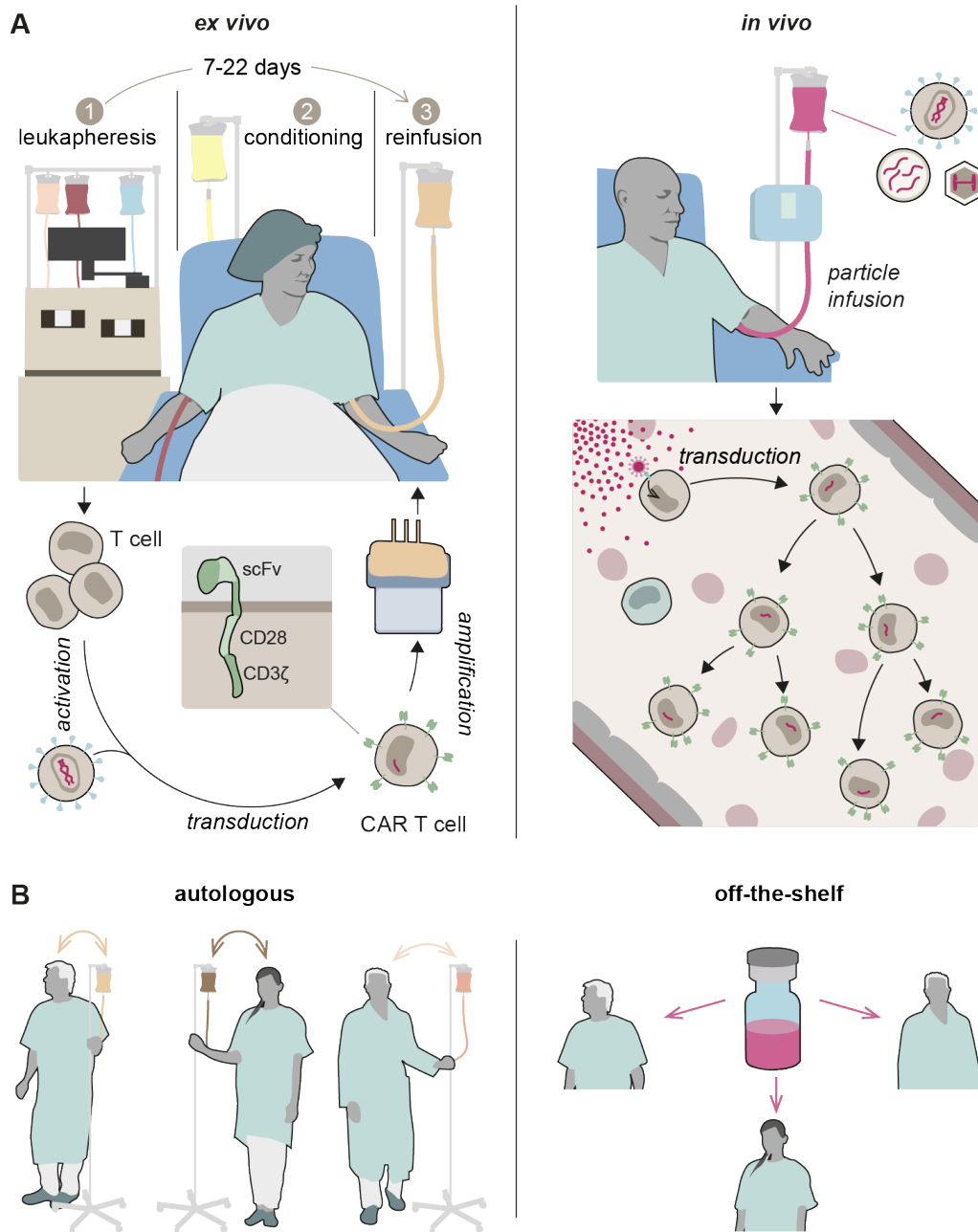
1.4 *In Vivo* CAR Therapy

Constrained by a complex manufacturing process which renders it expensive and, through the necessary manipulations of patients' T lymphocytes, can alter their phenotype and activity, CAR therapy well-exemplifies the challenges currently faced by clinical gene therapy (see Chapter 1.2.2). Consequently, various paths are being pursued in preclinical and clinical research to improve CAR technology.

Strategies aiming at facilitating the manufacturing process reach from automated systems [Lock et al., 2017] to allogeneic CAR T cells [Qasim, 2019]. Although automation combined with the possibility to generate CAR T cells close to the patient's bedside will greatly facilitate the logistics of manufacturing, this will not change the autologous, highly individualized nature of the product. In the allogeneic approach, CAR T cells prepared from a healthy donor are genetically manipulated to decrease their alloreactivity in the recipients. This is a step toward off-the-shelf CAR T cells, although the resulting products will most likely not be completely universal, owing to human leukocyte antigen barriers that necessitate adaptation to patient subgroups [Smirnov et al., 2021].

Graft-versus-host reactions as well as manufacturing complexity are circumvented when CAR cells are generated directly *in vivo* (see Figure 1.3). Here, a single, universally applicable medicinal product in the form of systemically administered vectors encoding the CAR would be used to transduce the patient's cells directly in their body. The resulting CAR cells would be truly autologous. In theory ideally suited to make CAR therapy more widely available, *in vivo* CAR therapy has long been considered impractical, chiefly because suitably sophisticated vectors were not available.

In the last five years, however, several groups have reported the successful *in vivo* generation of CAR cells in mouse models. These thirteen reports, of which ten made use of receptor-targeted vectors, demonstrate the transformative potential as well as the current state-of-the-art of receptor-targeting technology (see Table 1.2). Spanning the entire breadth of the vector spectrum from lentiviral and adeno-associated

FIGURE 1.3: *Ex vivo* **versus** *in vivo* **CAR therapy**
The two strategies for converting T cells into CAR T cells are compared **A** on the cellular level and **B** regarding their implications for clinical use. **A** *Ex vivo* generation of CAR T cells usually entails isolation of T cells from patient blood (1), followed by activation, transduction, and ex vivo expansion. After conditioning treatment (2), CAR T cells are infused into the patient (3). In the *in vivo* approach, vector particles (depicted as red dots) are infused directly into the patient, where they encounter T cells and selectively deliver genetic material encoding the CAR (red). **B** Due to their autologous nature, ex vivo-generated CAR cell products currently have to be prepared individually for each patient (left). The vector preparations currently under evaluation for in vivo CAR therapy constitute universally applicable off-the-shelf medicinal products (right). Reprinted from [Michels et al., 2022].

vectors to synthetic vectors[4] like polymer nanocarriers (NC) and lipid nanoparticles (LNP), they provide crucial proof-of-principle for *in vivo* CAR generation, but leave important questions regarding the short-, medium- and long-term safety and efficacy of the transfer approaches unanswered. Among these are concerns about the precise biodistribution of the vectors, the fate and longevity of the transferred genetic material, the persistence of the modified cells and the immune response to single and repeated vector administration, i.e. the host response [Michels et al., 2022].

Recent [Wilson and Flotte, 2020; Philippidis, 2020; Micklethwaite et al., 2021; Bishop et al., 2021] and earlier [Hacein-Bey-Abina et al., 2003; Raper et al., 2003] fatalities in gene therapy are a reminder not to take these questions lightly, but to thoroughly examine vectors' effects on a model host in long-term preclinical studies to help eliminate critical issues before advancing to first-in-human trials.

1.5 Mouse Models Beyond Proof-of-Principle

As the most pressing open questions in *in vivo* gene therapy research currently pertain to the host response to vector administration on different timescales, which, by all indication, is tightly linked to an interplay of different immune processes and compartments, a mouse model addressing them should be as representative as possible of a normal human immune system and enable long-term observations. Two distinct but complementary approaches are commonly used to assess immune responses to treatment in pre-clinical mouse models, each with its advantages and drawbacks. [Shultz et al., 2019]

1.5.1 Human Vectors, Human Cells

Most of the proof-of-concept experiments on *in vivo* CAR therapy summarized in **TABLE 1.2** made use of humanized mouse models. This preference is most pronounced for studies using viral vectors, which relied on them for twelve of fourteen experiments. In humanized mouse models, human immune cells are transplanted into mice which have been rendered immunodeficient through germline mutations. Able to accommodate human cells and immune processes, they are crucial tools in immunology research, enabling both preclinical testing of advanced therapy medicinal products designed for human use as well as bottom-up basic research in molecular

---

[4]Research into the clinical use of synthetic vectors, increasingly important and themselves the product of decades of basic research, is an emerging and highly dynamic field. Although a transformative technology in their own right and the basis for internationally successful SARS-CoV-2 vaccines, they are largely ignored in this manuscript for the purposes of conciseness and clarity. For an overview of approaches for their receptor-targeting, please refer to [Michels et al., 2022].

TABLE 1.2: Preclinical reports of *in vivo* CAR transfer. Based on [Michels et al., 2022].

Vector Platform	Targeted receptor	Dosing and route[b]	Mouse model Strain[d]	Immune transplants[e]	CAR Configuration[f]	Target cells[g]	Reference
NiV-LV	Human CD8	2E6 TU (i.p.)	NSG	Activated human PBMCs (i.p.)	hCD19-28ζ-CAR	Raji (i.p.)	[Pfeiffer et al., 2018]
	Human CD8	2E6 TU (i.v.)	NSG	Human CD34+ CB cells	hCD19-28ζ-CAR	Endogenous B cells	
NiV-LV	Human CD8	2.5E11 particles (i.v.)	NSG	Activated human PBMCs (i.v.)	hCD19-28ζ-CAR	Nalm-6 luc, (i.v.)	[Agarwal et al., 2019]
MV-LV	Human CD4	4E10 particles (i.p.)	NSG	Activated human PBMCs (i.p.)	hCD19-28ζ-CAR	Endogenous B cells	[Agarwal et al., 2020]
		1E11 particles (i.v.)	NSG	Activated human PBMCs (i.v.)	hCD19-28ζ-CAR	Nalm-6 luc, (i.v.)	
		4E10 particles (i.v.)	NSG	Human CD34+ CB cells	hCD19-28ζ-CAR	Endogenous B cells	
MV-/NiV-LV	Human CD4	0.9-2.4E11 particles (i.v.)	NSG-SGM3	Human CD34+ CB cells	hCD19-28ζ-CAR	Endogenous B cells	[Ho et al., 2022]
	Human CD8	0.8-2.8E11 particles (i.v.)	NSG-SGM3	Human CD34+ CB cells	hCD19-28ζ-CAR	Endogenous B cells	
NiV-LV	Human CD3	2E11 particles (i.v.)	NSG	Human CD34+ CB cells	hCD19-28ζ-CAR	Endogenous B cells	[Frank et al., 2020a]
SINV[i]-LV	Human CD3	5E10 particles (i.v.)	NSG	Activated human PBMCs (i.v.)	hCD19-28ζ-CAR	BV-173 luc (i.v.)	[Huckaby et al., 2021]
VSV-LV	LDLR	3.6-4.0E6 IU (i.v.)	B6	N/A	hCD19-4-1BBζ-CAR[h] or mCD19-4-1BBζ-CAR[h]	Endogenous B cells	[Rive et al., 2022]
		2.04E6 or 2.04E7 IU (i.v.)	B6	N/A	mCD19-4-1BBζ-CAR[h]	Endogenous B cells	
AAV-DJ	N/A[a]	1E11 vg (i.p.)	NCG	Human PBMCs (i.p.)	hCD4-28-4-1BBζ-CAR	Endogenous CD4 T cells	[Nawaz et al., 2021]
		2E11 vg (i.p.)	NCG	Human PBMCs (i.p.)	hCD4-28-4-1BBζ-CAR	MT-2 ATL (i.p.)	
DNA-NC	Mouse CD3	3E11 particles / day on five consecutive days (i.v.[c])	Albino B6	N/A	mCD19-4-1BBζ-CAR	N/A	[Smith et al., 2017]
		3E11 particles / day on five consecutive days (i.v.)	Albino B6	N/A	mCD19-4-1BBζ-CAR	Eμ-ALL(i.v.)	
DNA-NC	N/A	10 µg plasmid (i.t.) / d on 2 d, 3 d apart	A/J	N/A	mALK-28ζ-CAR-IFNγ-GFP	Neuro-2a (s.c.)	[Kang et al., 2021]
		25 µg plasmid (i.p.)	A/J	N/A	mALK-28ζ-CAR-IFNγ-GFP	Neuro-2a (s.c.)	
mRNA-NC	Human CD8	6 weekly doses; 50 µg mRNA / dose (i.v.)	NSG	Human T cells (i.v.)	hCD19-28ζ-CAR	Raji-luc (i.v.)	[Parayath et al., 2020]
		6 weekly doses; 50 µg mRNA / dose (i.v.)	NSG	Human T cells (i.v.)	hROR1-4-1BBζ-CAR	LNCaP C42 prostate cancer cells (orthotopic)	
	Mouse CD3	4 weekly bursts of 3 daily doses; 15 µg mRNA / dose (i.v.)	Albino B6	N/A	mCD19-28ζ-CAR	Eμ-ALL (i.v.)	
mRNA-LNP	Mouse CD5	10 µg LNPs (i.v.)	B6	N/A	mFAP-28ζ-CAR	Endogenous fibrotic cardiac fibroblast	[Rurik et al., 2022]
DNA/shRNA-LNP	Human CD3	5 µg plasmid / g bodyweight (i.v.)	NSG	T cells	hCD19-CAR-shIL6	Raji luc	[J.-E. Zhou et al., 2022]

[a] (N/A) not applicable.
[b] (TU) transducing unit; (i.p.) intraperitoneal injection; (i.v.) intravenous injection; (vg) vector genome.
[c] over 20 min with infusion pump.
[d] (NSG) NOD.Cg.Prkdc^scid IL2rg^tmWjl/SzJ; (NSG-SGM3): NOD.Cg.Prkdc^scid IL2rg^tmWjl Tg(CMV-IL3,CSF2,KITLG)1Eav/MloySzJ; (NCG) NOD/ShiLtJGpt-Prkdc^em26Cd52 Il2rg^em26Cd22 /Gpt; (Albino B6) C57BL/6J-Tyr^c-2J/J; (B6) C57BL/6.
[e] (CB) cord blood-derived.
[f] (h) anti-human; (m) anti-mouse.
[g] (luc) luciferase expressing.
[h] -2A-GFP; [i] Sindbis virus

17

immunology.

While cruder humanized models using activated, mature human T cells from PBMCs, which are very permissive to transduction and produce large amounts of transprotein, are ideal for short proof-of-concept studies, the activated nature of the transplanted cells results in the onset of Graft-versus-Host-Disease (GvHD) after several weeks, severely limiting the observation period. The onset of GvHD can be delayed by the engraftment of hematopoietic stem cells (e.g. CD34+ cells from human cord blood). Additionally, through this use of stem cells, a more complex, quiescent human immune system forms. Advanced models, which include the insertion of human genes into the mouse context, even further improve immunological complexity: In the NSG-SGM3 model used in the host lab, the engraftment of human myeloid and regulatory T cells is improved by transgenic expression of human IL3, GM-CSF and KitL.

Still, the immune systems formed in these models are not representative of the complexity of a typical human immune system in terms of cell frequencies, phenotypes, and activity, as well as in the morphology of immune tissues: A case in point, $IL2r\gamma^{null}$ mouse models, which include the popular NSG strains, display poor lymphatic architecture and suboptimal lymph node development [Shultz et al., 2019]. Complicating matters further, immunodeficient (especially stem cell-humanized) animals are expensive and fragile.

1.5.2 Murinization Required

An alternative to elaborate humanized models are syngeneic models, in which all cells share the genetic background of the host animal. Crucially, no immune transplantation or genetic manipulation is required. Instead, experiments in these models rely on the complex, natural immune system intrinsic to robust, cost-effective inbred laboratory mice. As these models do not contain non-self cells, the observation period is only limited by the animal's lifespan. Although there are marked differences in murine and human genetics and immune systems, such as the differential biodistribution of MHC class II and the dissimilar genetics of inflammation and innate immunity [Shultz et al., 2019], syngeneic models offer clinically valuable insights about the behaviour of complete mammalian immune systems which can inform the treatment of humans, either by themselves or through the complementation of information from humanized models. In fact, preclinical data submitted for the regulatory assessment of Yescarta was generated using a syngeneic mouse model based on the C3H inbred mouse strain [Kochenderfer et al., 2010; Elsallab et al., 2020].

For all of their desirable features, however, substantial differences in the molecular makeup of mouse and man, as are e.g. apparent for murine CD8, which only has negligible (<50%[5]) protein-level identity to its human counterpart [Michels et al., 2021], often preclude the direct testing of reagents for human treatment, such as human-specific CARs, antibodies or vectors targeted to human surface markers, in syngeneic preclinical models. Instead, surrogate, mouse-compatible reagents have to be developed. Breaking ground for syngeneic models of *in vivo* gene (i.e. CAR) therapy with viral vectors, this thesis describes the generation and characterization of mouse-compatible receptor-targeted lentiviral and adeno-associated vectors.

---

[5]`uniprot.org`, P01731 v. P01732.

1.5.3 Aims

Performed as part of a coordinated effort to characterize *in vivo* CAR therapy beyond proof-of-principle in advanced mouse models, the work summarized in this thesis aimed to establish the use of mouse receptor-targeted lentiviral vectors transferring mouse-compatible CAR and evaluate the host response to *in vivo* CAR generation in syngeneic mouse models, which at the time of the project's inception was thought to consist of reactions similar to the cytokine release syndrome (CRS) observed in 'conventional' clinical *ex vivo* CAR therapy (Milestones 1-3).

A starting point for the project was the pioneering work of A. Frank, who employed ribosome display to select DARPins specific for both human CD8 [Frank et al., 2020a] and mouse CD8 [Michels et al., 2021], using clone MSE10 to generate MV-pseudotyped LVs selective for mouse CD8α (mCD8-LV). Meeting Milestone 1, mCD8-LV was complemented by a vector targeted to mCD4 via a scFv (mCD4-LV), and both mCD4- and mCD8-LV were thoroughly characterized, both with regard to the particles' physical characteristics in nanoparticle tracking analysis and to their transfer behaviour on primary murine lymphocytes (Chapter 2.1.1).

Having established the vectors' efficacy on murine cells, the extent of their selectivity was examined in *ex vivo* binding (Chapter 2.1.3) and transduction (Chapter 2.1.2) assays on whole mouse blood. Additionally, mCD8-LV was used to ablate endo- and exogenous target cells by *in situ* transfer of αmCD19-CAR to an established culture of murine splenocytes (Chapter 2.1.4), completing Milestone 2.

As the LVs performed satisfactorily in cell culture, Milestone 3 was addressed in two experiments in BALB/c mice. The first, preparatory, experiment assessed the biodistribution of systemically administered GFP-transferring LVs and gauged the host response to their administration (Chapter 3.1). Based on these results, an experiment to determine the performance of phagocytosis-shielded, CAR-transferring mCD4- and mCD8-LVs in an immunocompetent model of *in vivo* CAR therapy was set up (Chapter 3.2).

MILESTONES

1. Generate and characterize the molecular tools required for a syngeneic mouse model of *in vivo* CAR therapy, most importantly mouse-compatible receptor-targeted lentiviral vectors.

2. Induce the *in vitro* ablation of target cells through the cell type-specific transfer of mouse compatible CAR.

3. Induce the ablation of target cells directly in mice through systemic administration of CAR-transferring vector and evaluate the side effect profile elicited by such treatment.

The utility of MSE10 in mouse-compatible LVs motivated its use beyond the original scope of the project. In collaboration with and building on the foundational work of D.M. Günther, who established a new generation of DARPin-targeted AAVs in the host laboratory, an AAV specific for mouse CD8α (mCD8-AAV) was generated by insertion of the DARPin into the GH2/GH3 loop of VP1 of AAV2. Modified particles were produced and biochemically characterized via quantitative PCR and Western Blot before functional evaluation on primary murine lymphocytes were carried out to determine the efficiency, specificty and kinetics of gene transfer (**CHAPTER 2.2**).

Found to display unexpectedly high transduction efficiencies *in vitro*, mCD8-AAV transferring cre-recombinase was examined in an *in vivo* biodistribution assay in Ai9 reporter mice to determine the effect of receptor-targeting on both on-target transduction efficiency and gross vector biodistribution (**CHAPTER 3.3**).

2

RESULTS I

Of Mice and Men and Viral Vectors

2.1 Lentiviral Vectors

The first and pivotal step towards the setup of the syngeneic models of *in vivo* gene therapy described later in this thesis was the generation and thorough character-ization of mouse-compatible viral vectors. As a substantial fraction of preclinical reports on *in vivo* CAR therapy published so far had relied on them (Table 1.2), receptor-targeted lentiviral vectors were the focus of the murinization efforts at the outset of the project. The first LV type to be established was mCD8-LV, targeted to murine CD8 via the anti-mCD8α MSE10 DARPin (see p. 20). An overview of all lentiviral vectors used in this thesis is provided in Table 2.1.

2.1.1 Murine Lymphocytes are Permissive to Lentiviral Transduction *In Vitro*

In mCD8-LVs, the C-terminus of receptor-blinded, truncated hemagglutinin (HΔ18) protein from MV is fused genetically to the N-terminus of the MSE10 DARPin via a G4S linker (Figure 2.1a). Pseudotyped LV stocks were purified and concentrated from cell culture supernatant by sucrose cushion centrifugation. Characterization of eleven stocks of mCD8-LV and nine stocks of VSV-LV (pseudotyped with the G protein of vesicular stomatitis virus) by nanoparticle tracking analysis revealed a consistently smaller size of VSV-LV than mCD8-LV, with mean particle sizes of 118.0 nm for VSV-LV and 130.9 nm for mCD8-LV (Figure 2.1bd). This is in line with previous data describing receptor-targeted LVs pseudotyped with modified paramyxovirus glycoproteins to be larger than VSV-LVs [Weidner et al., 2021]. Particle counts of the LV stocks were usually slightly higher for VSV-LV than for mCD8-LV after 150-fold

TABLE 2.1: Lentiviral vectors used in this thesis.

Vector	Receptor	Pseudotype	Binder	Transgene[a] Promoter	ORF	See Figure
mCD8-LV-SFFV-GFP	mCD8	MV	MSE10[b]	SFFV	GFP	2.1, 2.2, 2.3, 2.4, 2.5, 2.6, 3.7
mCD8-LV-MCMV-GFP	mCD8	MV	MSE10	MCMV	GFP	2.2
mCD8-LV-EF1α-GFP	mCD8	MV	MSE10	EF1α	GFP	2.2
mCD8-LV-PGK-GFP	mCD8	MV	MSE10	PGK	GFP	2.2, 3.1, 3.2, 3.4, 3.5
mCD8-LV-SFFV-CAR	mCD8	MV	MSE10	SFFV	αmCD19-CAR	2.6
mCD8-LV-PGK-CAR	mCD8	MV	MSE10	PGK	αmCD19-CAR	2.4, 2.5, 3.6, 3.7, 3.9, 3.10
mCD4-LV-PGK-GFP	mCD4	MV	GK1.5[c]	PGK	GFP	3.1, 3.2, 3.4, 3.5
mCD4-LV-PGK-CAR	mCD4	MV	GK1.5	PGK	αmCD19-CAR	2.4, 2.5, 3.6, 3.9, 3.10
VSV-LV-SFFV-GFP	LDLR	VSV	N/A	SFFV	GFP	2.1, 2.2, 2.3, 3.2
VSV-LV-MCMV-GFP	LDLR	VSV	N/A	MCMV	GFP	2.2
VSV-LV-EF1α-GFP	LDLR	VSV	N/A	EF1α	GFP	2.2
VSV-LV-PGK-GFP	LDLR	VSV	N/A	PGK	GFP	2.2, 3.1, 3.2
VSV-LV-SFFV-mCD19-CAR	LDLR	VSV	N/A	SFFV	αmCD19-CAR	3.7
VSV-LV-SFFV-hCD19-CAR	LDLR	VSV	N/A	SFFV	αhCD19-CAR	3.7

[a] All LV transgenes contain woodchuck hepatitis virus posttranscriptional regulatory element (WPRE) downstream of the ORF;
[b] DARPin; [c] scFv;

or 333-fold concentration (Figure 2.1c). Both vector stocks were produced using identical amounts of packaging plasmid. The difference in particle counts between LVs pseudotyped with VSV-G and paramyxovirus glycoproteins has been observed previously and may arise from the vesicle-forming activity of VSV-G protein [Mangeot et al., 2011] and/or the use of two versus three plasmids with a cytomegalovirus (CMV) promoter during production, which may have resulted in sequestration of transcription factors.

After establishing the nominality of mCD8-LVs' particle characteristics, their functionality was assessed by titrating their GFP transfer activity at doses ranging from 2.5E5 to 3.2 particles/cell on activated primary murine Pan T cells. Remarkably, mCD8-LV was very active in gene delivery, its transducing titer five days post vector addition, 1.17E8 transducing units (TU) per mL, being within one order of magnitude of the transducing titer of VSV-LV, 1.07E9 TU/mL (Figure 2.2ab). This difference was well in line with the obtained vector copy numbers (VCNs), which were approximately one order of magnitude higher for cells transduced with VSV-LV compared to cells incubated with mCD8-LV for all particle counts (range: 5.0- to 11.5-fold) (Figure 2.2c). At 2E9 particles/well, mean VCNs were 30.5 for VSV-LV-transduced cells and 2.9 for mCD8-LV-transduced cells.

In contrast to VSV-LV however, gene delivery by mCD8-LV was highly selective for CD8+ splenocytes, even resulting in a decrease in CD8 intensity at a dose of 1E10 particles/well, which was likely due to masking of the epitope for antibody staining (Figure 2.2d). This highest dose (i.e. 2.5E5 particles/cell) resulted in approximately 60% GFP+ cells for VSV-LV and 40% for mCD8-LV. Notably, mCD8-LV already reached a plateau of 40% GFP+ cells at 2E9 particles/well. The earlier plateau and steeper increase in mean fluorescence intensity (MFI) of cells treated with mCD8-LV is consistent with mCD8-LV only transducing a subpopulation of target cells (i.e., CD8+ cells).

As work by another group had suggested the choice of promoter to be a critical factor determining the success of mouse T cell transduction [Gilham et al., 2010], the performance of VSV-LV and mCD8-LVs carrying the GFP reporter under the control of promoters from the spleen focus-forming virus (SFFV), the human elongation factor 1a (EF1a), phosphoglycerate kinase (PGK), or the murine CMV (MCMV) immediate early promoter was evaluated in titrations on Pan T cells. No relevant differences in GFP expression were observed, indicating that all four promoters are equally suitable for gene expression in short-term mouse cultures and, conversely, that there are no principal objections to the use of non-virally derived promoters such as PGK or EF1a – which literature had suggested may be less prone to epigenetic inactivation than virally-derived promoters [Herbst et al., 2012] – for work towards syngeneic mouse models of *in vivo* gene therapy (Figure 2.2e).
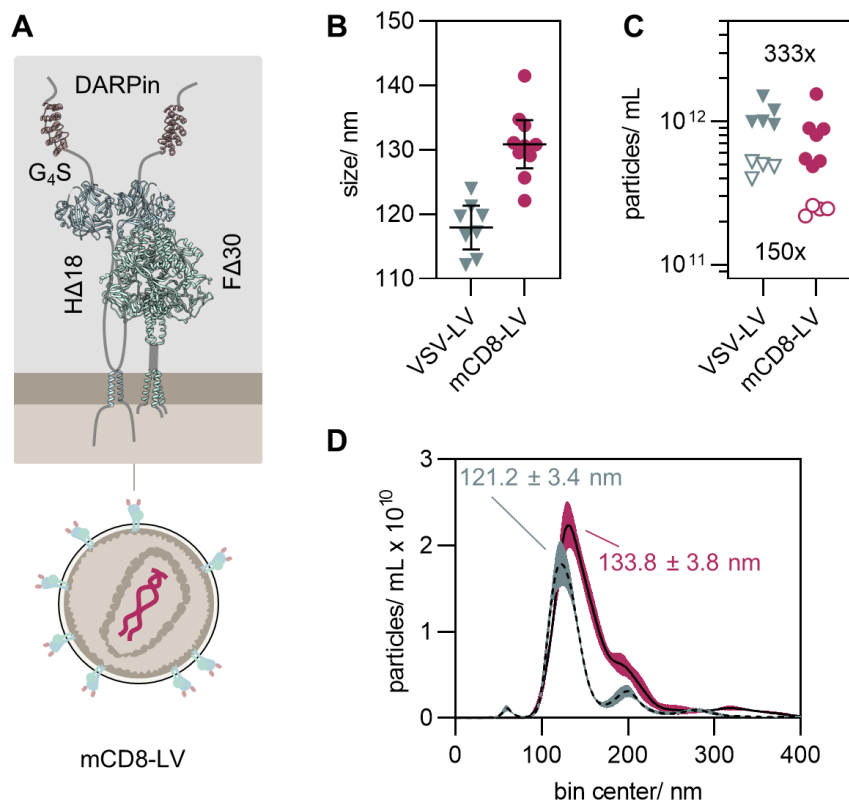
FIGURE 2.1: mCD8-LV displays nominal particle characteristics
A To-scale approximation of vector mCD8-LV structure. MV H protein is blinded for its natural receptors by point mutations and fused at its C terminus with DARPin MSE10 directed against mCD8. The inlay illustrates the envelope protein complex. MV HΔ18 is shown as a dimer, MV FΔ30 as a trimer. The illustration was created using structures PDB: 5YZD, 2ZB5, and cellPACK recipe HIV-1_0.1.6. **B-D** Characterization of mCD8-LV stocks by nanoparticle tracking analysis. Particle size distribution and concentration were determined using a NanoSight NS300 analyzer. VSV-LV served as a reference. **B** Particle sizes and **C** particle concentrations of 9 VSV-LV stocks and 11 mCD8-LV stocks from 5 measurement sessions, respectively. Each symbol represents one vector stock. Solid lines in **B** are arithmetic means. Error bars represent 95% confidence intervals (CIs). Empty symbols in **C** indicate 150-fold concentration, colored symbols 333-fold concentration. **D** Example histograms from one measurement. Size modes $\pm$ standard error of VSV-LV (dashed line, blue bands) and mCD8-LV (solid line, red bands) are indicated. Bands represent standard error of n = 4 sequential technical replicates.
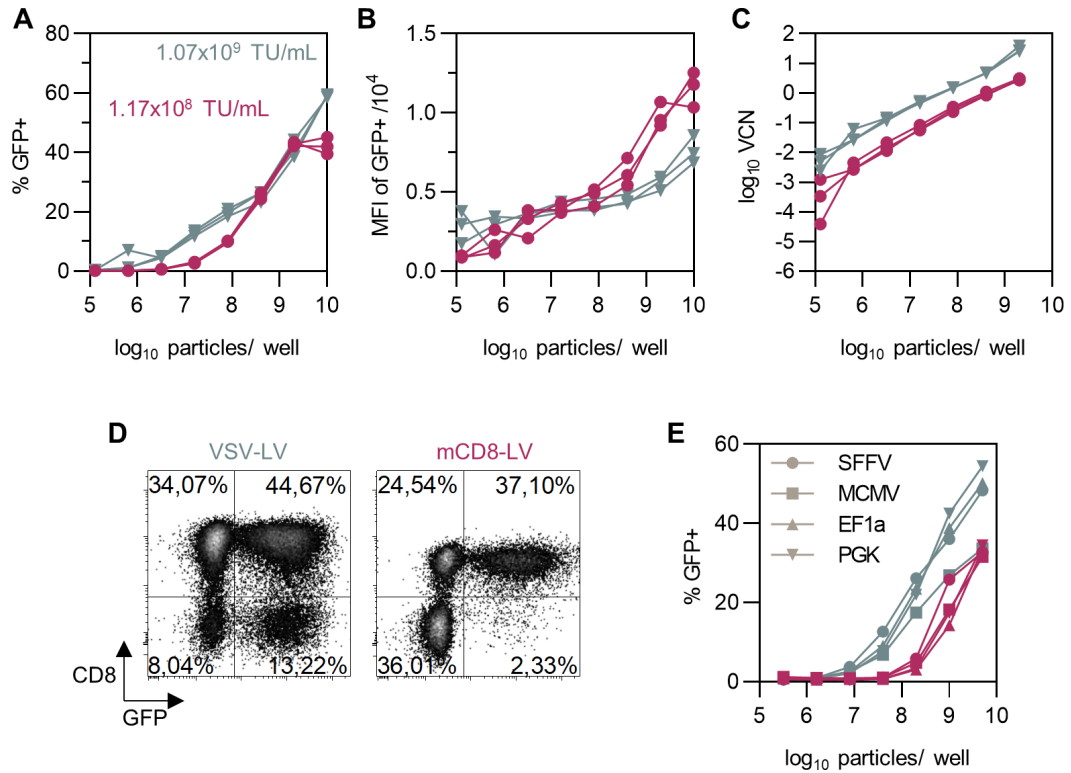
FIGURE 2.2: **Displaying MSE10 on lentiviral vectors mediates selective gene transfer**

AB Titration of gene transfer activity on murine Pan T cells. Splenic Pan T cells from BALB/c mice were thawed. 4E4 cells/well stimulated with αmCD3/αmCD28-beads and recombinant human IL7 and IL15 (rhIL7+15) were transduced with serial dilutions of GFP-transferring VSV-LV or mCD8-LV by spinfection. Cells were analyzed by flow cytometry and qPCR 5 days post spinfection. Symbols represent data from n = 3 mice. **A** Percentage of GFP+ viable singlet cells. Transducing titers for VSV-LV (blue triangles) and mCD8-LV (red circles) stocks are shown. **B** Geometric MFIs of GFP+ viable singlet cells at the indicated particle doses. **C** Numbers of integrated vector copies per cell for VSV-LV (blue triangles) and mCD8-LV (red circles) stocks. DNA was extracted from total cells, without prior sorting. **D** Representative flow cytometry plots showing GFP versus CD8 signals of viable singlet cells from one mouse. Vector dose was 1E10 particles/well. **E** Titration of VSV-LV and mCD8-LV stocks equipped with promoter variants. 4E4 Pan T cells per well, stimulated with αmCD3/αmCD28-beads and recombinant human IL7 and IL15 (rhIL7+15) were transduced with the indicated amounts of GFP-transferring VSV-LV (blue) or mCD8-LV (red) stocks carrying GFP under control of either SFFV (●), MCMV (■), EF1a (▲), or PGK (▼) promoter. Cells were analyzed by flow cytometry 5 days after vector treatment. Percentages of GFP+ cells among viable singlets are shown. Symbols represent means of data from n = 3 mice. Red symbols indicate mCD8-LV, blue symbols VSV-LV. Adapted from [Michels et al., 2021].

2.1.2 Receptor-Targeted LVs Selectively Transduce Lymphocyte Subsets in Whole Blood

In light of the satisfactory performance of mCD8-LV on primary splenocytes, its gene transfer activity in a more complex cell mixture, i.e. whole mouse blood, was examined. Blood from BALB/c mice was incubated with 2E10 particles/150 μL (i.e., approximately 5E4 particles/leukocyte) in the presence of rhIL7. The cultures were agitated on a shaker at 37°C for 6 h to simulate vector binding in circulating blood. After allowing for vector binding, erythrocytes were cleared, and the remaining cells were activated with αmCD3/αmCD28-beads and cultivated for 5 days in the presence of rhIL7+15 before cells were analyzed by flow cytometry and qPCR (**FIGURE 2.3A**).

Surprisingly, both LV treatments yielded similar overall GFP-positivities (**FIGURE 2.3BC**) and genomic integration rates (**FIGURE 2.3E**), even though VSV-LV-SFFV-GFP had previously displayed transducing titers per particle approximetaly 15-fold higher than those of mCD8-LV-SFFV-GFP on Pan T cells. In light of the concomitant large discrepancies between mCD8-LV and VSV-LV in mean GFP-positivities among CD8+ cells (22.7& v. 4.9%) and selectivities, i.e. CD8-positivities among GFP+ cells (99.2% v. 25.5%, **FIGURE 2.3D**), the similar overall protein and genome-level transduction rates observed here may be explained as a consequence of the selectivity of mCD8-LV, or – more precisely – the loss of VSV-LV-transduced relative to mCD8-LV-transduced blood cells to erythrocyte elimination and cell culture conditions that favor T cells, of which nearly half were CD8+ at the time of measurement.

To enable similarly effective and selective transduction of the second major lymphocyte subtype, i.e. CD4+ T cells, mCD4-LV was generated by replacing MSE10 with a mouse CD4-specific scFv derived from the GK1.5 hybridoma line monocloncal antibody. Overall, mCD4-LV behaved similarly to mCD8-LV, safe for an inverted preference in T cells. Nanoparticle tracking analysis of mCD4-LV stocks yielded size modes and particle concentrations within the range observed for mCD8-LV (**FIGURES 3.1BCD** & **3.6BC**, p. 43 & 50). Titrated on murine splenocytes, mCD4-LV-PGK-GFP (**TABLE 2.1**) achieved a transducing titer of 1.29E7 TU/ mL, similar to the titer of mCD8-LV-PGK-GFP (1.49E7 TU/ mL)[1]. At a dose of 1.5E9 particles/ well of mCD4-LV-PGK-GFP, >95% of GFP-positive cells were CD4+; approximately half of the CD4-positive population was GFP-positive (**FIGURE 3.2ACD**, p. 44), demonstrating the versatility of the paramyxovirus-based approach to receptor targeting of LVs.

---

[1]The transducing titer per volume reported here for mCD8-LV-PGK-GFP on whole splenocytes is 7.8-fold lower than that reported for mCD8-LV-SFFV-GFP on Pan T cells (**FIGURE 2.2A**). This discrepancy is likely a result of the different promoter and the approximately 2.3-fold lower particle concentration of mCD8-LV-PGK-GFP (6.65E11 particles/ mL) compared to mCD8-LV-SFFV-GFP (1.55E12 particles/ mL).
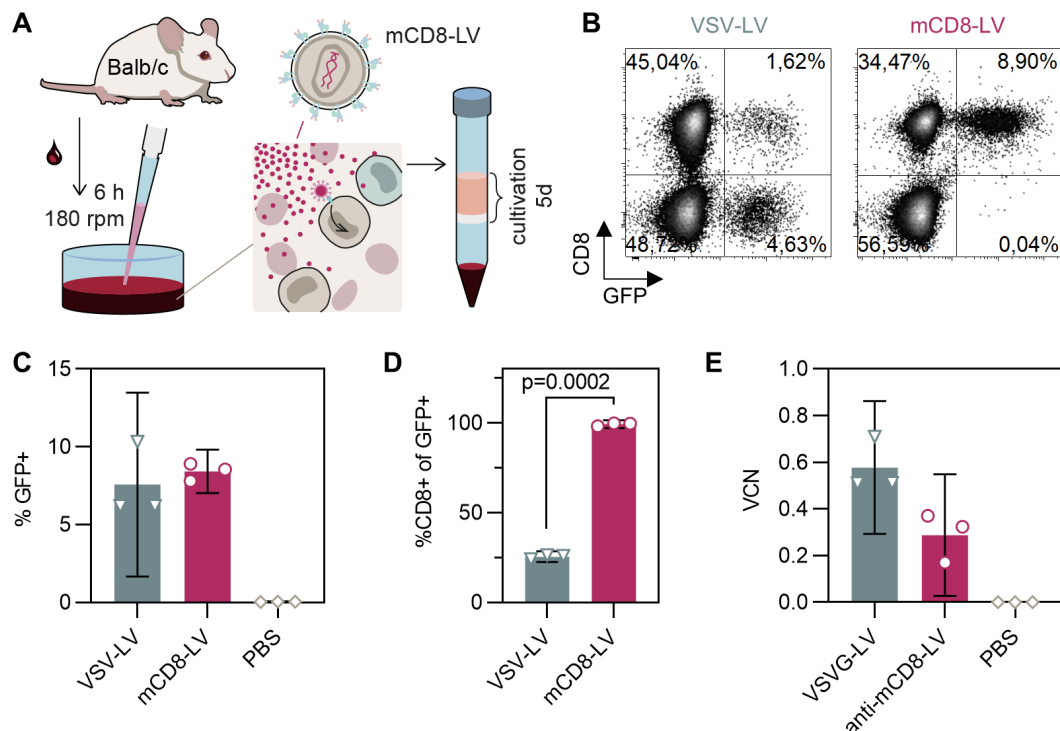
**FIGURE 2.3: mCD8-LVs specifically transduce CD8+ cells in murine whole blood**
A Blood from three BALB/c mice collected in lithium heparin tubes was transferred to 48-well plates and mixed with rhIL7 before VSV-LVs or mCD8-LVs were added at 2E10 particles/well. Blood was incubated under shaking at 37°C for 6 h. Subsequently, erythrocytes were removed by centrifugation over a Histopaque cushion. Purified cell preparations were then mixed with αmCD3/αmCD28-beads and rhIL7+15 and cultured for 5 days before analysis by flow cytometry and qPCR. **B** Representative flow cytometry plots showing GFP versus CD8 signals of viable singlet cells from one mouse. **C** Percentage of GFP+ viable singlet cells, determined by flow cytometry. **D** Percentage of CD8+ cells among GFP+ cells. P value is from paired t test. **E** Vector copies/cell. DNA was extracted from total cells, without prior sorting. Symbols represent data from n = 3 mice, bars represent means, error bars represent 95% CIs. Adapted from [Michels et al., 2021].

2.1.3 Selectivity is Achieved at Binding

To gain further insights – unbiased by prolonged cell culture – into the mechanics underlying the selective transduction observed for both mCD4- and mCD8-LV, a binding assay was performed (FIGURE 2.4 & 2.5). Whole blood from three BALB/c mice was collected in lithium heparin tubes. Then, 100 μL of blood/ 48-well were treated with 1E10 particles/ well of mCD4-LV-PGK-CAR, mCD8-LV-PGK-CAR or mCD8-LV-SFFV-GFP or an equivalent volume of PBS. Blood was incubated at 37°C under shaking for 2 h. Afterwards, nucleated cells were isolated via centrifugation over a histopaque cushion and analyzed via flow cytometry. The presence of LVs, i.e. receptor-targeted MV H proteins, on cells was detected via a His-tag on the C-terminus of H.

Notably, cell yields for each mouse were markedly different, with measurement of the material from the one mouse yielding several thousand viable singlet events per treatment while material from the other two mice only yielded hundreds of viable singlet events per treatment and measurement (FIGURE 2.4A). As the cellular yield varies more with mouse than with treatment (i.e. tube or well) this discrepancy is likely not due to handling errors. Despite the differences in cell yield, samples from all three mice displayed similar cellular composition, with CD3+ cells (T cells) making up approximately two-thirds of the obtained material. The vast majority of these were CD3+CD8-; CD3+CD8+ events only made up around 10% of the cells of untreated samples. Similar frequencies were observed for NKp46+ cells (NK cells) and CD11b+NKp46- myeloid cells. Unexpedctedly, B cells (i.e. CD19+ cells) only made up a sub-10% fraction of measured cells (FIGURE 2.4BD). Indeed, the fluorescent signal generated by the VioBlue-labeled antibody used for detection of mCD19 was only weakly shifted, whereas more clearly defined positive populations were obtained for all other markers (FIGURE 2.4C).

Despite these oddities, the experiment offered valuable insights into vector specificity and binding. In line with the high abundance of CD3+CD8- cells compared to CD3+CD8+ cells, His signal was more weakly shifted for cells from blood treated with mCD4-LV than for those treated with mCD8-LV (FIGURE 2.5A). Still, 6.2% of CD8- cells from blood treated with mCD4-LV were found to be His-positive; no CD8+ cells were His-positive. Likely due to the relatively low abundance of CD8+ cells, treatment of blood with mCD8-LV-PGK-CAR (TABLE 2.1) or mCD8-LV-SFFV-GFP resulted in His-positivities among CD8+ cells of 92.5% and 100%, respectively. Both mCD8-targeted vectors elicited His signal among CD8-negative cells; 2.2% of CD3+CD8- cells from mCD8-LV-SFFV-GFP-treated blood were His-positive (FIGURE 2.5B).
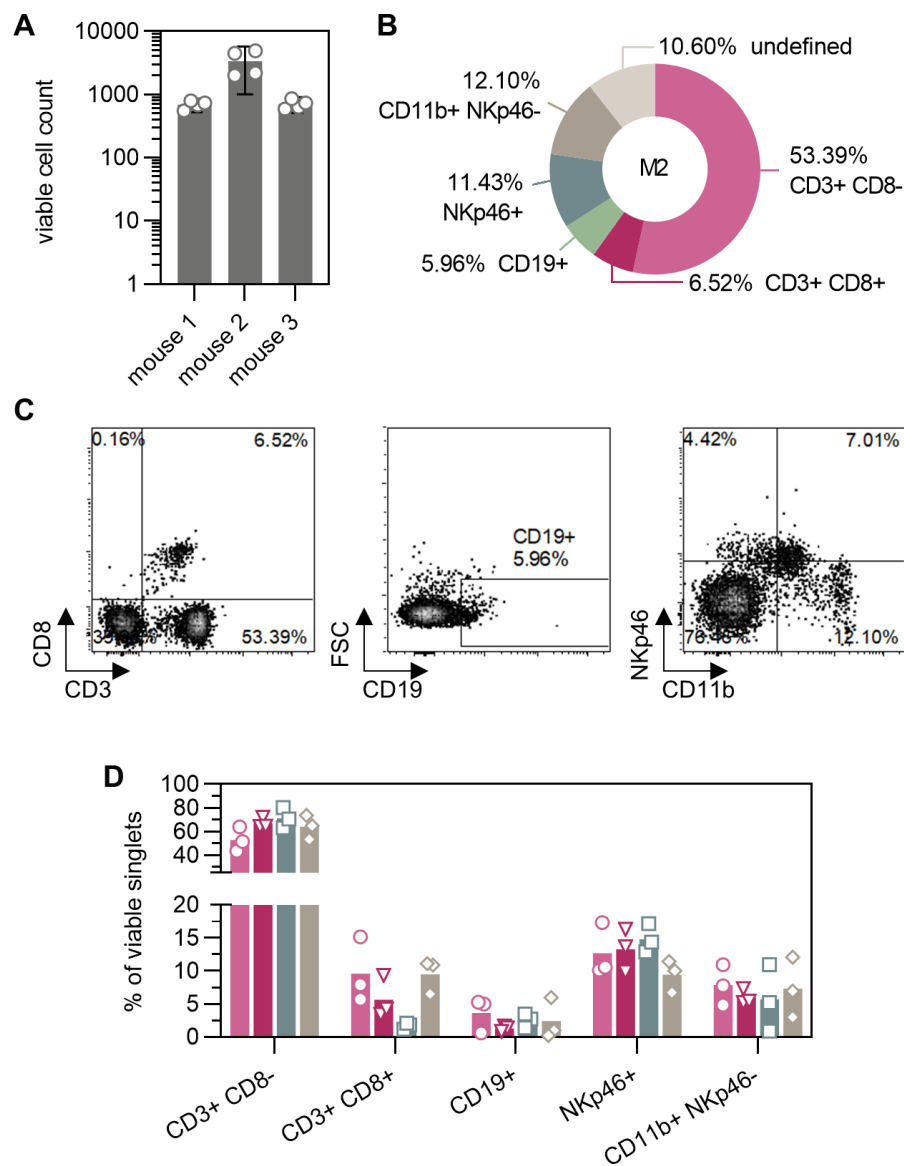
**FIGURE 2.4: MSE10 masks CD8α in whole blood**
A binding assay similar to the experiment described in FIGURE 2.3 was performed. Blood from three BALB/c mice was collected in lithium heparin tubes and transferred to 48-well plates before 1E10 particles/well of mCD4-LV-PGK-CAR, mCD8-LV-PGK-CAR or mCD8-LV-SFFV-GFP (or PBS) were added. Note that due to suboptimal sampling, the blood of mouse 1 was diluted 2:5 in warm DPBS. Blood was incubated at 37°C for 2 h at 400 rpm. Subsequently, erythrocytes were removed by centrifugation over a Histopaque cushion. Purified cell preparations were then analyzed by flow cytometry. Bound vector was detected via a C-terminal His-tag on MV H. **A** Viable cells measured per mouse. Symbols represent data from n = 4 treatments, bars represent means, error bars represent 95% CIs. **B** Cellular makeup of Histopaque-purified blood cells from mouse 2. Gating is shown in **C**. Gates were set using full minus one (FMO)-stained samples. **D** Apparent cellular makeup of samples after treatment with mCD4-LV-PGK-CAR (pink ●), mCD8-LV-PGK-CAR (red ▼), mCD8-LV-SFFV-GFP (blue ■) or PBS (grey ◆). Symbols represent data from n = 3 mice, bars represent means. Continued to FIGURE 2.5.

Much of this apparent off-target binding can be explained as masking of the entry receptor to flow cytometry detection antibodies by receptor-targeted vector particles. A decrease in CD8 MFI and the frequency of CD8+ cells was described above for mCD8-LV on primary murine T cells (FIGURE 2.2D). Here, incubation with mCD8-LV-PGK-CAR and especially mCD8-LV-SFFV-GFP also brought about a marked decrease in CD8 MFI. Suggesting a particle binding-dependent mechanism, this decrease was most pronounced for mCD8-LV-SFFV-GFP-treated cells, which also displayed the highest His MFI (FIGURE 2.5A). In fact, treatment with mCD8-LV decreased the mean apparent frequency of CD3+CD8+ cells from 9.4% in untreated samples to 5.7% in mCD8-LV-PGK-CAR-treated and 1.7% in mCD8-LV-SFFV-CAR-treated samples (FIGURE 2.4D). Accordingly, approximately 34% of His-positive events in samples treated with mCD8-LV-SFFV-GFP seemed to reside in the CD3+CD8- compartment. (FIGURE 2.5C). As its entry receptor was not directly detected in this assay, it could not be discerned whether mCD4-LV-PGK-CAR masks mCD4.

Strangely, it appears as though mCD8-LV-SFFV-GFP has substantial affinity for CD11b+ cells. It should be noted however that CD11b signal was measured via FITC in the B1 channel. His-positive (i.e. vector-binding) events likely appeared CD11b-positive because of GFP protein bound to the vector particles, a phenomenon known as protein transfer. Indeed, treatment of blood with mCD8-LV-SFFV-GFP shifted the entire population of His+ events towards higher B1 channel fluorescense (data not shown). Taken together, the binding patterns observed here suggest that the cell type selectivities which GK1.5 and MSE10 confer to mCD4- and mCD8-LV, respectively, are achieved at the stage of cell binding.

Further stressing the critical role of (high affinity) binders in the determination of cellular tropism, the incorporation of a transgene encoding a chimeric antigen receptor against murine CD19 seems to induce limited but genuine off-target binding of LV-CAR particles to CD19+ cells, i.e. off-target signal which cannot be explained by MSE10-mediated masking and protein transfer effects. The CAR-transferring LVs used here (characterized in anticipation of *in vivo* trials of the vector platform) harbored a transgene encoding a CAR based on the mouse CD19-specific 1D3 scFv (FIGURE 2.6B). When mCD4-LV-PGK-CAR or mCD8-LV-PGK-CAR were added to whole blood, an average of 1.8% and 4.1%, respectively, of vector-bound, i.e. His+ cells, were CD19+. No His+CD19+ cells were obtained from blood treated with mCD8-LV-SFFV-GFP or untreated blood (FIGURE 2.5C). Such binding, which is thought to be mediated by CAR protein carried over from the production cell membrane to the lentiviral envelope, has been described before [Cordes et al., 2021] and was also observed here when the effect of CAR transfer into mixed murine cell cultures was examined.
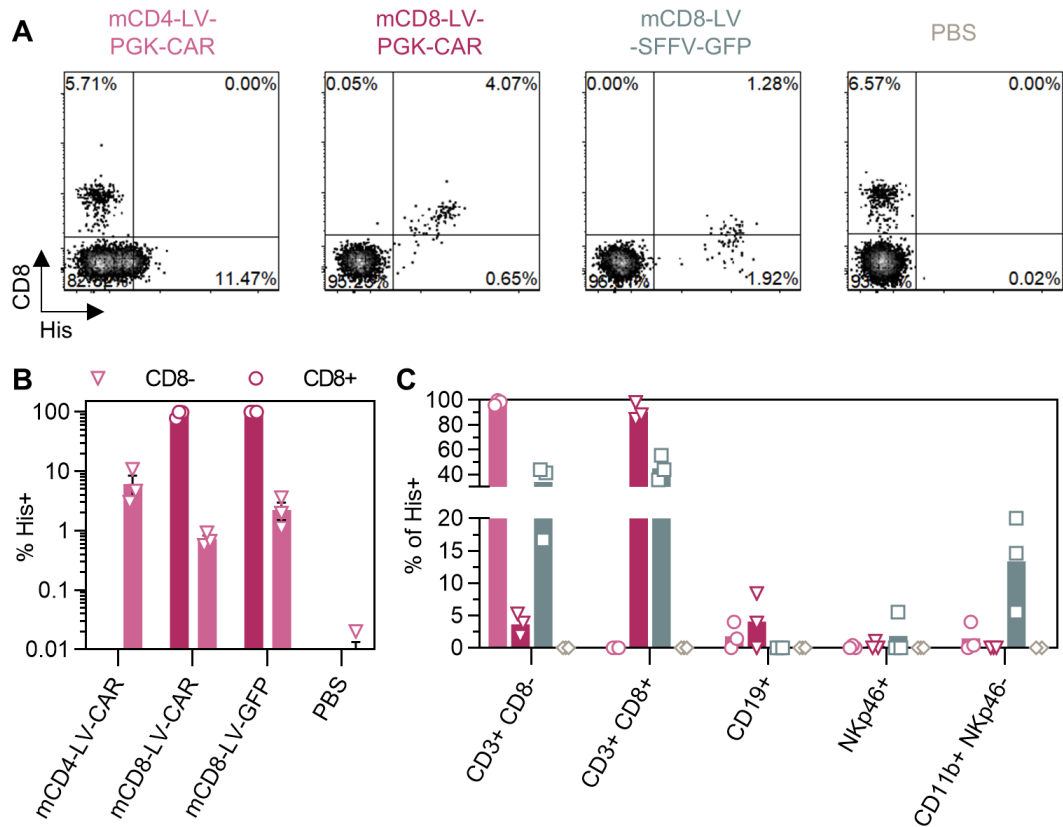
FIGURE 2.5: Targeting confers specificty at the stage of cell binding
Continued from FIGURE 2.4. **A** Flow cytometry plots showing His versus CD8 signals of viable singlet cells from mouse 2. **B** His-positivity of viable CD8- (pink ▽) and CD8+ (red ●) cells. Symbols represent data from n = 3 mice, bars represent means, error bars represent standard errors of means (SEMs). **C** His-positivity by cell type after treatment with mCD4-LV-PGK-CAR (pink ●), mCD8-LV-PGK-CAR (red ▽), mCD8-LV-SFFV-GFP (blue ■) or PBS (grey ◆). Symbols represent data from n = 3 mice, bars represent means.

2.1.4 Target Cell Ablation & Receptor Masking by *In Situ* CAR Transfer

These experiments, devised to simulate the eventual *in vivo* application of mouse-compatible CAR-transferring LVs, made use of mCD8-LV for transfer of a CAR gene (**Figure 2.6**). The αmCD19-CAR used throughout this thesis was derived by insertion of a myc tag from a published framework which covers the 1D3 scFv specific for murine CD19 as well as murine CD3ζ stimulatory and CD28 costimulatory domains [Kochenderfer et al., 2010] (**Figure 2.6b**). Whole splenocytes (containing endogenous CD19+ cells) from BALB/c mice were cultivated without full activation, i.e. only in the presence of IL7, either alone or as 10:1 coculture with CD19+ A20 cells, a murine lymphoma cell line derived from BALB/c. Cultures were treated with mCD8-LV-CAR or the corresponding GFP-transferring mCD8-LV-GFP as control and analyzed by flow cytometry and qPCR 2 days later (**Figure 2.6a**).

Confirming the particles' specificity and the equivalence of the applied mCD8-LV-GFP and mCD8-LV-CAR doses, both vector treatments induced similar dose-dependent decreases in CD8 MFI, likely as a consequence of masking of the epitope of the CD8 detection antibody by the bound vector particles (**Figure 2.6g**). Additionally, no relevant differences in VCNs were observed between vector treatments of splenocyte-only cultures at doses of approximately 2E9 particles/well (**Figure 2.6c**).

Still, a dose-dependent decrease of CD19 signal was observed for splenocyte-only cultures treated with mCD8-LV-CAR, but not for those treated with mCD8-LV-GFP, with the highest dose of 2E9 particles/well more than halving CD19 MFI compared to untreated control cultures, almost completely eliminating CD19 signal (**Figure 2.6de**). As the αmCD19-CAR uses a scFv derived from the same antibody clone used for detection of mCD19, 1D3, this decrease is likely due to epitope masking. In light of this, the CAR-specific ablation of cells observed at high vector doses both for splenocyte-only and A20-containing cultures (**Figure 2.6fhi**) may not be due to the activity of CAR T cells, but rather an effect of CAR-mediated binding of LVs to CD19-expressing cells (**Chapter 4.2.2**, p. 69). Transgene-derived binding interference, such as that suspected to underlie the phenomena described above, would likely not be an issue for non-enveloped vectors, which do not have a lipid membrane that could hold proteins which may skew the vector's carefully engineered tropism.
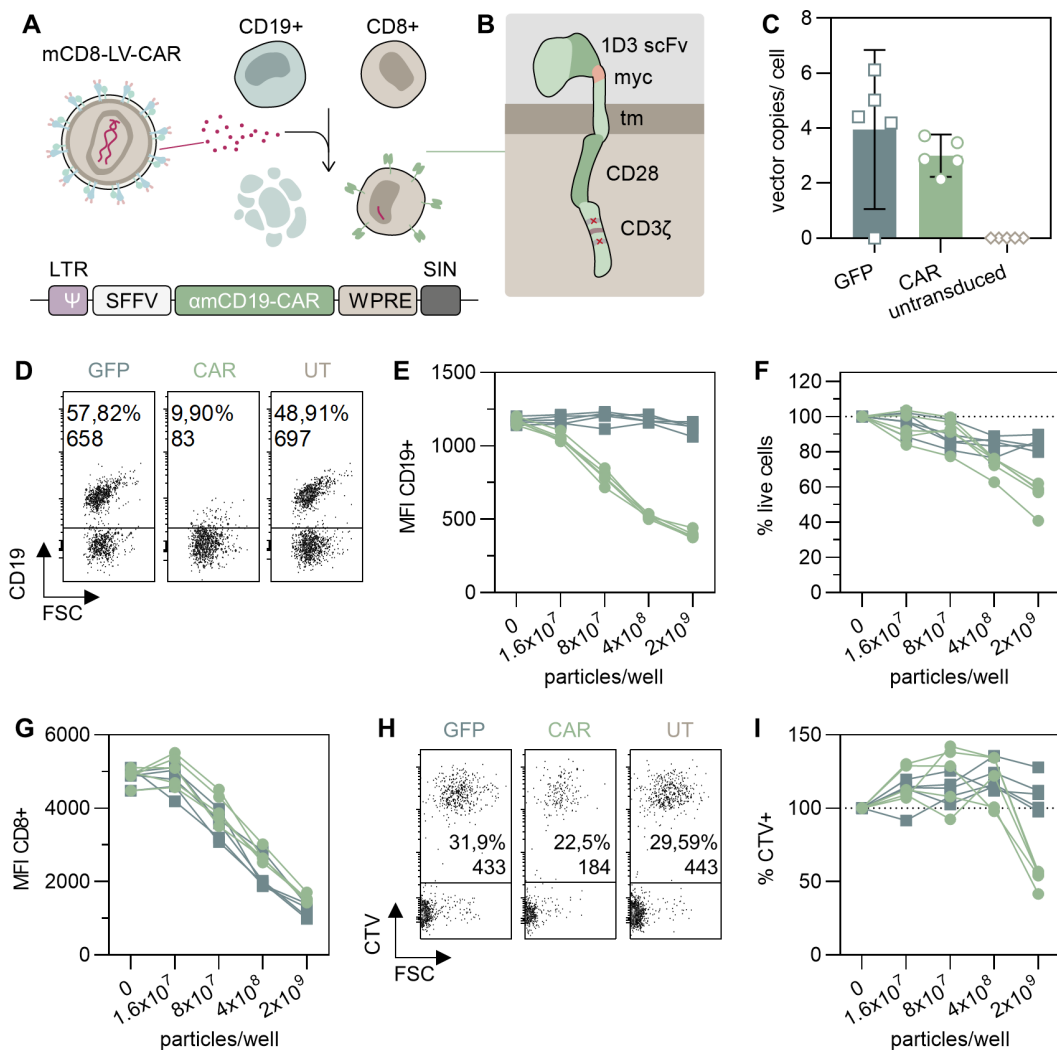
FIGURE 2.6: CAR gene delivery with mCD8-LV
A 4E4 BALB/c splenocytes were cultivated alone or in co-culture with 4E3 A20 tumor cells stained with Cell Trace Violet (CTV). Cultures were treated with defined particle amounts of mCD8-LV encoding GFP or a chimeric antigen receptor directed against mCD19. After spinfection, cells were cultivated for 2 days in the presence of rhIL7 before analysis by flow cytometry and qPCR. **B** CAR structure. The CAR used in this experiment was derived from a previously published receptor by addition of a myc tag (orange) between scFv and transmembrane domain (tm) to facilitate detection of the CAR. It employs a scFv of the 1D3 monoclonal antibody against mouse CD19. It is a second-generation CAR with a CD3ζ stimulatory and CD28 costimulatory domain. The first and third immunoreceptor tyrosine-based activation motifs (ITAMs) were ablated by mutation to decrease T cell apoptosis and increase survival in vivo [Kochenderfer et al., 2010]. **C** Similar VCNs in splenocyte-only cultures were obtained for both vector stocks at doses of 2E9 particles/well. Symbols represent data of lymphocytes from n = 5 mice. Bars represent means. Error bars represent 95% CIs. DNA was extracted from total cells, without prior sorting. **D-G** Killing of CD19+ B lymphocytes in splenocyte-only cultures. **D** Representative flow cytometry plots from one mouse showing CD19 signals of viable singlet cells after no treatment (UT: untreated/untransduced) or transduction with 2E9 particles/well. Percent CD19 positivity and CD19+ cell counts are reported. **E** Geometric MFI of CD19+ cells. **F** Percentage of viable cells relative to untransduced control. **G** Geometric MFI of CD8+ cells. Symbols in **E-G** represent data of lymphocytes from n = 5 mice treated with mCD8-LV-GFP (blue squares) or mCD8-LV-CAR (green circles). **H & I** Killing of A20 target cells in cocultures. Flow cytometry data, obtained from viable singlet cell populations are reported. **H** Representative flow cytometry plots from one mouse after no treatment or transduction with 2E9 particles/well. CTV+ cells are A20 tumor cells. **I** Percentage of CTV+ (A20) cells relative to untransduced control. Symbols represent data from n = 5 mice treated with mCD8-LV-GFP (blue squares) or mCD8-LV-CAR (green circles). Modified from [Michels et al., 2021].

2.2 Adeno-Associated Vectors

Capitalizing on the auspicious intersection of complementary lines of inquiry pursued in the host laboratory, non-enveloped mouse receptor-compatible vectors were generated by displaying the LV-proven MSE10 DARPin in the context of a DARPin-targeted adeno-associated vector platform newly established in the host laboratory (p. 21), yielding mCD8-AAV. An overview of all AAVs used in this thesis is provided in TABLE 2.2.

2.2.1 MSE10 Renders AAV2 Lymphocompatible

To make mCD8-AAV, MSE10 was displayed on the surface of AAV2 vector particles (FIGURE 2.7A). The coding sequence of MSE10 was inserted into the GH2/GH3 loop of VP1 and the production of VP2 and VP3 was prevented by deletion of the splice acceptor site downstream of the VP1 translation initiation site resulting in pRC-mCD8. In pRC-VP1KO, the VP1 start codon was deleted, thus encoding VP2 and VP3 only (FIGURE 2.7B). In both plasmids, the natural affinity for HSPG was ablated by point mutations, as demonstrated before [Münch et al., 2013].

The corresponding mCD8-AAV particles were produced by packaging the GFP reporter followed by purification via an iodixanol gradient. Vector genome (vg) counts in mCD8-AAV stocks and stocks with an unmodified AAV2 capsid were similar (FIGURE 2.7C), suggesting that DARPin insertion does not relevantly interfere with particle assembly. This may be partly due to the low incorporation rates of VP1 in both mCD8-AAV and AAV2, which became apparent in Western blot analysis: While the band pattern observed for mCD8-AAV exhibited the expected large shift in electrophoretic mobility for MSE10-VP1 as well as slight shifts due to the point mutations in VP2 and VP3, the intensity of the VP1* signal was similarly low as that observed for VP1 of AAV2. (FIGURE 2.7D).

Despite their similar vector genome titers, performance of the vectors on primary cells was markedly different. The normalized transducing titer of mCD8-AAV (1.6 TU/ 1E6 vg) was 5.7-fold higher than that of AAV2 (0.28 TU/ 1E6 vg), with mCD8-AAV2 inducing GFP-positivity in 38.1% of cells at the highest dose while exhibiting strong preference for CD8+ cells (FIGURE 2.7EF). These results, together with the observations made for lentiviral vectors (see CHAPTER 2.1.1), which are molecularly quite dissimilar to AAVs (see CHAPTER 1.2), implicate receptor-incompatibility as a principal barrier in mouse lymphocyte transduction.
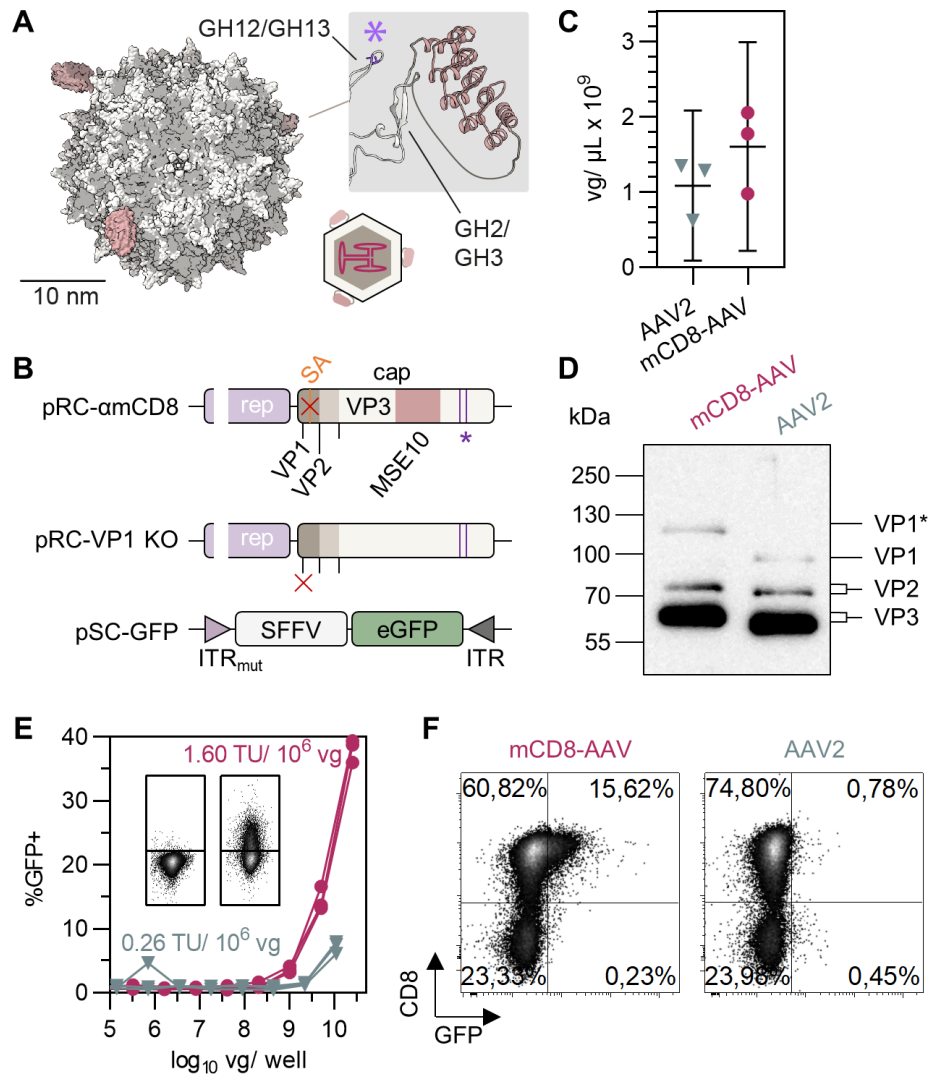
FIGURE 2.7: Generation and characterization of mCD8-AAV

A Structure of mCD8-AAV. To-scale approximation of electron density surfaces of AAV2 capsid (gray) decorated with DARPins (red). Cartoon shows cross-section of particle with self-complementary genome. Inlay shows ribbon representation of DARPin inserted in the GH2/GH3 loop of AAV2 VP1 from FIGURE 1.2C. Purple asterisk and residues indicate locations of point mutations, which ablate HSPG binding (R585A, R588A). Panel was created using structures PDB: 1LP3, 4J8Y. **B** Generation of mCD8-AAV. Vectors were produced by transfection of HEK293T cells with the indicated plasmids. The genetic structure of cap (shades of gray) is visualized. Start codons for VP1, VP2, and VP3 are indicated by black ticks. Point mutations ablating natural affinity for HSPG (R585A, R588A; $HSPG_{mut}$) are indicated by purple lines and asterisk, the splice acceptor site downstream of VP1 (SA) in orange, deletions of SA or start codon with red crosses. The inverted terminal repeats are indicated. **C** Vg titers. Symbols represent technical replicates from three PCRs. Error bars represent 95% CIs. **D** Detection of MSE10-VP1 (labeled with VP1*) by western blotting. 6.5E9 genome copies of vector stock were lysed in urea buffer and run on SDS-PAGE. After blotting, AAV2 capsid was visualized using the B1 monoclonal antibody. Blot was exposed for 7 s. Contrast was adapted, retaining relative pixel intensities. **E-F** Pan T cells (4E4 cells/well) from BALB/c mice fully activated with αmCD3/αmCD28-beads and rhIL7+15 were transduced by spinfection with AAV2 (blue ▼) or mCD8-AAV (red ●) at the indicated doses of vg/well. Cultures were analyzed 5 days post transduction by flow cytometry. **E** Graph summarizes the percentage of GFP+ viable singlet cells. Symbols represent data from n = 3 mice. Transducing titers of the vector stocks, normalized to vgs, are given in corresponding colors. Representative flow cytometry plots in inlay from one mouse show GFP signals versus forward scatter (FSC) in wells treated with 6.5E4 vg/well (left) and 2.5E10 vg/well (right) mCD8-AAV. **F** Representative flow cytometry plots show percentages of GFP+ versus CD8+ cells from one mouse. Adapted from [Michels et al., 2021]. Since publication, a flaw in the calculation procedure for the lab's AAV vg titer determination workflow has been corrected; this figure was changed to reflect the correction.

2.2.2 Transduction by mCD8-AAV is Selective and Transient

In line with observations made for LVs, MSE10 not only rendered mCD8-AAV lymphocompatible, but also highly selective for CD8+ cells: On whole splenocytes, more than 99% of GFP-positive viable singlet cells were CD8+ throughout a 156 hour experiment (**Figure 2.8a**). This specificity was observed regardless of whether the transferred gene was driven by an SFFV or EF1α core-promoter. While use of the latter, short promoter, derived from the human *EEF1A1* gene, resulted in roughly half the protein-level transduction efficiencies achieved using the SFFV promoter, its smaller size may enable AAVs with self-complementary genome architecture to accommodate larger, therapeutically relevant transgenes, such as CARs or immunomodulatory antibodies.

In keeping with the mostly episomal nature of AAV transgenes, the rate of GFP+ cells among rapidly proliferating murine lymphocytes peaked between 2 and 4 days after addition of either vector and decreased to approximately a fourth of peak level within a week. (**Figure 2.8b-d**). This transiency of AAV-mediated gene delivery into fast-replicating tissue holds exciting possibilities for temporally limited gene therapeutic approaches. Simultaneously, it represents a confounding factor which needs to be accounted for when assessing AAVs' properties *in vivo*.
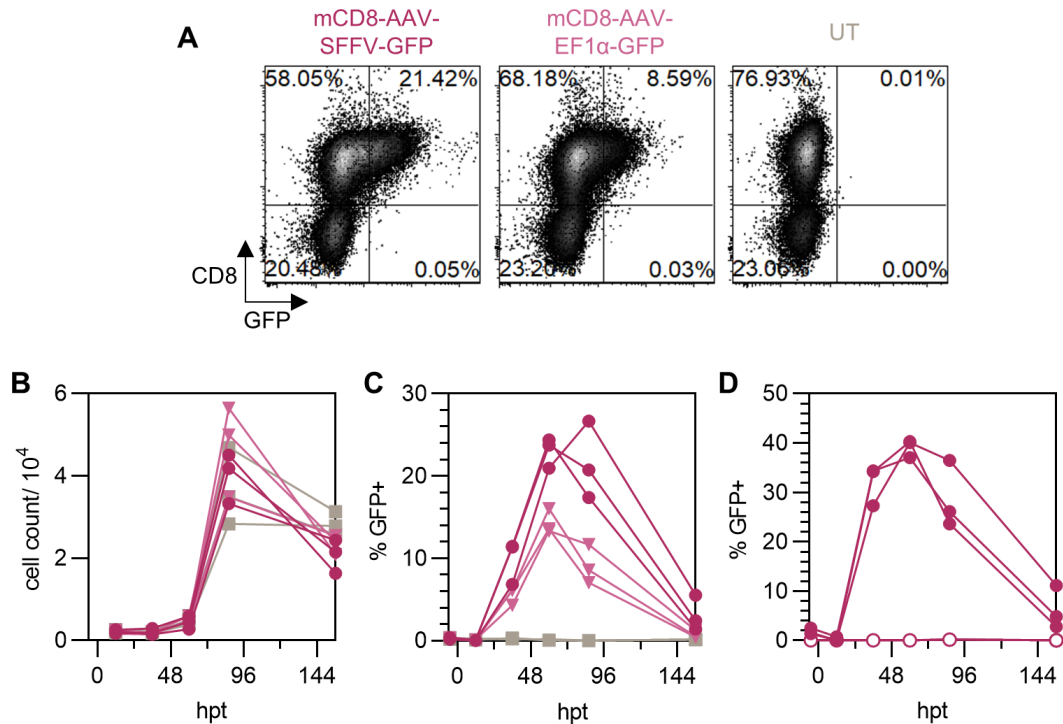
FIGURE 2.8: Selective and transient transduction of murine splenocytes by mCD8-AAV
Whole splenocytes from BALB/c mice were activated and transduced with 1E10 vg/well (2.5E5 vg/cell) of mCD8-AAV-SFFV-GFP (red ●) or mCD8-AAV-EF1αcore-GFP (pink ▼) or left untransduced (grey ■). **A** Flow cytometry plots of viable singlet cells from one mouse at 86 h post transduction. **B-D** Transduction kinetics on primary cells. Symbols represent single technical replicates from from n = 3 mice. Viable cell counts **B** and frequency of GFP-positive cells among viable singlets **C** are plotted over a timeframe of 161 hours around vector treatment (hpt: hours post transduction). **D** As a measure of specificity of transduction, the frequency of GFP+ cells among CD8+ cells (solid red circles) or CD8- cells (empty red circles) after treatment with mCD8-AAV-SFFV-GFP was plotted. Based on data previously published in [Michels et al., 2021].

Table 2.2: Adeno-associated vectors used in this thesis.

| Vector | Receptor | Serotype | Binder | Transgene | | | See Figure |
				Type	Promoter	ORF	
mCD8-AAV-SFFV-GFP	mCD8	AAV2	MSE10[a]	sc[b]	SFFV	GFP	2.7, 2.8, 3.11, 3.12
mCD8-AAV-EF1α core -GFP	mCD8	AAV2	MSE10	sc	EF1α core	GFP	2.8
mCD8-AAV-SFFV-cre	mCD8	AAV2	MSE10	sc	SFFV	cre	3.11, 3.12, 3.14, 3.15, 3.16
AAV2-SFFV-GFP	N/A	AAV2	N/A	sc	SFFV	GFP	2.7
AAV2-SFFV-cre	N/A	AAV2	N/A	sc	SFFV	cre	3.11, 3.12, 3.14, 3.15, 3.16

[a] DARPin;
[b] sc: Self-complementary;

RESULTS II

In Vivo Veritas

3

> *The truth is rarely pure and never simple.*
>
> — Algernon to Jack
> *The Importance of Being Earnest*
> **Oscar Wilde**

Due to the fully integrated nature of syngeneic mouse models (CHAPTER 1.5), the generation of mouse-compatible vectors is both necessary and sufficient, i.e. the first and only step required, to enable the setup of basic syngeneic models of *in vivo* gene therapy. Accordingly, after their principal efficacy and selectivity had been confirmed on primary cells, the mouse receptor-targeted vectors described in the previous CHAPTER 2 were used in three subsequent mouse experiments, with each setup informed by the results obtained from the previous experiments. The first experiment was performed in preparation for a longer-term investigation involving CAR transfer, and was designed to gauge the general feasibility of LV-mediated gene transfer into immunocompetent BALB/c mice.

3.1 Short-Term Biodistribution of GFP-Transferring LVs in BALB/c Mice

3.1.1 Two Stocks Pass QC

To enable such an evaluation of the *in vivo* performance of mouse-compatible LVs, mCD4-LV, mCD8-LV and VSV-LV stocks for *in vivo* use were produced in three separate runs. As concerns about the medium-term inactivation of virus-derived promoters by methylation had been raised [Herbst et al., 2012], PGK-GFP transgene (TABLE

2.1, p. 24) was chosen over SFFV-GFP, despite the marginally lower transducing titer achieved with the former *in vitro* (FIGURE 2.2E, p. 27). On the day of vector harvest, syncytia were observed in cells transfected to produce mCD4-LV-PGK-GFP, but not in those producing mCD8-LV-PGK-GFP or VSV-LV-PGK-GFP (FIGURE 3.1A). The formation of macro- and/or microscopically visible syncytia in production cells had been observed before in the host laboratory, both in cells producing mCD4-LV and in cells producing LV targeted to human CD4 and did not seem to be an indicator of vector stock quality (personal communication).

More concerningly, VSV-LV-PGK-GFP displayed an approximately 500-fold lower gene transfer activity on BALB/c splenocytes than a VSV-LV-SFFV-GFP control stock (FIGURE 3.2BCD). Moreover, the particle size mode of the stock was 140.2 nm, well outside of the established size range of VSV-LVs (FIGURE 3.1BE), and its particle concentration was unusually low (approximately 3E11 particles/ mL, FIGURE 3.1C), indicating a serious flaw in its production run.

In contrast to this, the quality parameters of mCD4-LV-PGK-GFP and mCD8-LV-PGK-GFP were nominal: Both stocks yielded titers around 1E7 TU/mL on BALB/c splenocytes, with mCD4-LV-PGK-GFP reaching an earlier and lower plateau of GFP-positivity reflective of the lower frequency of CD4+ cells compared to CD8+ cells in the culture at the time of measurement (FIGURE 3.2A). Additionally, GFP signal in cultures transduced with mCD4-LV or mCD8-LV originated almost exclusively from the CD4+ or CD8+ compartment, respectively. Again, treatment with mCD8-LV lowered the MFI of the CD8 signal. No such decrease was observed for treatment with mCD4-LV (FIGURE 3.2CD). Both mCD4-LV and mCD8-LV stocks displayed particle size modes and concentrations well-within the established range (FIGURE 3.1BCD). In light of these results, only the mCD4- and mCD8-LV-PGK-GFP stocks were used *in vivo*.

3.1.2 Minimal Reporter Signal *In Vivo*

To facilitate transgene expression *in vivo*, BALB/c mice received two intravenous 200 ng doses/ animal of recombinant human IL7 (which cross-reacts with mouse receptors). These injections were motivated by previous reports on the critical role of common γ-chain cytokine IL7 in enabling *in vitro* GFP transfer to mouse splenocytes [Gilham et al., 2010] as well as in inactivating SAMHD1, which restricts reverse transcription by decreasing cellular dNTP-levels [Behrendt et al., 2013; Coiras et al., 2016; Wittmann et al., 2015].

The first dose was administered one day before vector injection, the second dose was mixed into the injected vector material or PBS. To maximize gene transfer, mice were injected with the maximum permissible volume of 200 μL/ animal of
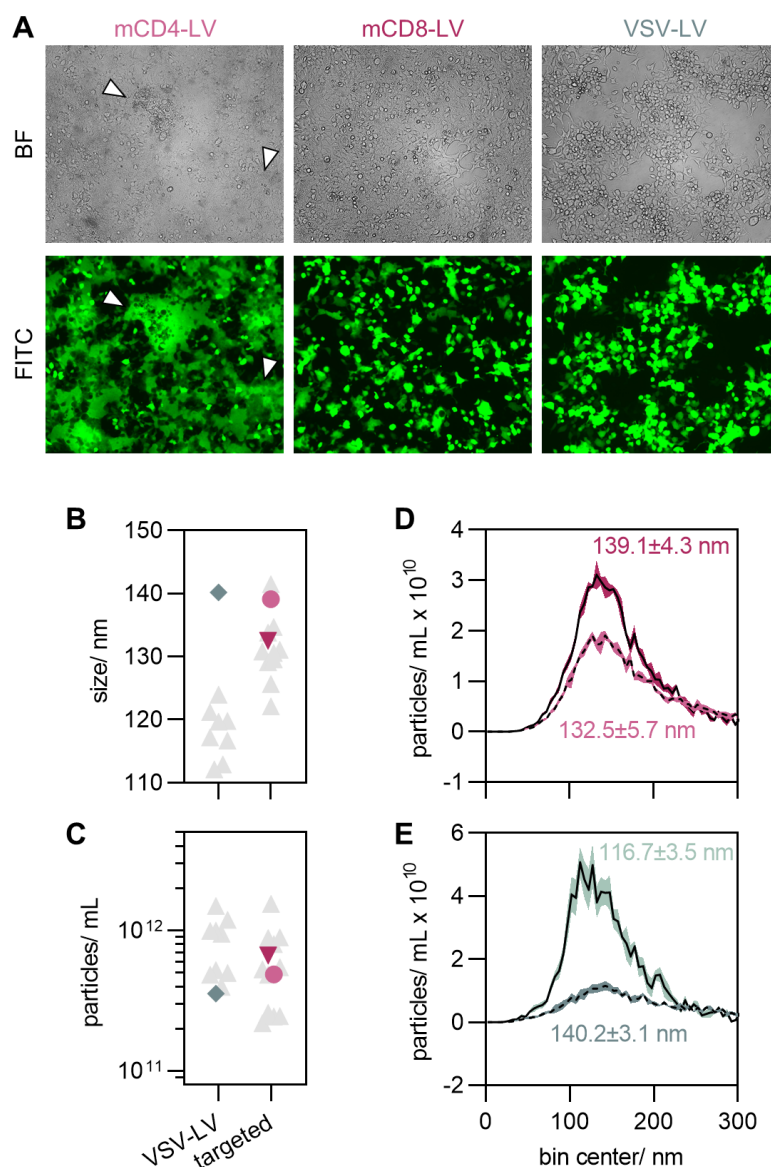
**FIGURE 3.1: Physical characterization of LVs for *in vivo* use**
A Prior to harvest of vector-containing supernatant, LentiX 293T cells producing mCD4-LV-PGK-GFP, mCD8-LV-PGK-GFP and VSV-LV-PGK-GFP were documented by brightfield (BF) and epifluorescense (FITC) microscopy. Examples of syncytia observed in cells producing mCD4-LV are indicated by white arrowheads. Brightness and contrast of brightfield micrographs were adapted to improve readability. **B-E** Characterization of stocks by nanoparticle tracking analysis. Particle size distribution and concentration were determined using a NanoSight NS300 analyzer. **B** Particle sizes and **C** particle concentrations of mCD4-LV-PGK-GFP (pink ●), mCD8-LV-PGK-GFP (red ▼) VSV-LV-PGK-GFP (blue ◆) stocks. Each symbol represents one vector stock. Grey reference symbols in **BC** represent the measurements first reported in FIGURE 2.1BC. **DE** Histograms for each vector stock. Size modes ± standard error of VSV-LV-SFFV-GFP (solid line, green bands), VSV-LV-PGK-GFP (dotted line, blue bands), mCD8-LV-PGK-GFP (solid line, red bands) and mCD4-LV-PGK-GFP (dotted line, pink bands) are indicated. Bands represent standard error of n = 4 sequential technical replicates. Continued to FIGURE 3.2.

43
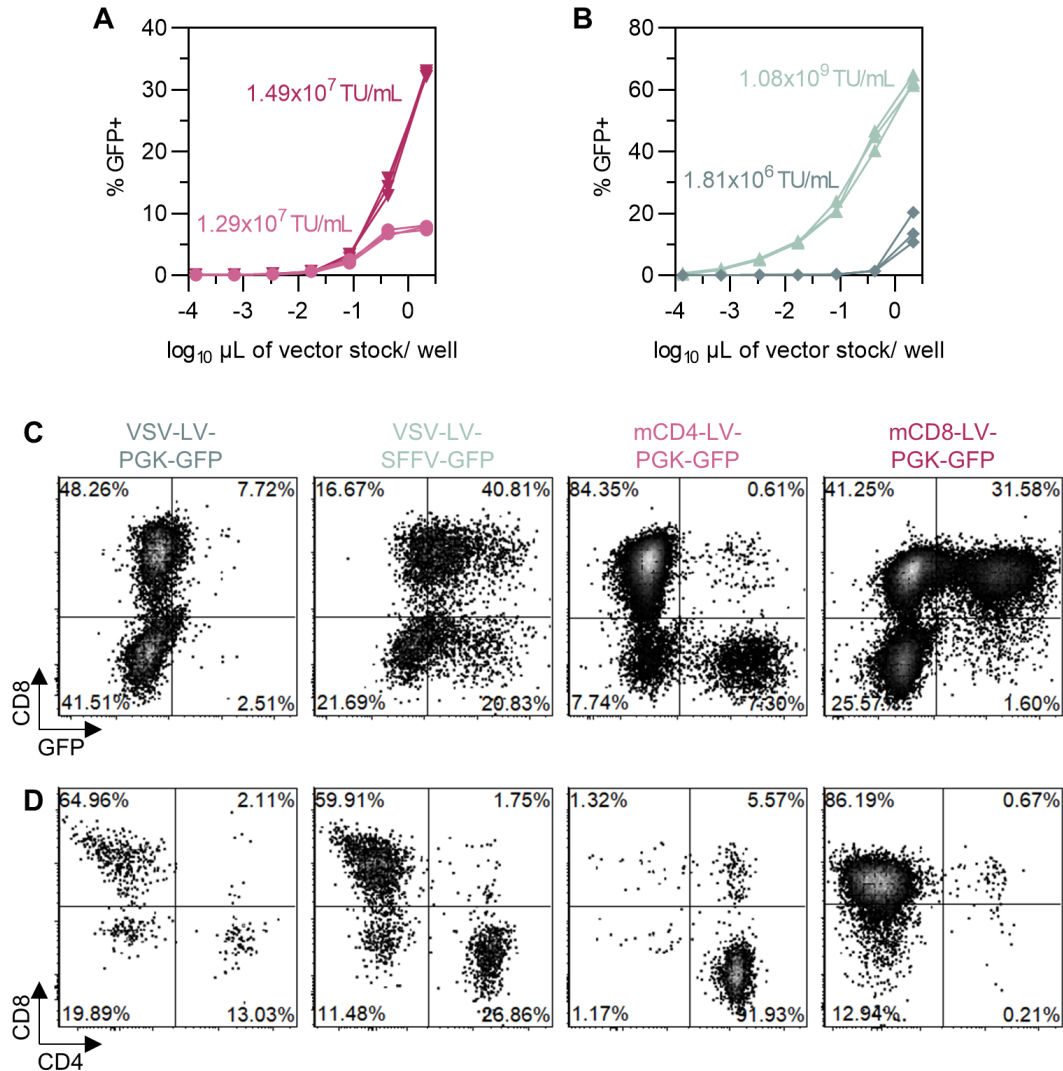
FIGURE 3.2: Functional characterization of LVs for *in vivo* use
Continued from FIGURE 3.1. Characterization of vector stocks on freshly isolated BALB/c spleno-cytes. 4E4 cells/well stimulated with αmCD3/αmCD28-beads and recombinant human IL7 and IL15 (rhIL7+15) were transduced with serial dilutions of mCD4-LV-PGK-GFP (pink ●), mCD8-LV-PGK-GFP (red ▼) VSV-LV-PGK-GFP (blue ◆) or a VSV-LV-SFFV-GFP reference stock (green ▲; used in FIGURE 2.2ABC). Cells were analyzed by flow cytometry 4 days post spinfection. **AB** GFP-positivity of viable singlet cells. Symbols represent technical triplicates. Transducing titers of the stocks are shown next to the curves in corresponding colors. **CD** Cell material from wells treated with the highest vector dose (3 µL/ well) was stained for murine CD4 and CD8 to assess the specificity of gene transfer. Repre-sentative flow cytometry plots show **C** GFP versus CD8 signal of viable singlet cells and **D** distribution of GFP+ viable singlet events on the CD4 CD8 plane.
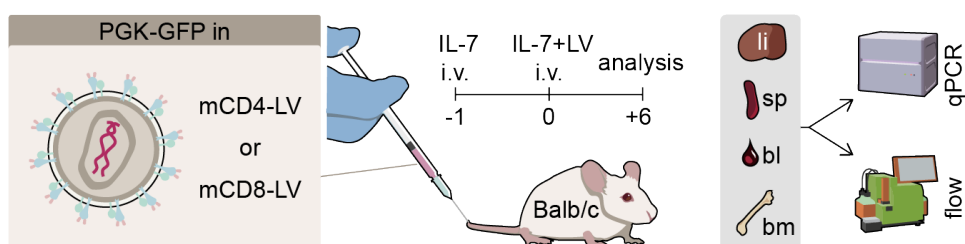
FIGURE 3.3: **Assessing the biodistribution of receptor-targeted LVs**
Prior to vector administration, male BALB/c mice received intravenous injections of 200 ng of human IL7/ animal. One day later, they were treated via tail vein injection with 200 µL of PBS-based injection mix/ animal, each mix containing 200 ng/ animal of human IL7 and either 1.0E10 particles/ animal of mCD4-LV-PGK-GFP, 1.3E10 particles/ animal of mCD8-LV-PGK-GFP or no vector. Six days after vector injection, animals were euthanized and nucleated cells were extracted from spleens (sp), blood (bl) and bone marrow (bm) of all mice. Additionally, cells were extracted from the livers (li) of three animals per group. Cell material was analyzed by flow cytometry and qPCR. Notably, flow cytometry was not only used to analyze fixed samples stained with immune panels, but also to count samples' cell content after sample preparation using a simple propidium iodide-based stain and measuring unfixed cells. Continued to FIGURES 3.4 & 3.5.

vector stock (undiluted, except for approximately 10% v/v of IL7) and accordingly received 1.0E10 particles/ animal of mCD4-LV-PGK-GFP or 1.3E10 particles/ animal of mCD8-LV-PGK-GFP. Six days after vector injection, the animals were euthanized and spleens, bone marrow and blood from all animals as well as livers from three animals/ group were analyzed by flow cytometry and qPCR (FIGURE 3.3).

In flow cytometry, GFP signal in samples from vector-treated mice was at the lower detection limit. In fact, no GFP signal was observed in fixed samples fully stained with a panel meant to help ascertain the specificity of transgene expression (data not shown). GFP-positivity was only observed inadvertently: During final analysis, after cells were isolated from the extracted tissues, a MACSQuant flow cytometer - which has automated staining capabilities - was used to add propidium iodide viability stain to unfixed tissue samples and determine viable cell count, which would inform further sample deposition and freezing of leftovers. During the measurements, the machine recorded not only the relevant scatter and B3 channels, but all channels, including B1, in which GFP is measured.

In spleen, GFP-positive cells were observed in five of seven animals in each vector-treated group; a maximum frequency of GFP+ cells of 0.026% was observed in an animal treated with mCD4-LV. Similar maximum transduction efficiencies were observed in blood, again for an mCD4-LV-treated animal, but GFP-positive cells were only observed for two vector-treated animals per group. In bone marrow, GFP-positive events were only found for one animal; none were observed in liver samples. Among all measured samples, none contained more than nine GFP-positive viable cells. (FIGURE 3.4AB). Considering the scarcity of positive events and their low MFI, their absence in fixed and stained samples might be explained by the additional background incurred by fluorescent staining and the loss of weak signal through

fixation-related quenching.

Protein-level signals, although few and faint, were in good agreement with genome-level VCN data; both were stronger in blood and spleen than in bone marrow and liver. In line with observations *in vitro* (FIGURE 2.2C), qPCR suggested approximately tenfold higher gene transfer rates than flow cytometry, consistent with the assumption that only a fraction of genomic integrations result in detectable expression of the transgene. In spleen, mean VCNs were 2.2E-3 and 1.7E-3 for mCD4-LV and mCD8-LV, respectively. Similar rates were found in blood (mCD4-LV: 1.7E-3; mCD8-LV: 1.6E-3). Likely due to the more pronounced signal, more samples appeared positive in qPCR than in flow cytometry. All seven samples from each vector-treated group appeared positive for vector integration in spleen, as well as 6/7 of each group in blood, all six liver samples from vector-treated mice and a total of six samples from the bone marrow of vector treated mice. Notably, no sample from a PBS-treated mouse appeared positive in VCN qPCR (FIGURE 3.4C).

Taken together, flow cytometry and qPCR data suggest that both mCD4-LV and mCD8-LV mediated *in vivo* gene transfer. Although the way in which GFP-positivity data was ultimately collected precluded a direct analysis of the selectivity of transfer, close examination of sample makeups in flow cytometry yielded cellular compositions not inconsistent with cell-type specific vector binding.

3.1.3 LV Treatment Alters Lymphocyte Makeup

Strikingly, the strength of protein- and genome-level transfer signals observed for both vectors seems to correlate with the relative abundance of T cells in the respective tissue in PBS-treated mice: Spleen and blood samples, which were found to contain the highest (42.0%) and second-highest (21.2%) mean proportions of T (i.e. CD3+) cells, respectively, among the four analyzed tissues, also displayed the highest (mCD4-LV: 0.010%; mCD8-LV: 0.006%) and second-highest (mCD4-LV: 0.005%; mCD8-LV: 0.005%) mean GFP-positivities and VCNs (see above). Similarly, liver samples, which had a higher CD3-content (9.7%) than bone marrow samples (1.3%), yielded higher average VCNs for mCD4-LV (8E-4 v. 3E-4) and mCD8-LV (3E-4 v. 1E-4) (FIGURES 3.4BC & 3.5ADGJ). This signal distribution may be indicative of the specific transduction of mCD4+ and mCD8+ cells, which were mainly T cells (91.7% of CD4+/CD8+ cells were CD3+ in spleen; blood: 88.1%; bone marrow: 64.3%; liver: 86.4%), by mCD4-LV and mCD8-LV, respectively. In that case, the higher overall signal obtained through treatment with mCD4-LV compared to CD8-LV may be explained as a result of the overall higher proportion of CD4+ cells among T cells, which made up >60% of CD3+ cells in spleen, blood and liver samples from PBS-treated (i.e. negative control) animals (FIGURE 3.5BEHK).
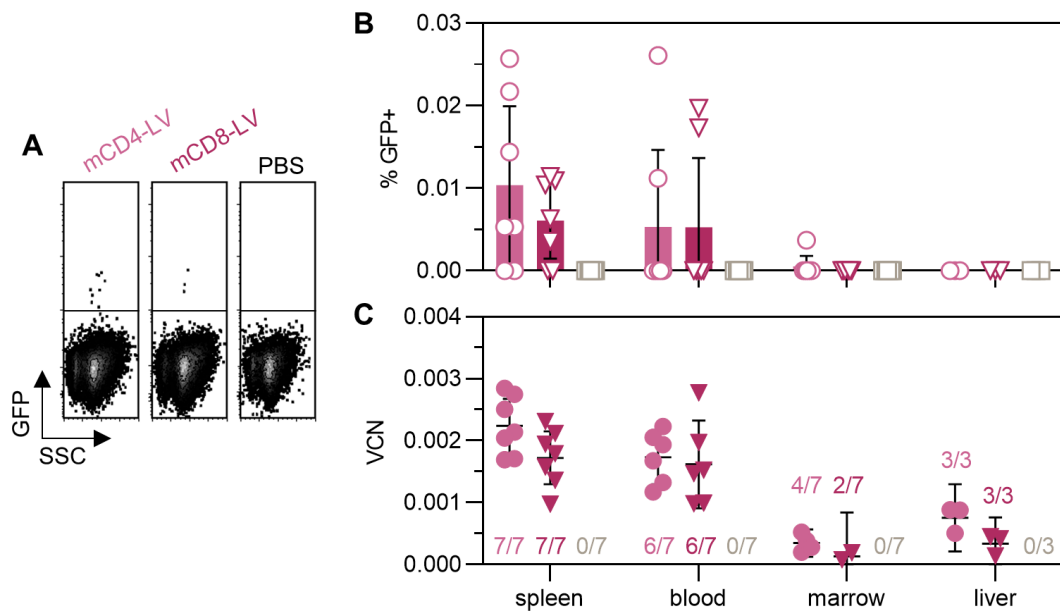
FIGURE 3.4: Transfer signal near the limit of detection
Continued from FIGURE 3.3. Transfer signal on the **AB** protein and **C** genomic level after injection of mCD4-LV-PGK-GFP (pink ●), mCD8-LV-PGK-GFP (red ▼) or no vector (grey ■). Symbols represent data from n = 7 mice/ group (total: 21 mice) for spleen, blood and bone marrow and n = 3 mice/ group (total: 9 mice) for liver. **A** Representative flow cytometry plots from propidium iodide-based cell counting of unfixed splenocytes showing GFP signal versus sideward scatter (SSC) of viable singlet cells. **B** GFP-positivity of viable singlet cells. Symbols in represent single technical replicates, bars represent means, error bars represent 95% CIs. **C** VCNs (i.e. copies of woodchuck hepatitis virus posttranscriptional regulatory element (WPRE)/ cell) in total cell samples. Samples were considered WPRE-positive if all three technical replicates yielded a treshold/quantification cycle (C_T/C_Q). Proportion of WPRE-positive samples is given for each condition. Symbols are arithmetic means of technical triplicates, solid lines represent arithmetic means, error bars represent 95% CIs. See SUPPLEMENTARY FIGURE 6.1 for visualization of qPCR input quality.

Additionally, pronounced remodelling of the lymphoid compartment upon vector treatment was observed. Readily apparent was a shift towards lower relative frequencies of T cells upon vector injection. This effect was most pronounced for mCD4-LV, which lowered the mean frequency of CD3+ cells in spleen and blood by roughly 5% compared to untreated mice. This decrease was accompanied in blood by an increase in the frequency of CD3-CD19- double negative cells, i.e. non-T-non-B cells (**FIGURE 3.5AD**). Furthermore, the administration of mCD4-LV caused a pronounced decrease in the frequency of CD4+ cells among T cells and a concomitant increase in CD4-CD8- double negative T cells in blood (**FIGURE 3.5E**), as well as, curiously, an uptick of double negative T cells in bone marrow, accompanied by a slight decrease in the frequency of CD8+ T cells (**FIGURE 3.5H**). Most notably, the administration of both mCD4-LV and mCD8-LV caused a shift in T cells in spleen and liver towards higher forward and sideward scatter, i.e. an increase in cell size and granularity, which usually is a hallmark of T cell activation. Additionally, mCD4-LV induced such a shift in blood (**FIGURE 3.5CFIL**). This remodelling, most pronounced in animals

treated with mCD4-LV, which yielded stronger overall protein and genome level transfer signals than mCD8-LV in all four tissues (**FIGURE 3.4ABC**), may be indicative of immune response toward vector-binding or recently transduced, transprotein-displaying cells, in the course of which non-T/B cells accumulate in the blood and T cells become activated, migrating from the spleen to the periphery.
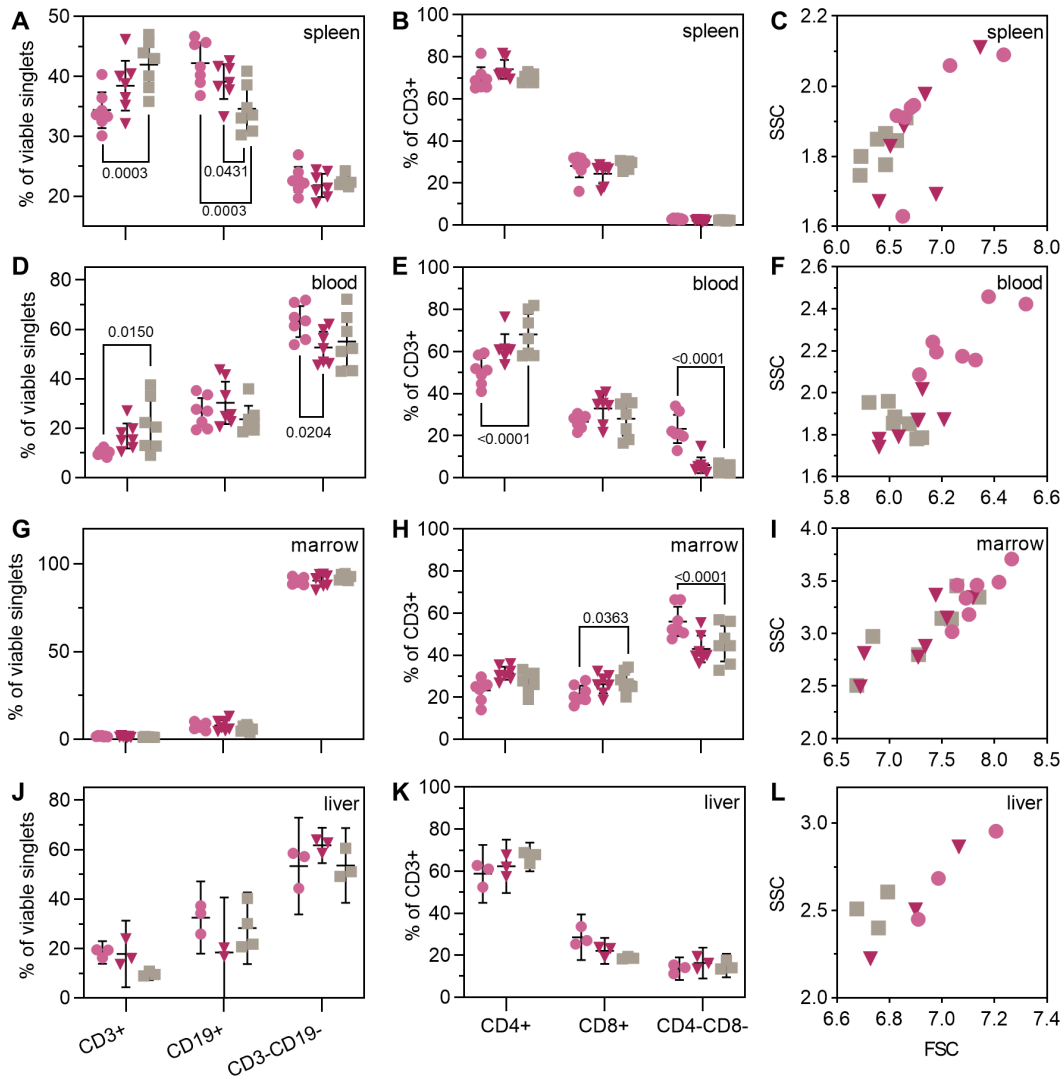
FIGURE 3.5: Changes in the lymphoid compartment
Continued from FIGURE 3.3. Visualization of a putative immune response in **A-C** spleen, **D-F** blood, **G-I** bone marrow and **J-L** liver after administration of mCD4-LV-PGK-GFP (pink ●), mCD8-LV-PGK-GFP (red ▼) or no vector (grey ■). Symbols represent data from n = 7 mice/ group (total: 21 mice) for spleen, blood and bone marrow and n = 3 mice/ group (total: 9 mice) for liver. Solid lines represent means, error bars represent 95% CIs. Select multiplicity-adjusted p values from two-way ANOVA with Tukey's multiple comparisons test are reported. **ADGJ** Frequencies of CD3+, CD19+ and CD3-CD19- cells among viable singlet cells. **BEHK** Frequencies of CD4+, CD8+ and CD4-CD8- cells among CD3+ viable singlets. **CFIL** Arithmetic means of forward and sideward scatter of CD3+ viable singlets.

3.2 LV-Mediated CAR Transfer in BALB/c Mice

Immune interference with transduction was thought to be less of a concern for *in vivo* CAR transfer experiments than for GFP transfer experiments, as it was assumed that while both the CAR and GFP would register as foreign antigen with the BALB/c immune system, the CAR, in the presence of ample CD19+ target cells, would – in contrast to GFP – provide transduced T cells with activatory signals, improving their persistence *in vivo*. To additionally improve transfer rate, phagocytosis-shielded vectors, which display the human phagocytosis inhibitor CD47 on their surface, were used.

mCD4- and mCD8-LVs were produced in the *B2M* knockout CD47hi cells using a PGK-driven CAR transgene (Table 2.1, p. 24). The CAR had previously been shown to mediate cell ablation in *in vitro* assays in our hands (Figure 2.6, p. 35). Having been derived by the insertion of a myc tag between scFv and hinge from the CAR described in [Kochenderfer et al., 2010], it featured an attenuated CD3ζ domain in which the first and third ITAMs were ablated by point mutation to improve CAR T cell survival (Figure 3.6a).

After transduction of the 58m8ab murine T cell line (which overexpresses mouse CD8α and CD8β), αmCD19-CAR could be detected similarly well using either soluble mCD19-Fc fusion protein or an αmyc-antibody. Underlining the specificity of αmCD19-CAR for mouse CD19, a myc-tagged control CAR specific for human CD19 could be detected via its myc tag, but not via mCD19-Fc (Figure 3.7ab). The mCD4-LV-PGK-CAR and mCD8-LV-PGK-CAR stocks produced for *in vivo* use were within specification, with particle concentrations in the range expected for receptor-targeted LVs and particle size modes above those commonly observed for VSV-LV (Figure 3.6bc). Vectors enabled stable transfer of CAR; apparent transducing titers of mCD8-LV-PGK-CAR on 58m8ab cells were not markedly different on days 3 and 7 after vector addition (Figure 3.7c).

It should be noted that the observed transducing titers of mCD8-LV-PGK-CAR were roughly an order of magnitude lower than those observed for an mCD8-LV-SFFV-GFP control stock. While most of this difference can be explained by the different particle concentrations, transgenes and detection modes of the two stocks, this observation, especially in the light of the very low GFP signal observed in the previous setup, indicated that mCD19-CAR would be difficult to detect *in vivo*.
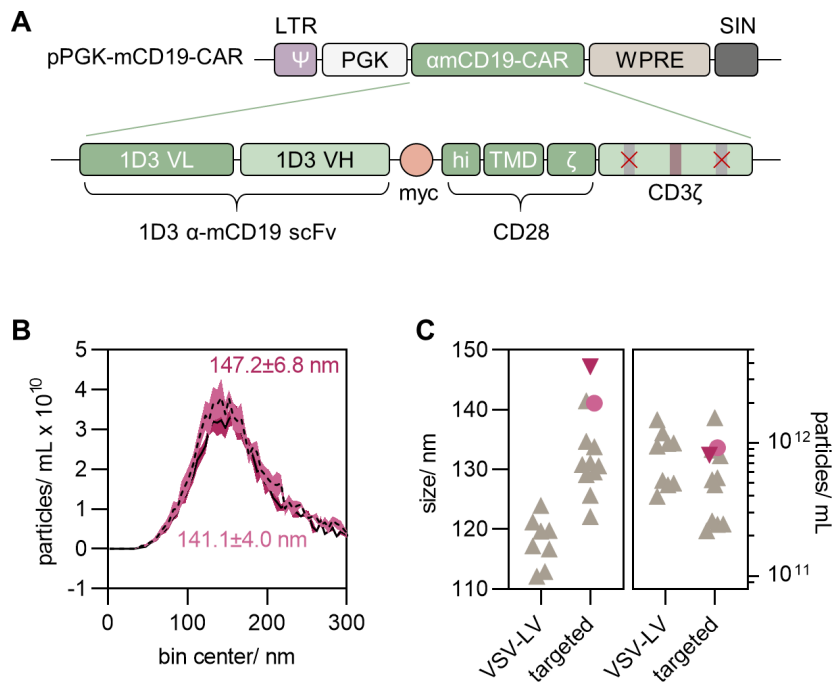
FIGURE 3.6: Physical characterization of vectors for *in vivo* CAR transfer
A Structure of the αmCD19-CAR-encoding transgene used for *in vivo* experimentation. The myc-tagged αmCD19-CAR described in FIGURE 2.6AB is flanked by a PGK promoter and WPRE. Hi: Hinge; TMD: Transmembrane domain; VH/VL: Variable chain heavy and light domains. **BC** Characterization of stocks by nanoparticle tracking analysis. Particle size distribution and concentration were determined using a NanoSight NS300 analyzer. **B** Histograms. Size modes ± standard error of mCD4-LV-PGK-CAR (dotted line, pink bands) and mCD8-LV-PGK-CAR (solid line, red bands) are indicated. Bands represent standard error of n = 4 sequential technical replicates. **C** Particle sizes and particle concentrations of mCD4-LV-PGK-CAR (pink ●) and mCD8-LV-PGK-CAR (red ▼) stocks. Each symbol represents one vector stock. Grey reference symbols represent the measurements first reported in FIGURE 2.1BC. Continued to FIGURE 3.7.
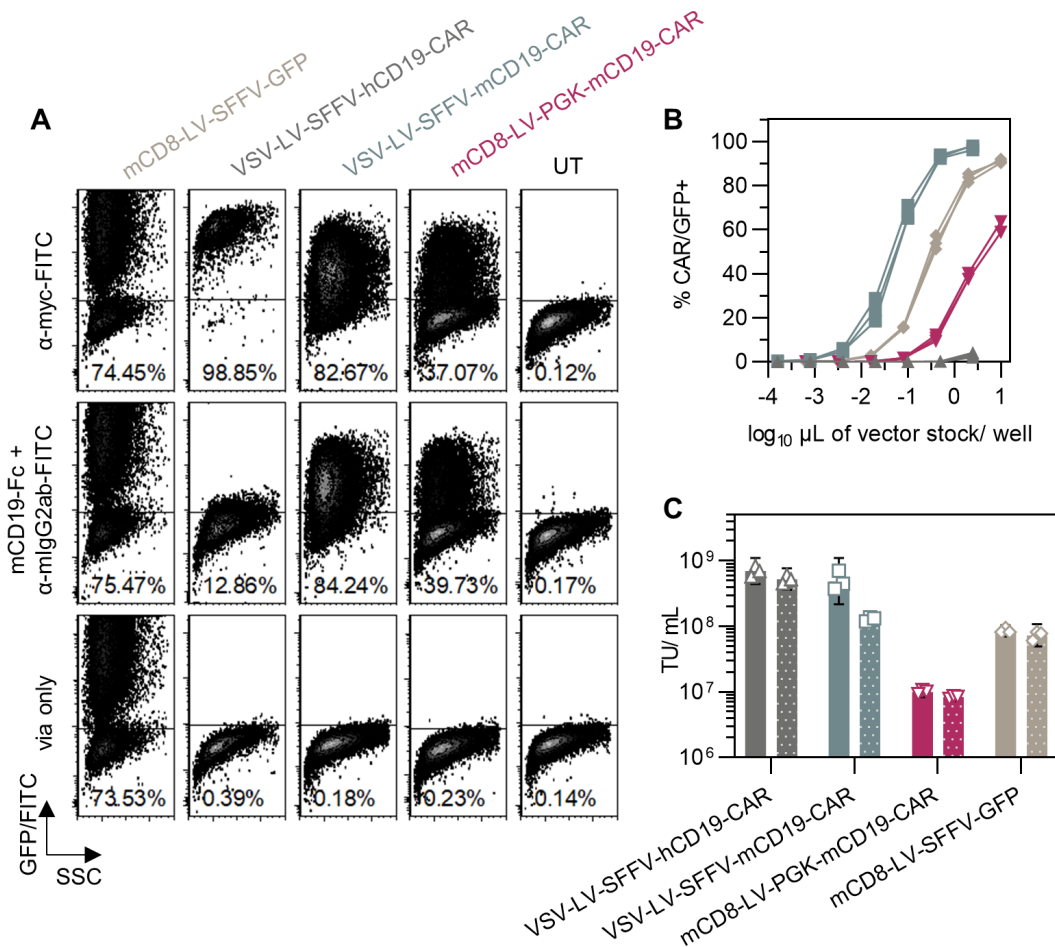
FIGURE 3.7: Functional characterization of vectors for *in vivo* CAR transfer

Continued from FIGURE 3.6. **A** Detecting αmCD19-CAR. 5E4 cells/ 48-well of the murine 58m8ab T cell line overexpressing murine CD8α and CD8β were treated with fixed volumes (1 μL of VSV-LV, 10 μL of mCD8-LV) of mCD8-LV-SFFV-GFP, VSV-LV-SFFV-mCD19-CAR, mCD8-LV-PGK-mCD19-CAR and VSV-LV-SFFV-hCD19-CAR (a positive control transferring a myc-tagged anti-human CD19-CAR) or left untreated. Cells were washed one day after transduction and analyzed by flow cytometry 3 days post transduction (dpt). CARs were detected either via α-myc antibodies or via a two-step staining involving recombinant soluble FC-tagged mCD19 and α-mIgG2b secondary antibodies. Flow cytometry plots show CAR/GFP signal of viable singlet cells. Cells in plots labeled 'via only' were only stained with viability dye. **BC** Assessment of the stability of CAR expression. 1E4 58m8ab cells/ well were treated with serial dilutions of mCD8-LV-SFFV-GFP (grey ◆), VSV-LV-SFFV-mCD19-CAR (blue ■), mCD8-LV-PGK-mCD19-CAR (red ▼) and VSV-LV-SFFV-hCD19-CAR (dark grey ▲) . Cells were washed 1 dpt and interrogated for CAR expression by flow cytometry on 3 and 7 dpt. Sampling for CAR expression on day 3 post transduction resulted approximately in 1:5 subculturing. **B** CAR/GFP-positivity of viable singlet cells. CAR signal is from two-step staining with soluble Fc-tagged mCD19 and α-mIgG2b secondary antibody. Symbols represent technical triplicates. **C** Transducing titer of vector stocks, determined via GFP or myc-tag, at 3 dpt (smooth bars) and 7 dpt (coarse bars). Symbols represent technical triplicates. Bars represent geometric means, error bars represent 95% CIs.
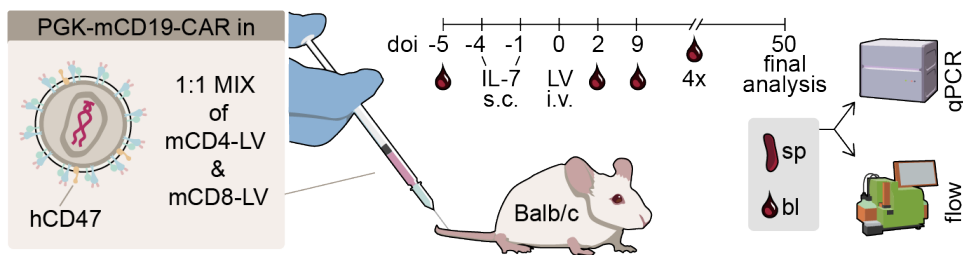
**FIGURE 3.8: Modelling *in vivo* CAR therapy in immunocompetent mice**
Four and one day before vector administration, male BALB/c mice received subcutaneous injections of 200 ng of human IL7/ animal and injection. On the day of (vector) injection (doi 0), animals received either a mix of mCD4-LV-PGK-CAR (0.9E10 particles/ animal) and mCD8-LV-PGK-CAR (0.8E10 particles/ animal) in a volume of 200 µL/ animal (MIX) or PBS via tailvein injection. Drops of peripheral blood were taken from the retroorbital nexus on doi -5, +2 +9, +16, +23, +30 and +44; nucleated cells were analyzed by flow cytometry. On doi +50, mice were euthanized and nucleated cells were extracted from whole blood (bl) and spleens (sp) of all mice. Cell material was analyzed by flow cytometry and qPCR. Continued to FIGURES 3.9 & 3.10.

3.2.1 No CAR Signal in Peripheral Blood

As in the previous experiment, IL7 was administered to improve lentiviral transduction and provide early support to transduced cells, i.e. CAR T cells. This time however, for slower kinetics and greater ease of handling, 200 ng/ animal of IL7 were administered subcutaneously four and one days before vector administration. Animals received intravenous injections of either a 1:1 mix (by volume) of mCD4-LV-PGK-CAR (0.9E10 particles/ animal) and mCD8-LV-PGK-CAR (0.8E10 particles/ animal), resulting in a dose of 1.7E10 particles/ animal or PBS. Animals were bled regularly and nucleated cells were analyzed by flow cytometry (**FIGURE 3.8**).

Vector administration did not have detectable effects on bodyweight over the entire observation period and, as before, no acute reactions to injection were observed (**FIGURE 3.9A**). Likewise, both PBS- and vector-treated mice appeared healthy by macroscopic inspection throughout the experiment, save for the results of treatment-independent infighting.

Interestingly and somewhat disappointingly, no effects of vector treatment were observed on the cellular level in peripheral blood. While exclusion by gating of non CD3+ cells reduced the background CAR signal substantially (**FIGURE 3.9CD**), instances of CAR-positivity in the blood of vector-treated mice were caused by single events straddling the gate boundary (**FIGURE 3.9BD**). As *in vitro* CAR transfer experiments and the previously performed *in vivo* GFP transfer experiment (see p. 41) had indicated that CAR may be difficult to detect, especially in peripheral blood samples – in which, due to the maximum permitted sampling volume, mean and median viable cell contents of 3.7E4 and 2.8E4 cells, respectively, were measured over the course of the experiment – and CAR positivity had been described to lag
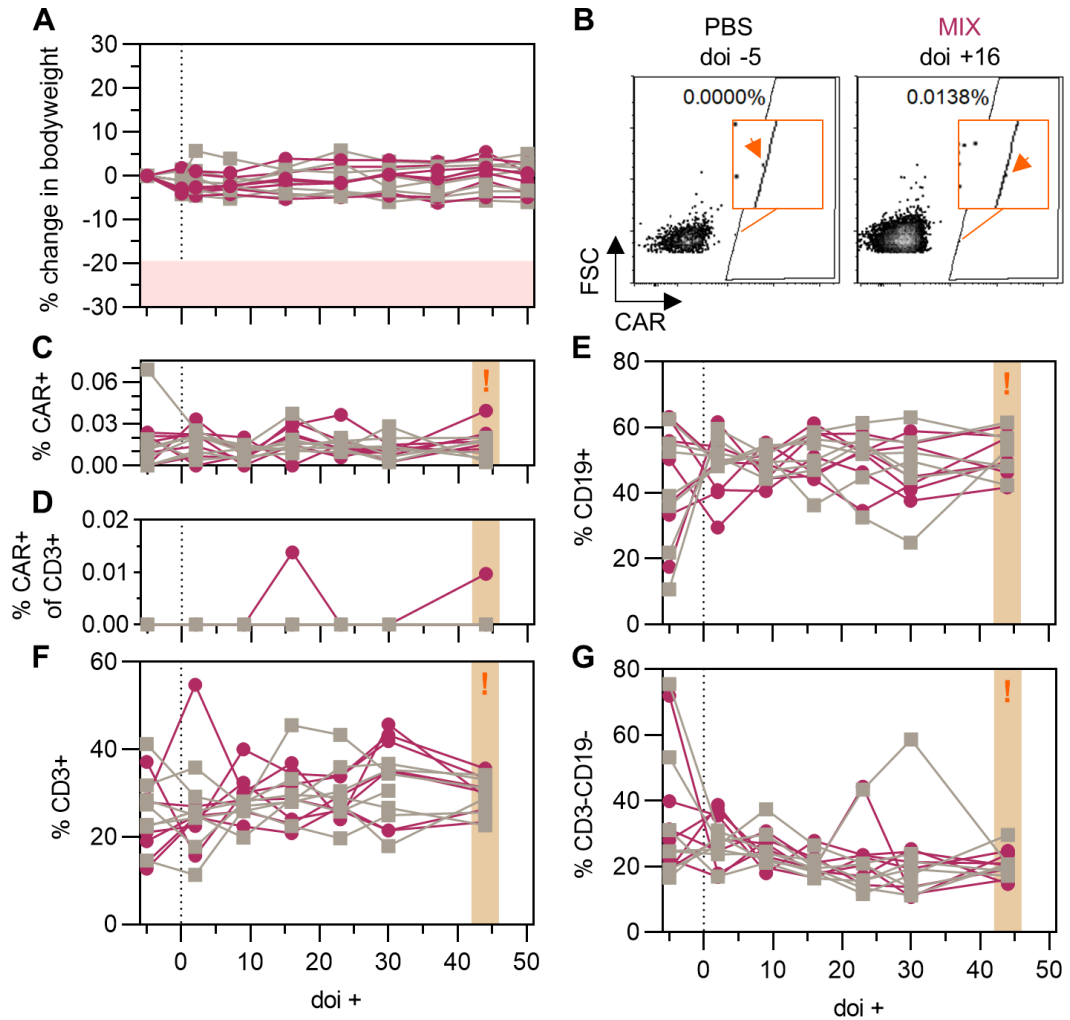
FIGURE 3.9: No signs of CAR activity in peripheral blood after LV infusion
Continued from FIGURE 3.8. Mice were monitored by weighing and flow cytometric analysis of peripheral blood nucleated cells before and after injection of MIX (red ●) or PBS (grey ■). Symbols represent single technical replicates from n = 7 mice/ group (total: 14). **A** Bodyweight relative to doi -5. **B-G** Flow cytometric analysis of peripheral blood. **B** FACS plots showing CAR/myc-positivity of viable singlet CD3+ cells in samples from PBS- and MIX-treated mice on doi -5 and +16, respectively. Orange inlays and arrows magnify single events at the gate boundary to provide context for the signals reported in **D**. **C-G** Kinetics of CAR/myc-positivities of **C** total and **D** CD3+ cells as well as frequencies of **F** CD3+, **E** CD19+ and **G** CD3-CD19- cells among viable singlets from peripheral blood. Cave: A mistimed vortex step during sample processing on doi +44 resulted in cross-contamination of unknown extent (ocre bars, orange exclamation marks). Also note that the excursion in CD19+ and CD3-CD19- frequencies of one PBS-treated mouse on doi +30 was detected shortly after the respective animal was wounded by a cage mate. See SUPPLEMENTARY FIGURE 6.2 for additional plots on peripheral blood cell kinetics.

behind target cell ablation [Ho et al., 2022], the experiment's main readout was the frequency of CD19+ (i.e. B) cells in peripheral blood over time.

Notably however, the lowest readings of CD19+ frequency occured in PBS- and vector-treated animals alike. Furthermore, decreases in CD19 levels were transient, i.e. were only observed at one timepoint, and were accompanied by spikes in the frequency of CD3-CD19- non-T-non-B cells, possibly suggesting inflammatory responses. Indeed, the excursion in CD19+ and CD3-CD19- frequencies in the peripheral blood of one PBS-treated mouse on doi +30 was detected shortly after the respective animal was wounded by a cage mate. The three animals with the highest CD3-CD19- and lowest CD19+ levels on doi -5 were cagemates at the time (FIGURE 3.9EFG). Over the observation period, no notable differences in FSC, SSC, or CD4+, CD8+ and CD4-CD8- levels in the blood of vector- vs. PBS-treated mice were observed (SUPPLEMENTARY FIGURE 6.2B-F). Soberingly, the data summarized above suggests that vector treatment did not induce CAR T cell activity in peripheral blood.

3.2.2 Decreased Splenic B/T Cell Ratio

While vector treatment had no detectable effect on blood composition, on final analysis at doi +50, evidence of vector-induced lymphatic remodelling was observed in spleen. Splenocytes from vector-treated animals on average contained fewer CD19+ cells and more CD3+ cells, i.e. they had a lower CD19/CD3 ratio, than splenocytes from PBS-treated animals, indicating that some T cell proliferation and/or B cell depletion may have occured (FIGURE 3.10CD): In vector-treated animals, the mean frequency of splenic CD19+ cells was approximately 6% lower (48.9% v. 54.9%) and T cell frequency, conversely, was approximately 7% higher (44.3% v. 37.6%) than in PBS-treated animals. Notably, there were no relevant differences in mean spleen weight and splenocyte yield between PBS- and vector-treated animals (FIGURE 3.10AB).

On the protein level, CAR signal clearly above background was observed in neither blood nor spleen (FIGURE 3.10F), and mean T cell subsets, sizes and granularities were distributed similarly for vector-treated and PBS animals (FIGURE 3.10E & SUPPLEMENTARY FIGURE 6.2G). Unfortunately, no reliable VCN qPCR data was available to help discern the extent of gene transfer: While spleen samples from four of seven vector-treated animals were found to be positive for WPRE, confusingly, two of seven blood samples from both PBS- and vector-treated groups were positive for WPRE as well (FIGURE 3.10G). *Alb* copy numbers in the reactions varied over more than two orders of magnitude for both tissues, suggesting an unidentified error in the performed 96-well DNA extraction procedure as a cause for the anomalous readings (SUPPLEMENTARY FIGURE 6.2A). While frozen backup splenocyte samples
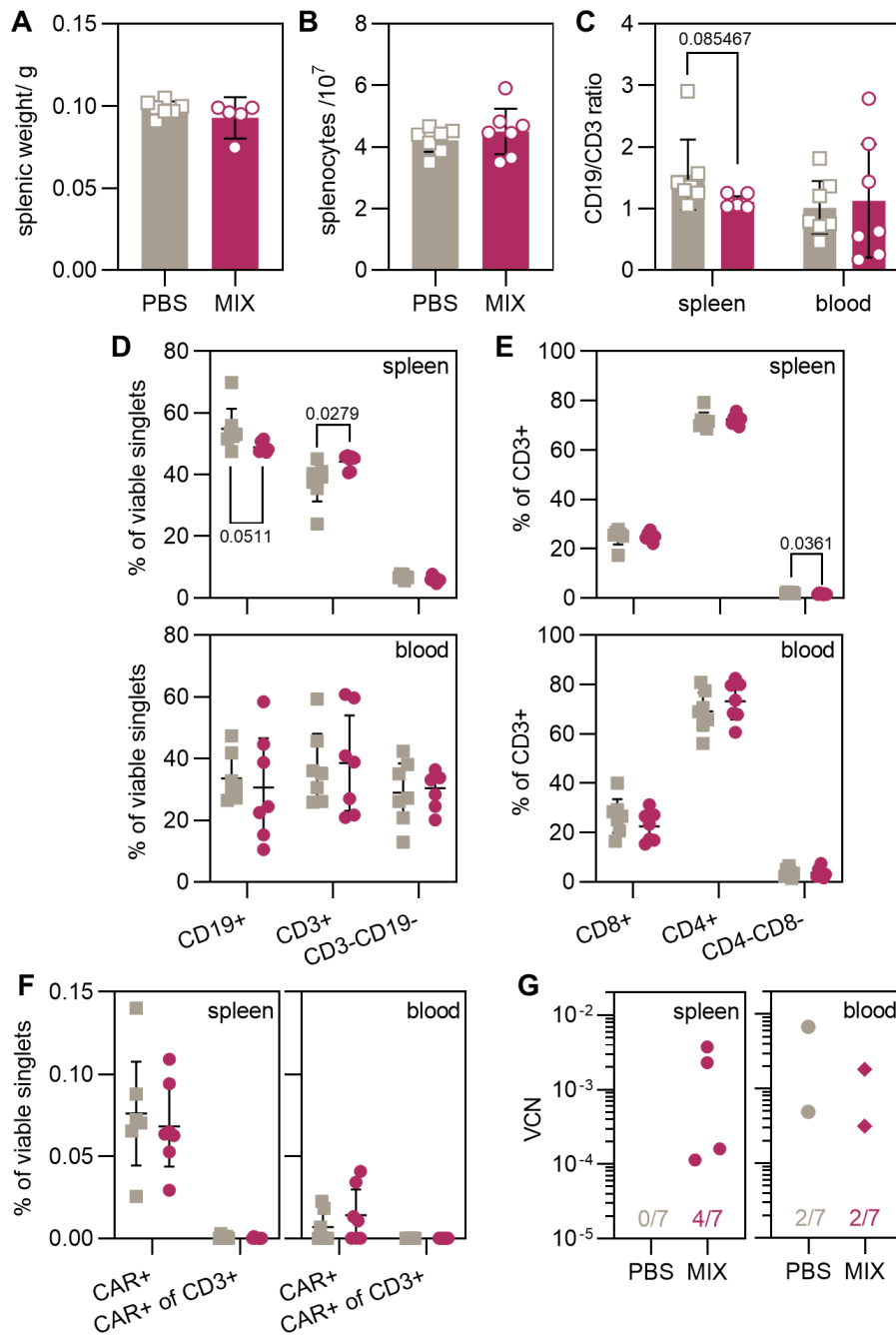
FIGURE 3.10: Altered cellular composition in spleen fifty days after treatment
Final analysis of mice treated with MIX (red ●) or PBS (grey ■) was performed as described in FIGURE 3.8. Symbols represent data from n = 7 mice/ group (total: 14 mice). Bars/ lines are means, error bars represent 95% CIs. Symbols in A-F represent single technical replicates, symbols in G are arithmetic means of technical triplicates. P-values are from unpaired t-tests without multiple comparisons correction. A Spleen weights. Due to an oversight during processing, no weights were recorded for two MIX-treated animals. B Splenocyte yields. C Ratio of CD19+ over CD3+ viable singlet cells. D Frequencies of CD3+, CD19+ and CD3-CD19- cells among viable singlet cells. E Frequencies of CD4+, CD8+ and CD4-CD8- cells among CD3+ viable singlets. F CAR/myc-positivities of (CD3+) viable singlet cells. G VCNs (i.e. WPRE copies/ cell) in total cell samples. Samples were considered WPRE-positive if all three technical replicates yielded a treshold/quantification cycle (C_T/C_Q). Proportion of WPRE-positive samples is given for each condition. See SUPPLEMENTARY FIGURE 6.2 for visualization of qPCR input quality and information on T cell size and granularity.

from the experiment are available, the author was unable to repeat DNA extraction due to time constraints. Accordingly, it is unclear at the time of this writing whether the observed shift in splenocyte composition in vector-treated animals was linked to the presence of CAR T cells.

3.3 AAV Biodistribution in Ai9 Reporter Mice

The two experimental setups summarized above provided crucial data on how receptor-targeted vectors may be received by immunocompetent subjects: Most importantly, they showed that even though mouse-targeted lentiviral vectors perform nominally *in vitro*, the transfer rates they elicit *in vivo* (if any can be discerned) are much lower than those expected for human-targeted LVs in humanized mouse models. Possibly a result of immune interference, the resistance of BALB/c mice to lentiviral transduction motivated a change of experimental system to enable a direct assessment of the impact of receptor-targeting on AAV biodistribution.

To this end, immunoreplete Ai9 reporter mice with a C57BL/6 background were used. These express tdTomato (tdT) reporter from the accessible *Gt(ROSA)26Sor* genomic locus upon introduction of cre recombinase (FIGURE 3.11A). Accordingly, transient cre expression is converted into a stable and bright fluorescent signal, conveniently removing the confounding factor of reporter transience from the analysis of AAV biodistribution. Additionally, through the natural leakiness of their reporter cassette, Ai9 mice should display some immunotolerance towards tdTomato protein, possibly reducing immune interference with the readout, which was characterized *in vitro* on primary Ai9 cells before vector was systemically administered into animals.

### 3.3.1 Bright and Binary Fluorescence Signal in Ai9 Cells

Stocks of cre-transferring mCD8-AAV and AAV2-cre were produced and yielded similar vg titers (FIGURE 3.11C). When splenic Pan T cells from an Ai9 mouse were transduced with either mCD8-AAV-cre, AAV2-cre or an mCD8-AAV-GFP control stock (TABLE 2.2, p. 40), cre transfer elicited much brighter signal than GFP transfer, with the MFIs of positive populations being roughly two orders of magnitude above baseline in flow cytometry. Importantly, because of the mechanism of action of the reporter cassette, tdTomato signal was binary, i.e. the MFI of the reporter-positive population was independent of the population's size, in contrast to GFP signal, for which MFI increased with increasing transduction efficiency (FIGURE 3.12ABC).
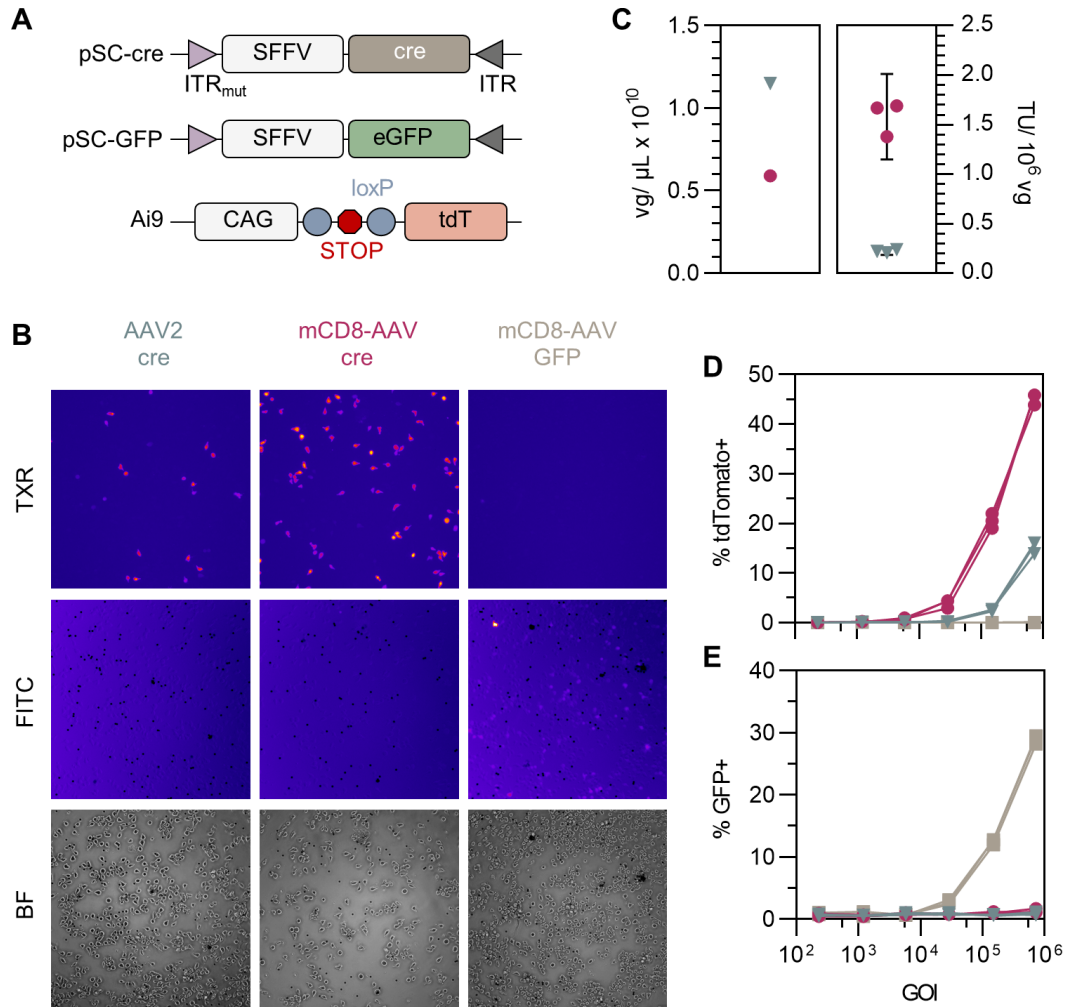
FIGURE 3.11: **Bright signal in Ai9 splenocytes after cre transfer by mCD8-AAV**
A Genetic structures of self-complementary AAV transgenes pSC-cre and pSC-GFP as well as the reporter cassette in the *Gt(ROSA)26Sor* locus of Ai9 mice. In the latter, a stop-codon is flanked by loxP sites. When cre recombinase is introduced, the stop codon is excised and tdT is expressed. **B-E** Characterization of AAVs on primary Ai9 splenocytes. Ai9 Pan T cells from one mouse were thawed and 4E4 cells/ well - stimulated with αmCD3/αmCD28-beads and recombinant human IL7 and IL15 (rhIL7+15) - were transduced with serial dilutions of mCD8-AAV-cre (red ●), mCD8-AAV-GFP (grey ■) or AAV2-cre (blue ▼). Cultures were documented **B** by microscopy 3 dpt and analyzed **C-E** by flow cytometry 5 dpt. **B** Brightfield (BF) and fluorescence (TXR and FITC channels) micrographs of cultures. **C** Vg titers were determined by qPCR (left panel). Symbols are means from technical duplicates. Transducing titers (TU/ mL) of the cre-transferring vector stocks were determined from the data plotted in *(C)* and normalized to vg titers (right panel). Symbols represent technical triplicates. Error bars represent 95% CIs. **DE** tdT and GFP signal of (viable) singlet cells at different genomes of infection (GOI, vg/ cell). Continued to FIGURE 3.12.
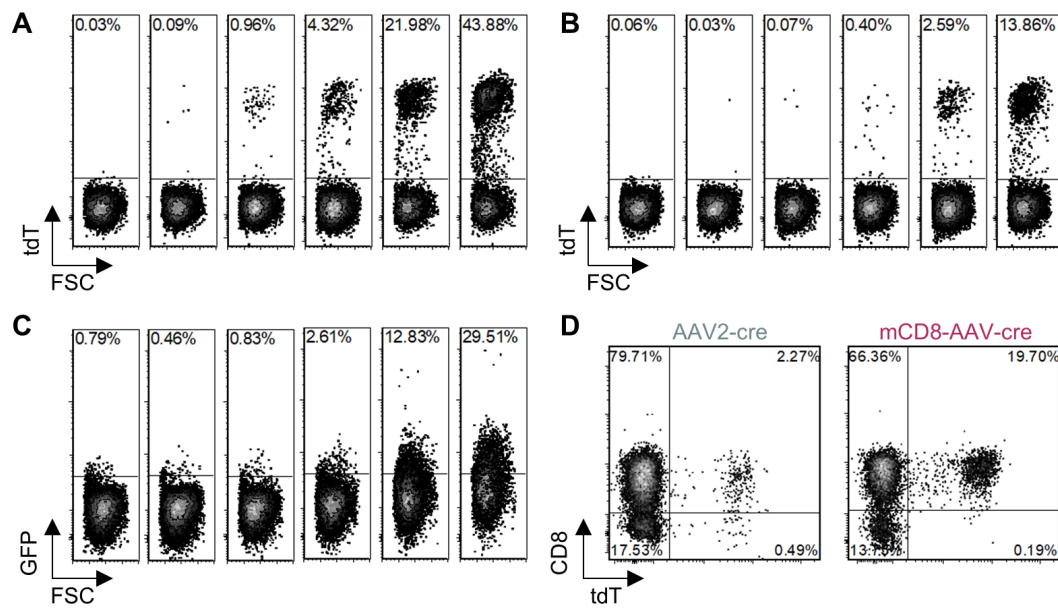
FIGURE 3.12: mCD8-AAV-cre elicits specific and binary signal in Ai9 splenocytes
Continued from FIGURE 3.11. **A-C** TdT/GFP vs. FSC flow cytometry plots of (viable) singlet Ai9 splenocytes treated with five-fold serial dilutions of **A** mCD8-AAV-cre, **B** AAV2-cre and **C** mCD8-AAV-GFP, resulting in GOIs ranging from 2.3E2 (leftmost plot in each panel) to 7.3E5 (rightmost plot in each panel). **D** Flow cytometry plots showing CD8 vs. tdT signal of (viable) singlet cells treated with mCD8-AAV-cre and AAV2-cre at GOI of 1.5E5. **A-D** Because of a temporary failure of the red laser of the flow cytometer, no signal from viability staining was available. Instead, viable cells were selected by their FSC and SSC.

Naturally, mCD8-AAV-cre selectively transduced mCD8+ cells, whereas AAV2-cre did not: In wells treated with 1.5E5 GOIs of the former, mean CD8-positivity among tdT+ events was 98.8% (**FIGURE 3.12D**). The normalized transducing titer of mCD8-AAV-cre (1.58 TU/ 1E6 vg) was 7.1-fold higher than that of AAV2-cre (0.22 TU/ 1E6 vg) (**FIGURE 3.11CDE**). This is similar to the 5.7-fold difference observed for GFP-transferring vectors earlier (**FIGURE 2.7EF**).

3.3.2 Reduced Liver Fluorescence Through Targeting

To harness the excellent sensitivity of the lox-STOP-lox-based reporter cassette for biodistribution studies, Ai9 mice were injected intravenously with 130 μL/ animal of PBS containing 1.7E11 vg/ animal of mCD8-AAV-cre or AAV2-cre or no vector. This was far from the maximum applicable dose, with the vector stock only making up approximately 29 or 15 μL of the injection volume per animal. Fourteen days after vector injection, animals were euthanized and gross biodistribution of the vectors was assessed by whole organ fluorescence imaging (**FIGURE 3.13**).

Administration of either vector had no apparent effect on the weight gain of the mice (**FIGURE 3.14AB**), and no acute or longer-term adverse reactions to injection
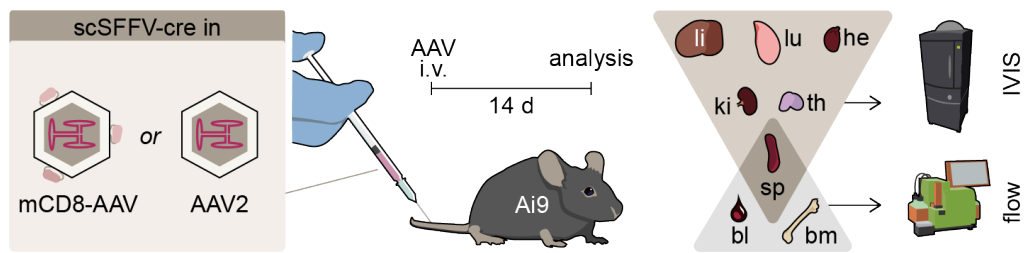
FIGURE 3.13: **Assessing the impact of receptor-targeting for AAV biodistribution**
Female Ai9 mice received 1.7E11 vg/ animal of mCD8-AAV-cre or AAV2-cre or no AAV in 130 μL of PBS/ animal via tailvein injection. Fourteen days after injection, animals were euthanized. Liver (li), lung (lu), heart (he), kidney (ki), thymus (th) and spleen (sp) were removed and whole-organ fluorescence was measured using an *in vivo* imaging system (IVIS). Additionally, nucleated cells were isolated from spleen, blood (bl) and bone marrow (bm) and analyzed by flow cytometry. Continued to FIGURES 3.14, 3.15 & 3.16.

were observed. As expected, AAV2-cre appeared to mostly localize to the liver: In animals treated with it, mean tdT signal in the liver was 22.7-fold over background (i.e. mean liver fluorescence in PBS-treated animals) and less than two-fold over background in all other imaged organs. Interestingly, the liver burden was much reduced in animals treated with mCD8-AAV-cre: In these, mean fluorescence in the liver was only 1.3-fold over background. Unexpectedly, however, mCD8-AAV displayed some preference for the heart, yielding signal 4.5-fold over background. It is unknown whether this signal is due to transduction of cardiomyocytes or heart-resident CD8+ cells (**FIGURE 3.14C**).

To help identify the cell types involved and rule out that putative, spatially inhomogeneous signal biases analysis in similar future experiments, the preparation of tissue lysates and isolation of nucleated cells from the tissues-of-interest should be considered. Notwithstanding the possibly confounding role of non-homogeneous signal distribution in whole organ fluorescence imaging, the data summarized above indicates that receptor-targeting can have a considerable impact on vector distribution in the body.

3.3.3 Selective Quasipercent Gene Transfer by mCD8-AAV

Flow cytomteric analysis of nucleated cells from blood, spleen and bone marrow revealed that targeting not only drastically affects macro- but also microscopic vector distribution.

In line with the preceding *in vitro* experiments, mCD8-AAV-cre far outperformed AAV2-cre both in terms of transduction efficiency and specificity. Among all viable nucleated cells, it achieved mean transduction rates of 0.053% in spleen, 0.096% in blood and 0.016% in bone marrow, which were 9.0-, 100.8- (sic), and 3.9-fold higher than those observed in the respective tissues of mice treated with AAV2-cre.
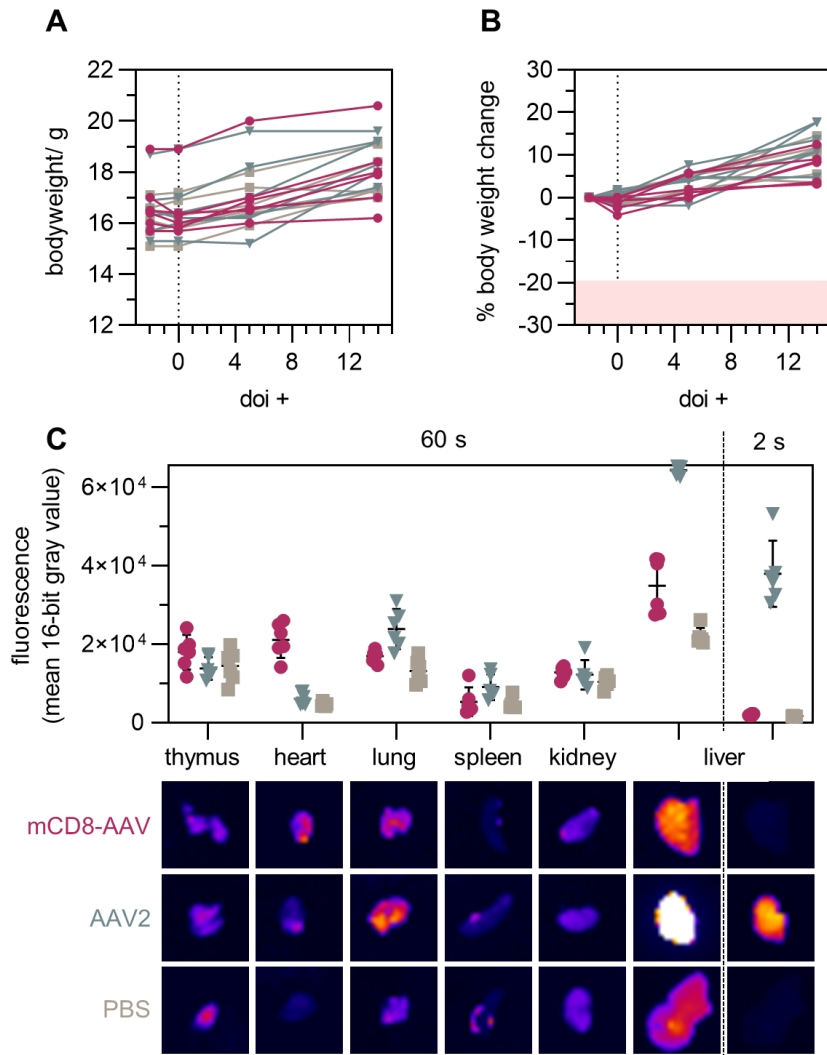
FIGURE 3.14: **Receptor-targeting drastically reduces liver burden *in vivo***
Continued from FIGURE 3.13. Macroscopic reactions to treatment with treated with mCD8-AAV-cre (red ●), AAV2-cre (blue ▼) or PBS (grey ■). Symbols represent single technical replicates from n = 6 mice/ group (total: 18 mice). **AB** Vector injection did not affect bodyweight. Plots show **A** absolute bodyweight and **B** percent change in bodyweight relative to doi -2 over the course of the experiment. **C** Whole-organ fluorescence was determined by IVIS. Summary graph shows mean 16-bit gray value for all animals by treatment. Exposure times are indicated above. The matrix below shows representative fluorescence photographs for each treatment and tissue. Lines are means, error bars represent 95% CIs. See FIGURES 3.15 & 3.16 for flow cytometry data.
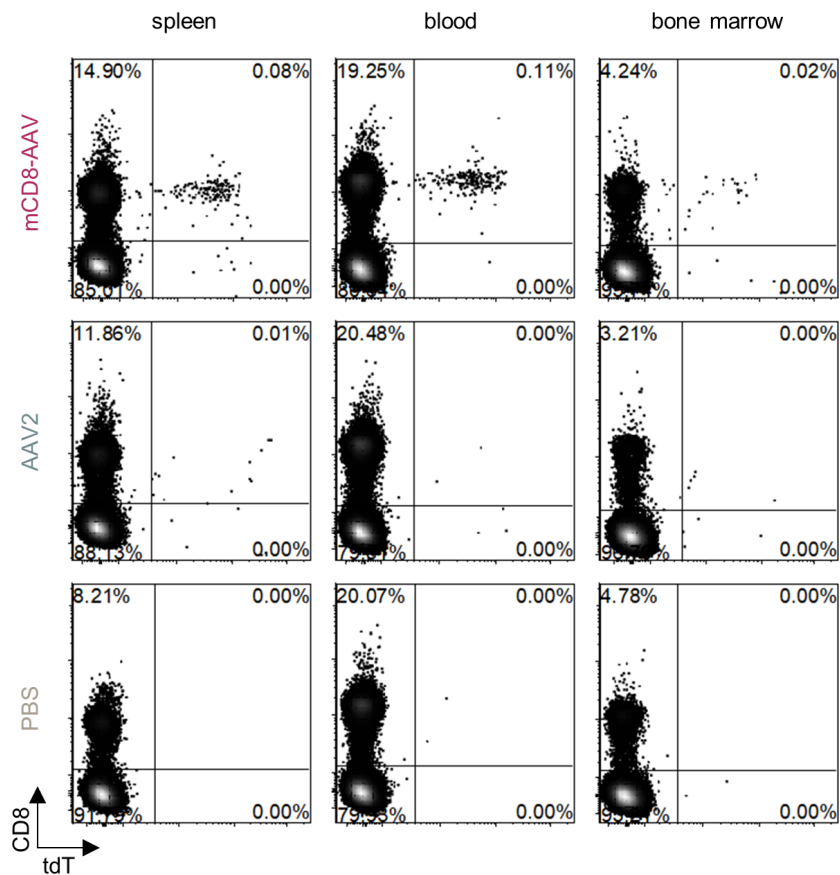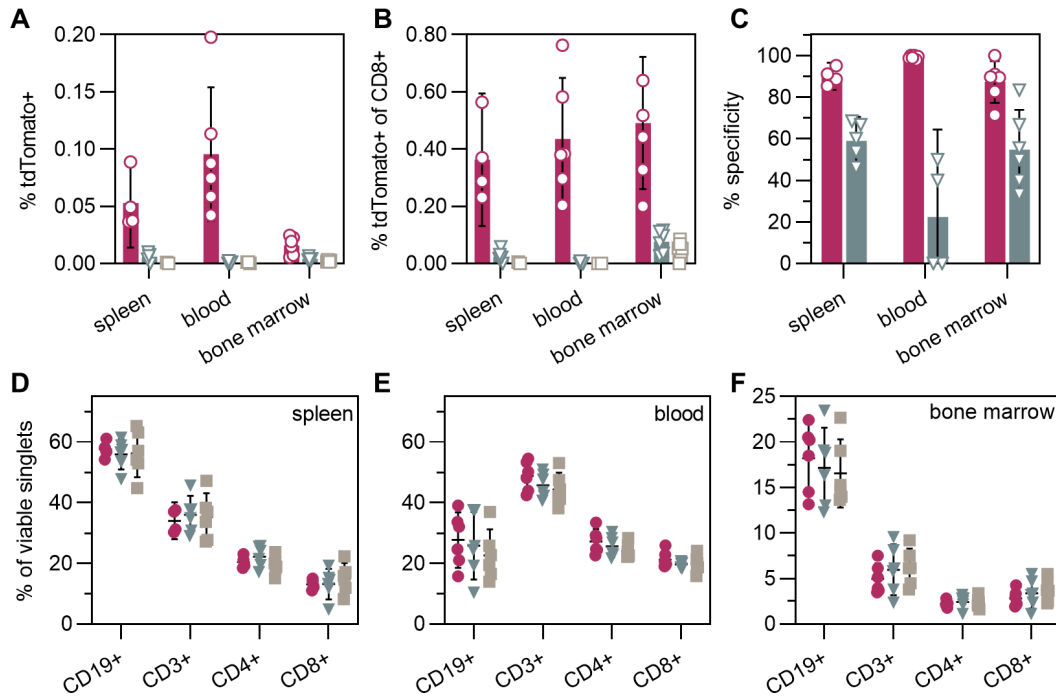
FIGURE 3.15: Selective *in vivo* transduction by mCD8-AAV
Continued from FIGURE 3.13. Representative flow cytometry plots showing tdT vs. CD8 signal. Autofluorescent signal was removed using a dump channel. See SUPPLEMENTARY FIGURE 6.3 for more information on gating. Continued to FIGURE 3.16.

Among CD8+ cells, mCD8-AAV2-cre achieved similar mean transduction rates across all tissues, ranging from 0.36% in spleen to 0.49% in bone marrow. In the blood of one mCD8-AAV-treated mouse, 0.76% of CD8+ cells were tdT+ (FIGURE 3.16AB).

Specificities of transduction (i.e. percentage of CD8+ cells among tdT+ cells) of mCD8-AAV-cre vs. AAV2-cre were 90.1% vs. 59.0% in spleen, 99.2% vs. 22.5% in blood and 87.4% vs. 54.8% in bone marrow (FIGURES 3.15 & 3.16ABC) consistent with the notion that the marked differences in gross biodistribution of mCD8-AAV and AAV2 and the substantially higher transduction rates achieved with the former on lymphoid tissues are a direct consequence of its re-directed tropism.

Finally, possibly as a result of the employed mouse model's supposed tolerance towards tdT, analysis of lymphocyte subsets found no obvious effect of administration of either vector on the frequencies of CD3+, CD19+, CD4+ and CD8+ cells, as well as on T cell viability, size or granularity in any organ (FIGURE 3.16DEF & SUPPLEMENTARY FIGURE 6.3).

Figure 3.16: Selective *in vivo* transduction by mCD8-AAV (continued)
Final analysis of mice treated with mCD8-AAV-cre (red ●) or AAV2-cre (blue ▼) or PBS (grey ■) was performed as described in Figure 3.13. Symbols represent single technical replicates from n = 6 mice/ group (total: 18 mice). Bars/ lines are means, error bars represent 95% CIs. **A-C** Efficiency and specificity of transduction. Plots show tdT-positivity among **A** all viable singlets and among **B** CD8+ viable singlet cells as well as **C** the CD8-specificity of transduction, i.e. the percentage of CD8+ cells among tdT+ cells, for all treatments and tissues. **D-F** Frequencies of CD19+, CD3+, CD4+ and CD8+ cells among viable singlet cells derived from **D** spleen, **E** blood and **F** bone marrow. Cells in spleen samples from two mice treated with mCD8-AAV-cre displayed viabilities <10%. These replicates were excluded from the analyses summarized here. See Supplementary Figure 6.3 for more information on cell size & viability.

DISCUSSION

Learning from Algernon

Mixed as the results obtained from the experiments in immunocompetent mice described here may appear, they - as well as the *in vitro/ ex vivo* assays leading up to them - hold unequivocal lessons (KEY FINDINGS 1-3) for *in vivo* gene therapy, which are discussed in the following in the context of established and emerging concepts in gene therapy.

4.1 Lentiviral Plasticity

To enable the syngeneic models of *in vivo* gene therapy which were the subject of this thesis (CHAPTER 1.5), mouse-compatible vectors which faithfully recapitulate the behaviour of their human-compatible counterparts had to be generated. A major proportion of the preclinical reports of *in vivo* CAR therapy published at the time of this writing made use of receptor-targeted lentiviral vectors (TABLE 1.2), a platform which was lacking suitable surrogate reagents at the outset of the thesis work.

Although the initial description of lentiviral vectors reported their successful use for *in vivo* gene delivery to rat neurons [Naldini et al., 1996], the rodent- and, more specifically, mouse-compatibility of LVs is a recurring concern in the field, one that is rooted in the inability of the parent virus, the human-pathogenic HIV-1, to productively infect mouse cells. Apart from the incompatibility of mouse CD4 and CCR5/CXCR4 with the HIV-1 fusion machinery, pre- and post-integrational blocks have been identified [Nair and Rein, 2014], which include blocks to nuclear import [Tsurutani et al., 2007] and chromosomal integration as well as post-integration blocks to Gag expression, processing, and release [Zhang et al., 2008]. In light of these findings, it is unsurprising that pivotal publications on CAR therapy in syngeneic mouse models did not rely on lentiviral, but instead on gamma-retroviral vectors derived from Moloney murine leukemia virus [Davila et al., 2013] or mouse stem cell virus [Kochenderfer et al., 2010; Kochenderfer et al., 2009] for the *ex vivo* generation of CAR T cells.

Still, the tropism of lentiviral vectors is famously plastic, and uses of appropriately pseudotyped particles in diverse applications beyond the transduction of human T cells are well-documented, including, i.a., the projection pattern-specific transduction of rat neurons by retrogradely transported LVs pseudotyped with a chimeric rabies/ vesicular stomatitis virus glycoprotein [Lockowandt et al., 2020], studies of the binding and cell-fusion properties of SARS-CoV-2 Spike protein via LVs or LV-derived virus-like particles pseudotyped with truncated Spike [Theuerkauf et al., 2021], genetic modification of hematopoetic stem cells with LV-derived nanoblades carrying VSV G and baboon retroviral envelope proteins [Gutierrez-Guerrero et al., 2021] or the *in vivo* transduction of murine B cells using LVs modified to display αmCD19 antibodies [Cascalho et al., 2018]. Additionally, productive transduction of murine cells with VSV-LVs has been described in literature [Gilham et al., 2010; Rive et al., 2022].

In line with this, use of mouse-targeted binders in paramyxo-pseudotyped LVs was found to enable nominal vector behaviour [Michels et al., 2021], an observation further supported by so far unpublished data reported in this thesis (CHAPTER 2.1.1): The mCD4- and mCD8-LV stocks assessed here not only displayed particle sizes and concentrations similar to those of their human-targeted counterparts, but also recapitulated their transduction behavior in terms of specificity and efficiency relative to VSV-LV [Weidner et al., 2021], indicating that receptor compatibility is a major determinant of LV performance on murine cells.

Further stressing the importance of receptor compatibility, Cordes et al. found that treatment of primary murine T cells with measles-pseudotyped, adapter-targeted lentiviral vectors only yielded GFP signal when antibody adapters specific for mCD4 or mCD8 were present [Cordes et al., 2022][1].

The central role of receptor compatibility in mouse cell transduction is not limited to LVs, as the use of the MSE10 DARPin for the targeting of adeno-associated vectors to mCD8+ cells, initially described in [Michels et al., 2021] and expanded upon in this thesis (CHAPTER 2.2.1), has demonstrated. Indeed, the insertion of mouse-specific binders into the receptor-targeting frameworks of both lentiviral and adeno-associated vectors was found to be sufficient to enable gene transfer to cultured mouse cells as well as in syngeneic mouse models of *in vivo* gene transfer (KEY FINDING 1).

---

[1]Interestingly, in their hands, 25-fold higher LV doses were required to achieve the same apparent transduction efficiencies on murine cells as in human cultures. As comparisons of the functional performance of LVs on murine versus human cells are naturally confounded by the necessary use of different cell material and culture protocols for each system, such observations of differential transduction performance likely reflect differences in experimental setups and not a principal incompatibility of mouse cell biology with lentiviral vectors.

> **Key Finding 1:**
>
> Receptor compatibility is a major determinant of the success of mouse lymphocyte transduction for two dissimilar classes of viral vector; targeting to mouse lymphocyte markers sufficiently murinized LVs and AAVs.

4.2 Immunity Matters

Featuring different schedules, transgenes, mouse strains and vector platforms, the three syngeneic models of *in vivo* gene therapy set up for this thesis (**Chapter 3**) were similar insofar as mean gene transfer rates did not exceed 0.25% of cells in any of them, although the vectors' principal efficacy had been demonstrated *in vitro* beforehand. Seeing that a primary difference between humanized and syngeneic mouse models is the latters' complete immune system, the transfer rates observed here, considerably lower than those reported for humanized mouse models in proof-of-concept studies for *in vivo* CAR therapy, (**Table 1.2**, p. 17) may be in large part a result of the host immune system interfering with treatment.

4.2.1 Immune Interference

In fact, reports suggest that even the immune systems of inbred mice kept in specific pathogen-free (SPF) conditions (such as the ones used in this thesis) are remarkably restrictive towards foreign antigen (**Figure 4.2d**). The popular fluorescent reporter GFP, for example, which was also used here, has been described to induce marked immune responses in immunoreplete mice. Overexpression of GFP in syngeneic BM185 leukemia cells drastically improved survival relative to animals which received unmodified BM185 cells in BALB/c mice, but not in Nu/Nu immunodeficient mice. Additionally, BALB/c mice rejecting BM185-EGFP cells for at least thirty days showed activity of cytotoxic lymphocytes against EGFP+ cells [Stripecke et al., 1999][2]. Similarly, take rates of syngeneic A20.Luc.GFP cells in BALB/c mice were much improved by cyclophosphamide lymphodepletive treatment prior to transplantation [Kueberuwa et al., 2018].

In line with this, in addition to protein-level transduction efficiencies in the range

---

[2]Notably, immune responses towards GFP in C57BL/6 mice were found to be less pronounced compared to those observed in BALB/c mice [Stripecke et al., 1999; Skelton et al., 2001]. In ignorance of these findings, BALB/c mice were favored over C57BL/6 mice for the *in vivo* LV gene transfer experiments described in this thesis mainly because of the more even ratio of CD4+ to CD8+ T cells and more placid character, which enabled easier handling during procedures, and because the bulk of preparatory *in vitro* experiments had been performed on BALB/c splenocytes.

of hundredths (sic) of percents, indicators for an immune response were observed when BALB/c mice were treated with GFP-transferring LVs in the context of this thesis (CHAPTER 3.1): Here, administration of mCD4- or mCD8-LV concurred with increases in T cell size and granularity in several tissues, as well as with decreases in T cell frequency in blood and spleen and its concurrent increase in the liver, which are consistent with the activation and redistribution of T cells. Additionally, a marked increase in non-T-non-B cells in the blood was observed, which may be indicative of an inflammatory response. As a close immunological examination of the deposited cell samples from this experiment – which may confirm the above conjecture and might entail, i.a., the quantification of inflammatory and antiviral cytokine levels, the staining of T cell activatory markers and the precise determination of the cellular distribution of viral integration and/or RNA – has not yet been performed, it is unclear at this time whether the observed response was caused by transduced cells or the vector particles themselves.

Immune responses to vector particles are a well-known phenomenon which is not only responsible for adverse reactions but also for clearance of administered particles, reducing the effective on-target dose. Broadly, antibody-mediated (FIGURE 4.2A) and phagocytotic (FIGURE 4.2B) mechanisms of particle clearance can be distinguished, although there is probably functional overlap between the two [Michels et al., 2022]. While both LVs and AAVs, because of their viral origin, are capable of eliciting strong (neutralizing) antibody responses even after one administration [Abordo-Adesida et al., 2005; Munis et al., 2019; Weber, 2021] and antibody-mediated mechanisms have been suggested as a major contributor to toxicity (namely thrombotic microangiopathies) in *in vivo* gene therapy with the latter platform [Ertl, 2022], antibody-dependent mechanisms of particle clearance were thought to not play an important role in murine models based on SPF animals which had never before encountered the vectors in question.

Instead, in light of recents findings by Naldini and colleagues, phagocytotic mechanisms were suspected of relevantly decreasing the on-target dose: When they attempted to transfer human Factor IX into the liver of C57BL/6 mice, they found a non-linear dose response, which, together with other findings, suggested a phagocytotic response of fixed capacity clearing most particles up to a certain dose threshold. They also found that gene transfer into the livers of compatible mouse strains and even non-human primates could be much improved by the use of MHC-free 293T cells overexpressing the human 'Don't eat me!' signal CD47 for LV production [Milani et al., 2019]. In line with this, Ho et al., modelling the *in vivo* generation of CAR T cells in stem cell-humanized NSG-SGM3 mice, found that use of phagocytosis-shielded hCD4- and hCD8-LVs produced on MHC-free hCD47^hi cells

resulted in higher transduction rates and more pronounced B cell ablation than use of similar unshielded vectors [Ho et al., 2022].

4.2.2 CAR-Mediated Responses

When such hCD47^{hi} shielded LVs were used in this thesis to model the *in vivo* generation of CAR T cells in BALB/c mice (**Chapter 3.2**), no CAR+ cells were observed in the peripheral blood of vector-treated animals at any time during the experiment. As the phagocytosis-shielded vectors were not expected to offset the poorer detectability of CAR compared to GFP, this was unsurprising. Indeed, Cunningham et al., injecting αCD20-CAR-transferring paramyxo-pseudotyped CD8-LVs into *Macaca nemestrina*, only reported genome-level positivity in peripheral blood. Crucially however, they found both transient and sustained B cell depletion [Cunningham et al., 2021]. This was not observed in this thesis. In fact, the only apparent difference found between vector- and PBS-treated mice was a slight but consistent decrease in the CD19/CD3 ratio of the former. In the absence of more conclusive data, one can only speculate about the possible cause(s) for this lack of clear CAR-mediated B cell ablation.

One possible contribution is an immune response against the CAR. As stated above, the CAR used here was derived from that used in a preclinical study providing proof-of-concept for the marketing application of Yescarta. In that study, C3H mice receiving αmCD19-CAR T cells after injection of 38c13 lymphoma cells only survived if they had been sublethally irradiated before lymphoma application, suggesting an immune-mediated ablation of CAR T cells [Kochenderfer et al., 2010]. Likewise, in a study using BALB/c mice, 1E7 *ex vivo*-generated αmCD19-CAR T cells per animal were almost completely lost within seven days after administration without prior total body irradiation at a dose of 5 Gy [Kueberuwa et al., 2018].

Contrasting these findings, a recent report describes the successful *in vivo* generation of αCD19-CAR T cells in C57BL/6 mice following a single, moderately dosed injection of approximately 4E6 TU per animal of VSV-LV [Rive et al., 2022] (also see **Table 1.2**). Interestingly, CAR was detected via GFP incorporated into the transgene. In their setting, αmCD19-CAR cells, i.e. GFP-positive cells, were first detected three weeks after vector administration and their appearance was followed by a sharp drop in B cell levels one to two weeks later. Somewhat confusingly however, they claim to obtain similar T cell expansion rates and target cell killing (in a mismatched setting) *in vitro* and similar expression and ablation kinetics *in vivo* using CARs based on the mouse CD19-targeted 1D3 scFv and those based on the human CD19-targeted FMC63 scFv. In the detection trials performed for this thesis, FMC63-based αhCD19-CAR could be detected via its myc tag, but, crucially, not via recombinant soluble murine CD19, whereas αmCD19-CAR could be detected via both. This may suggest

that some of the treatment effect described in the aforementioned report was due to antigen-independent CAR signaling and/or CAR-induced immune activation.

Notwithstanding this, the data of Rive et al. stresses an important point: While paramyxo-pseudotyped receptor-targeted lentiviral vectors have displayed far superior cell type selectivity, likely in part as a consquence of the bipartite nature of their entry machinery, their transducing capacity per particle is typically lower than that of LVs pseudtoyped with VSV G protein. In some cases, stocks of both human and mouse-targeted receptor-targeted LV register approximately 100-fold lower transducing titers than stocks of VSV-LV [Weidner et al., 2021; Michels et al., 2021; Parayath and Stephan, 2021][3].

Additionally, phagocytosis shielding may not have worked as intended[4]: Due to polymorphisms, the strength of the interaction of human CD47 and mouse SIRPα is dependent on strain: Human CD47 has been reported to interact strongly (K_d=2.5 nM) with the SIRPα variant of the NOD strain (on which many humanized mouse models are based). Interaction with the variant of a BALB/c strain was found to be more than 100-fold weaker (K_d=307.6 nM). This was still stronger than the interaction between C57BL/6 SIRPα and hCD47, which did not yield a K_d. [Milani et al., 2019; Iwamoto et al., 2014]. As a consequence of αCAR immunity and suboptimal suppression of phagocytosis, the administered dose of receptor-targeted LVs, limited by the inoculum volume and vector stock particle concentration, may have been too low to enable sustained CAR cell activity.

Lastly, in light of similar anecdotes, it cannot be ruled out that the insertion of a myc-tag into the Kochenderfer CAR [Kochenderfer et al., 2010] somehow impedes its function. As the mechanics of CAR signaling are still incompletely understood, such interference cannot be ruled out without further experiments, the completion of which was prevented by time constraints. While CAR-mediated target cell ablation has conclusively been shown using the construct in question (**CHAPTER 2.1.4**), it has never been assessed in a 'classical' killing assay.

Assuming impeded CAR function, the increase in CD3/CD19 ratio observed in vector-treated animals may not be the consequence of transient CAR T cell activity, but of CAR- and/ or vector-dependent immune activation, which may include CAR-mediated association of vectors with CD19+ cells and their subsequent clearance by host immune mechanisms reacting to vector components (**FIGURE 4.1**). Considering the evidence for CAR-mediated vector binding (and uptake) in literature [Cascalho

---

[3]Inclusion of VSV-LV into the *in vivo* GFP transfer experiment described in this thesis was planned, but prevented by an out-of-specification vector stock and scheduling issues. In the CAR transfer setup, VSV-LV was omitted because *in vitro* characterization had demonstrated a negative effect of high VSV-LV doses on the viability of fresh splenocytes, raising concerns about adverse events *in vivo*.

[4]It should be noted, however, that no increase in T cell FSC or SSC was observed in the CAR transfer setting. This may be explained by the MHC-free nature of the production cells used, which may have lowered the vector stocks' immunogenicity.
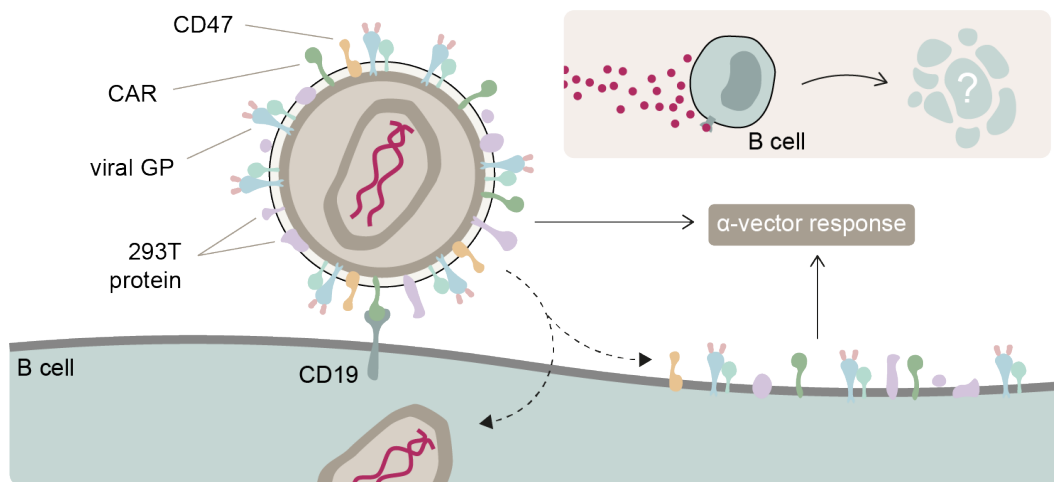
FIGURE 4.1: A possible mechanism for vector-mediated B cell-ablation
Lentiviral vectors, likely not only displaying viral glycoprotein (GP) and CD47, but also CAR and human protein from 293T production cells, bind (and perhaps fuse with) B cells via the CD19-CAR axis. Presentation of vector-derived protein or peptides may then induce an α-vector immune response resulting in B cell ablation (inlay).

et al., 2018; Cordes et al., 2021] and the CAR-mediated binding of LVs to CD19 observed *in vitro* in the context of this thesis (Chapters 2.1.3 & 2.1.4), the contribution by the latter mechanism should not be disregarded, whether the CAR is functional or not.

4.2.3 Dealing with Immunity

Although responses to vector administration in the syngeneic mouse model setups described in this thesis were minimal enough to preclude a direct assessment of vector biodistribution and cell type specificity in two of them, these experiments were not failures. On the contrary, in proving difficult to transduce, the setups reset the expectation horizon for future experiments, stressing the need for a better grasp of the extent of immune interference and the evaluation and implementation of approaches for its mitigation (Key Finding 2).

Strategies for overcoming immune restriction – whose evaluation will likely also aid in dissecting the mechanisms implicated in it – may include improvements on the side of the vector stock and its application as well as more direct immunomodulation (Figure 4.2). An immediate conclusion from the results presented here (and the lack of any apparent adverse events in all setups) is to increase the applied vector dose. If the maximum permitted injection volume is the limiting factor (like it was for dosing of LVs in this thesis), doses may be increased by further concentrating the vector or by administering multiple subsequent volumes of it within a short timeframe (e.g.

within a day), or a combination of both. As a prerequisite for greater concentration, vector stocks may have to be purified by (affinity) chromatography, which would have the added benefit of removing contaminants, thereby likely attenuating the stocks' immunogenicity.

Considering the poor compatibility of human CD47 with the SIRPαs of commonly used inbred mice strains, the feasibility of modifying MHC-free production cells for the expression of a mouse-derived phagocytosis inhibitor (such as mouse CD47) to improve on-target lentiviral vector dose should be explored. Such approaches may further benefit from recent advances in production cell engineering: Through
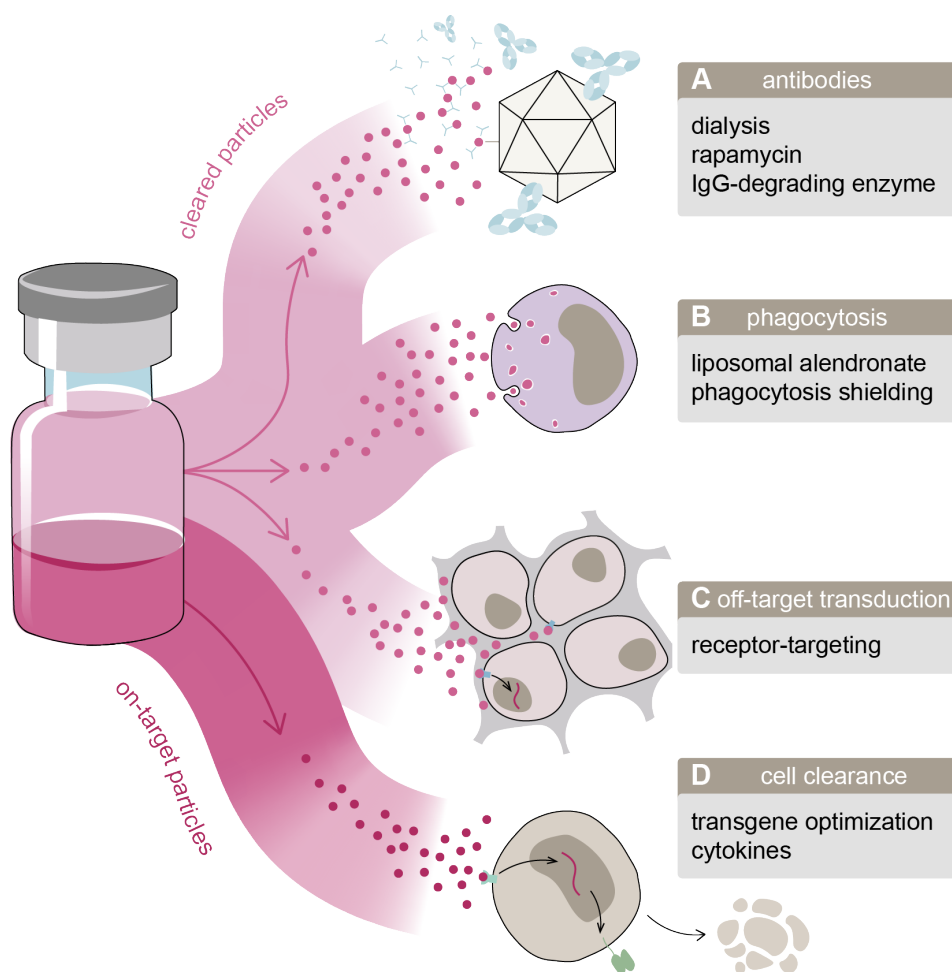
FIGURE 4.2: Mechanisms of host immunity interfering with *in vivo* gene therapy and possible approaches for their mitigation
Several host mechanisms can interfere with *in vivo* gene therapy. These include mechanisms of particle clearance, namely **A** the antibody-mediated incapacitation of particles, **B** their uptake by phagocytes and **C** off-target transduction, which reduce the effective on-target dose (shown as darker pink fraction). Furthermore, host immune responses can **D** clear productively transduced target cells. Approaches for circumventing or counteracting these host mechanisms are discussed in CHAPTER 4. Based on [Michels et al., 2022].

knockout of restriction factors *OAS1*, *LDLR* and *PKR* as well as the overexpression of transcription elongation factors *SPT4* and *SPT5* in 293T cells, approximately tenfold higher vector stock titers were achieved [Han et al., 2021].

For both LVs and AAVs, in an effort to minimize the immunogenicity of the vector and transduced cells, the transgene cargo may be optimized for a minimal immune footprint. Famously, a CAR featuring hinge and transmembrane domains from CD8αas well as an αhCD19 scFv from a fully human antibody was found to have a better safety profile in human trials than one which, i.a., still featured a scFv derived from a mouse antibody (FMC63) [Brudno et al., 2020]. 'Murinization' of transgenes, where possible, might have similar results.

In addition to vector-related optimization, procedures of immune modulation or suppression may have to be implemented to ensure sufficient transduction and persistence of transduced cells. Notably, broadband lymphodepletion (i.e. chemotherapy) before vector administration is already common practice in clinical *in vivo* gene therapy, not only to ensure effective gene transfer, but to minimize immunity-related adverse events [Ertl, 2022]. At the time of this writing, it is unclear whether such 'firehose' approaches are viable for gene immunotherapy as well. There, problematically, target cells are immune cells, whose function and survival may be impacted to the point of non-efficacy by broad lymphosuppressive treatment.

Aiming to address this problem, several reports have explored more nuanced approaches of immunomodulation in recent years. Addressing the issue of phagocytosis, liposomes carrying alendronate have been used to transiently and selectively ablate monocytes and macrophages in non-human primates, rats, rabbits and NSG mice [Burwitz et al., 2014; Danenberg et al., 2003; Haber et al., 2010; Hodgins et al., 2016]. Also using synthetic vectors, albeit polymer nanoparticles, Meliani et al. were able to prevent the induction of anti-capsid humoral and cell-mediated responses against AAV by co-administering the immunomodulator rapamaycin packaged in synthetic vaccine particles. This strategy enabled the re-administration of AAVs in C57BL/6 mouse and nonhuman primate models of liver therapy [Meliani et al., 2018]. Instead of preventing the formation of a (neutralizing) antibody response, other strategies rely on the removal of existing antibodies. For this, an alternative to the removal of serum IgG by plasmapheresis - which is a time-consuming process requiring complex instrumentation - is the use of streptococcal IgG-degrading enzymes such as IdeS. Systemic treatment with IdeS enabled not only liver transduction in macaques with pre-existing anti-AAV8 NAbs, but also effective multiple administrations [Leborgne et al., 2020].

Immune modulatory approaches such as those outlined above may enable resarchers and clinicians to harness the full potential of receptor-targeted viral vectors for gene therapy, drastically improving both safety and efficacy of treatment.

> **KEY FINDING 2:**
> Host immunity may relevantly interfere with *in vivo* gene therapy of immuno-competent subjects; nuanced immunomodulatory approaches may be required to enable gene immunotherapy.

4.3 Receptor Targeting is Key

The transformative power of receptor-targeting became apparent in the third and last setup of syngeneic mouse model examined in this thesis, in which receptor-targeted mCD8-AAVs were compared directly to unaltered serotype 2 vectors in Ai9 mice (CHAPTER 3.3). Mouse models based on recombination-activated fluorescent reporters in the *Gt(ROSA)26Sor* locus, mostly using the C57BL/6-derived Ai9 and Ai14 strains, are commonly used in vector research, as their properties make them ideal for studies of biodistribution. As confirmed here, the binary mechanism of action of their reporter cassette generate a brilliant, permanent signal, transforming even a transient transfer of recombinase into a persistent readout. When Lang et al. administered AAV8 carrying a transgene encoding both cre and GFP under the same promoter into Ai14 and C57BL/6 control mice, they found approximately fourfold higher hepatocyte transduction rates by tdT expression in Ai14 than by GFP expression in C57BL/6 mice as well as a previously unreported tropism of AAV8 for several types of splenic cells including B and T cells, leading them to conclude that conventional, e.g. GFP-based, methods of *in vivo* AAV screening underreport AAV transduction events [Lang et al., 2019]. Furthermore, the natural leakiness of the cassette likely results in some degree of immune tolerance towards the encoded tdT fluorescent reporter, facilitating analyses of biodistribution less confounded by potential anti-repoter host responses[5].

---

[5]It has not escaped the author's notice that Ai mice, for their favorable properties, might allow the productive assessment of the biodistribution of mCD4- and mCD8-LVs which could sadly not be provided in this thesis. When the author became aware of the advantages of the Ai system, however, time constraints made such experiments impossible. Researchers continuing his work may consider assessing bot cre- and tdT-transferring LVs in Ai mice.

4.3.1 AAV Safety

In this sensitive and tolerant reporter system, use of mCD8-AAV-cre resulted in selective, quasipercent gene transfer into CD8+ cells in flow cytometry and, crucially, drastically (i.e. approximately 18-fold) lower levels of whole organ liver fluorescence, compared to those elicited by AAV2-cre, in IVIS (**Chapter 3.3**). As AAV localization to the liver, either through direct transgene/ vector toxicity or discrete T cell responses, is thought to be the cause of fatal hepatotoxicities observed in clinical trials of AAV-based therapy [Ertl, 2022], the observed increase in on-target specificity, concomitant with a pronounced decrease in off-target (i.e. liver) signal, upon receptor-targeting represents a major advance towards safer, more effective vectors (**Key Finding 3**).

Interestingly, in a comparable experimental setting, targeting of synthetic vectors by surface-attached antibodies apparently does not alleviate liver burden to a similar extent: Five days after injection of Ai mice with polymer nanocarriers transferring cre-mRNA, Stephan and colleagues observed a marked increase in reporter signal in lymphoid tissues from mice treated with mCD3-targeted NCs relative to those from mice treated with isotype control-conjugated NCs, but found no relevant decrease in liver fluorescence between targeted and non-targeted vectors [Parayath et al., 2020].

While the apparently much-reduced liver burden of mCD8-AAV brought about by its vector targeting likely majorly improves its safety profile compared to untargeted AAVs, it is unclear if the (apparently equally targeting-dependent) slight increase in vector localization to the heart observed for mCD8-AAV in this thesis is a reason for concern. As myocarditis (i.e. an inflammation of the heart muscle) has been observed in patients treated for Duchenne muscular dystrophy with AAVs [Ertl, 2022] and is a well-known issue in the wider field of immunotherapy [Axelrod et al., 2022], future experiments should carefully assess the nature of the heart signal observed in IVIS, both to determine whether it is a result of the transduction of heart-resident CD8+ cells or off-target transduction and to examine whether this transduction results in relevant inflammation.

The considerable differences in biodistribution between mCD8-AAV and the serotype 2 AAV from which it was derived are likely a direct consequence of the engineering approach employed for the former's targeting, which enables extraordinarily effective and cell type-selective gene transfer.

4.3.2   Gene Transfer Efficiency

Indeed, mouse CD8-AAVs are unusual among AAVs as they offer both cell-type selectivity, and, through the manner of their targeting, high transduction efficiencies. While serotype 8 vectors were shown to transduce murine lymphoid cells upon systemic injection [Breuer et al., 2020], this is a consequence of their broad tropism, which results in the transduction of most tissues, including brain, heart, lung, liver, kidney, spleen, skeletal muscle and testes, upon intranveous injection [Lang et al., 2019].

Relying on N-terminal insertion into VP2, the host laboratory of this thesis did pioneering work into the receptor-targeting of AAVs via DARPins (CHAPTER 1.3.2.2). While this much improved selectivity, transducing titers of the modified vector stocks were poor: At the same vg dose, N-terminally modified AAV2 targeted to hCD4 (CD4-AAV) displayed eightfold lower transduction efficiencies than parental AAV2 on human PBMCs. Notably, transduction efficiency was much improved when non-DARPin-displaying particles were removed from the vector stocks by immobilized metal ion affinity chromatography (IMAC). Use of such IMAC-purified CD4-AAV stocks resulted in higher transduction efficiencies than those observed for AAV2, both *in vitro* and *in vivo*. Such purification also further improved cell-type selectivity [Münch et al., 2015].

Crucially, mCD8-AAV, in the context of this thesis, achieved approximately six- to sevenfold higher vector genome-normalized transducing titers than AAV2 *in vitro* (CHAPTER 2.2.1) and up to two orders of magnitude higher *in vivo* signal (CHAPTER 3.3) without IMAC purification, indicating that insertion of the DARPin into the GH2/GH3 loop of VP1 results in improved DARPin display on the particle surface compared to N-terminal insertion; detailed and direct comparisons of the two insertion sites will soon be provided in the context of another target receptor [Günther & Buchholz, in preparation]. Additionally, like all approaches of rational design (CHAPTER 1.3), receptor-targeting of AAVs by binder insertion into the GH2/GH3 loop affords unparalleled modularity, facilitating thorough, multidirectional preclinical evaluation of the platform.

4.3.3   Vector Platform Modularity

While approaches of directed evolution have been used successfully to generate particle variants which improved tissue tropism, they do not generally offer the same flexibility as approaches of rational design. A case in point is the recent work of Nyberg and colleagues, who, by screening a library of AAV6 mutants with heptamer

insertions in the equivalent VR-IV loop on C57BL/6 splenocytes, identified the Ark313 variant, which bears a peptide interacting with the MHCI component QA2, enabling highly efficient transduction of murine lymphocytes. Expression of QA2, however, is substrain-dependent, with BALB/c-derived splenocytes being largely refractory towards transduction by Ark313 [Nyberg et al., 2023][6]. Furthermore, Ark313, although explicitly designed to enable syngenic murine models of *in vivo* gene therapy, strangely does not appear to have a human counterpart of similar efficiency and receptor-specificity; the generation of such a reagent would likely require the selection of yet another AAV6 variant.

Conversely, a human-targeted counterpart for mCD8-AAV is easily generated by replacing the MSE10 DARPin with one selective for human CD8α [personal communication, Zinser & Buchholz]. Similar interoperability has been demonstrated for lentiviral vectors in this thesis, as the inclusion of binders specific for mouse immune receptors, in the absence of any other alterations, generated mouse-targeted LVs whose behaviour closely resembled that of the human-targeted LVs from which they were derived.

By enabling, through its modular nature, the generation of pairs of vectors with similar properties - one vector targeted to a human receptor, the other to its murine counterpart - which in turn facilitate the thorough preclinical assessment of therapies in paired syngeneic and humanized models, receptor-targeting continues to drive the development of *in vivo* gene therapies beyond proof-of-principle.

> **Key Finding 3:**
>
> By redirecting particles, receptor targeting can improve both safety and efficacy of gene transfer. The impact of targeting on macro- and microscopic biodistribution can be assessed in immunocompetent mouse models, whose setup is facilitated by the modular nature of receptor targeting approaches.

---

[6]In this way, the variant is oddly reminiscent of early iterations of PHP.B family AAVs, which, through their affinity for a substrain-specific isoform of *Ly6a*, only enabled transduction across the blood-brain-barrier in one set of strains, i.a. C57BL/6, but not in another set, which included BALB/c mice [Hordeaux et al., 2018; Hordeaux et al., 2019; Huang et al., 2019].

4.4 Coda

Integrated models will likely not only be instrumental in furthering the preclinical characterization of receptor-targeted lentiviral vectors but also indispensable for the new class of DARPin-targeted AAVs (DART-AAVs) of which mCD8-AAV is the first published example [Michels et al., 2021]. Its unprecedentedly high rate and fidelity of gene transfer impressively demonstrate the ability of receptor-targeting to enable novel functionalities (KEY FINDING 3) and make it a prime candidate for new approaches of gene therapy, such as the *in vivo* generation of CAR T cells.

Still, future attempts to use mCD8-AAV for *in vivo* gene transfer in syngeneic models more refractory to transduction than Ai-based models might turn out to be as sobering as the attempts using LVs described in this thesis. In fact, considering the evidence collected and reviewed here and elsewhere [Michels et al., 2022], one might expect host immune responses to interfere with all approaches of *in vivo* gene therapy, regardless of the vector system used.

This prospect must not dishearten the reader, as it is important to remember that similar interference will likely occur in the clinical setting if appropriate mitigation procedures are not in place. In light of this, 'stubborn' immunoreplete mouse models offer a valuable opportunity to better understand the host response to vector administration and assess the utility of existing immunomodulatory approaches before human health is needlessly put at risk.

This thesis has demonstrated that such informative syngeneic models can be set up with relative ease, requiring only the adaptation of the vector-in-question's receptor tropism. Incidentally, insights from these models will not only help advance *in vivo* CAR therapy down its developmental trajectory, but likely contribute to making *in vivo* therapies for hematologic, cardiac, infectious, and developmental diseases a clinical reality, and thus to bringing about a new era of safe, effective and affordable genetic therapy.

Materials and Methods

5

5.1 Vector Generation

Molecular Cloning

To generate plasmids encoding MV HΔ18 glycoproteins targeted to murine CD4, the coding sequence of GK1.5-derived αmCD4 scFv was transferred from the retroviral targeting plasmid H21A-mCD4 (kindly provided by Inan Edes and Wolfgang Uckert, Berlin) to pHnse-Δ18mut-L3 [Anliker et al., 2010] via SfiI/NotI, generating pHnse-Δ18mut-L3-mCD4.

To generate LV transfer vector plasmids encoding GFP or αmCD19-CAR under various promoters, sequences of PGK, MCMV, and EF1α promoters [Michels et al., 2021] were amplified by PCR with primers 1 and 2 (PGK), 3 and 4 (MCMV), or 5 and 6 (EF1a) from pGL3-PGK (kindly provided by Arne Auste), pMCMV3 (Addgene: 85711), and pTN-CD20.CAR (kindly provided by Michael Hudecek, Würzburg, Germany), respectively (TABLE 5.1). Amplified promoters were cloned into the CAR transfer plasmids via EcoRI/BamHI, resulting in plasmids pPGK-CAR-W, pMCMV-CAR-W and pEF1a-CAR-W. In a second step, promoters were transplanted to GFP transfer plasmids via BamHI/SbfI, yielding pPGK-GFP-W, pMCMV-GFP-W and pEF1a-GFP-W.

To generate plasmids encoding mCD8-targeted AAV2 capsid proteins, MSE10 DARPin (Table S3, [Michels et al., 2021]) was amplified by PCR from lentiviral envelope plasmid using primers 7 and 8 (TABLE 5.1). Amplified DARPin was cloned into an intermediate plasmid from which an insert containing the DARPin and the mutations knocking out the HSPG binding site (R585>A, R588>A) was cloned into pRC_RR_VP1_r1c3 (Addgene: 65724) by BsiWI/XcmI, generating pRC-αmCD8.

To generate a self-complementary AAV transfer plasmid encoding cre recombinase with an SV40 nuclear localization signal (pscAAV-cre), the GFP ORF in pscAAV-SFFV-GFP was exchanged for NLS-cre from a lentiviral NLS-cre-encoding transfer plasmid via SbfI/AscI.

Production of Lentiviral Vectors

LentiX-293T cells (Takara Bio) and β2M$^{-/-}$, CD47^{high} HEK293T cells (kindly provided by Michela Milani & Alessio Cantore, Milan, Italy) were cultivated in DMEM High Glucose (Sigma-Aldrich, D6546; Biowest, L0615-500) supplemented with 10% fetal bovine serum (FBS, Sigma, F7524) and 2 mM glutamine (Sigma, G7513) at 37°C, 5% CO_2, 90% relative humidity and subcultured twice a week at ratios between 1:8 and 1:10 using 0.25% trypsin in 1 mM EDTA-PBS without Ca^{2+} or Mg^{2+}.

RT-LVs were produced based on the protocol for the generation of LVs pseudo-typed with paramyxoviral glycoproteins established in the host laboratory [Weidner et al., 2021]. Production cells (β2M$^{-/-}$, CD47^{high} HEK293T for mCD4-LV-PGK-CAR and mCD8-LV-PGK-CAR, see **TABLE 2.1**) were transfected with the pHnse-Δ18mut-L3-MSE10/pHnse-Δ18mut-L3-mCD4 and pCG-FΔ30 [Funke et al., 2009] envelope plasmids, the transfer plasmid, and the packaging plasmid pCMVd8.9 (Addgene: 2221) in a 7.7:23:87:83 ratio. For VSV-LV production, VSV G envelope (pMD2.G, Addgene: 12259), transfer, and packaging plasmid were transfected in a ratio of 35:100:65. Supernatants harvested 36-48 h after transfection were clarified by 0.45 μm filtration. Filtrates were treated with Pierce Universal Nuclease (Thermo Fisher Scientific, 88702) at 50 U/mL for 30-60 min at 37°C. Particles were puri-fied and concentrated 150- to 500-fold into PBS from the clarified supernatant by overnight centrifugation through a 20% sucrose cushion at 4,500 x g and 4°C. Concentrated stocks were aliquoted and stored at -80°C.

Production of Adeno-Associated Vectors

AAV2 and mCD8-AAV particles were generated by transient transfection of HEK293T cells (cultivated ad subcultured as described in the section above). 24 h prior to transfection, 1.8E7 HEK293T cells were seeded per 14 cm dish. On the day of transfection, the cell culture medium was replaced by 12 mL DMEM High Glucose with 15% fetal calf serum and 2 mM L-glutamine. For the transfection mix, 30 μg of total DNA per dish were mixed in 2 mL of DMEM without additives, vortexed, and added to 1.9 mL DMEM supplemented with 120 μL of 18 mM polyethylenimine solution. For production of AAV2, helper plasmids pXX6-80 [Xiao et al., 1998], packaging plasmid pRC22 (Addgene: 104963), and the self-complementary transfer vector pscAAV-SFFV-GFP [Münch et al., 2013] were mixed in a ratio of 60:20:20. For production of mCD8-AAV, pXX6-80, and pscAAV-SFFV-GFP, the complementary capsid plasmid pRC-VP1-KO and pRC-mCD8 were mixed in a ratio of 15:5:5:5. The mixture was vortexed vigorously and incubated for 20 min at room temperature. A

total of 4 mL of transfection mix per dish was added to the HEK293T cells. Medium was changed after 5 h to 18 mL of DMEM supplemented with 10% FBS and 2 mM L-glutamine.

48 h after transfection, cells were scraped off, pelleted (1,800 xg, 30 min, 4°C) and lysed using Tris-HCl/NaCl (pH 8.5). Four freeze-and-thaw cycles in liquid nitrogen were conducted followed by a Benzonase treatment (50 U/mL cell lysate; Sigma-Aldrich, E1014-25KU) for 30 min at 37°C. Lysate was clarified (3,700 xg, 20 min, 4°C) before loading onto an iodixanol gradient [Reul et al., 2019]. The gradient was centrifuged for 2 h at 290,000 xg in a 70Ti rotor (Beckman Coulter), and AAV particles were harvested from the 40% iodixanol layer. For mCD8-AAV-cre and AAV2-cre (see **Table 2.2**), buffer was exchanged to PBS by centrifugation in Amicon Ultra-4 50 kDa cut-off size exclusion filters (Millipore, UFC805096) at 2000 xg. Stocks were aliquoted and stored at -80°C.

5.2 Biophysicochemical Particle Characterization

AAV Genome Copy qPCR

Three microliters of purified vector stock were used for DNA extraction using the DNeasy Blood & Tissue kit (QIAGEN, 69506). Genomic AAV vector titers were determined via ITR-specific qPCR using primers 14, 15, and probe 16 (**Table 5.1**) with the LightCycler 480 Probes Master mix (Roche, 04707494001) on a LightCycler 480 Real-Time PCR System (Roche). The transfer cassette from pssAAV-hSyn-eYFP transfer plasmid [Hartmann et al., 2019], isolated by PvoII-XmnI digest and gel purification, served as a standard.

Nanoparticle Tracking

Particle numbers were determined by nanoparticle tracking analysis using the NanoSight NS300 system (Malvern Instruments) and detection via a green laser. For this, LV stocks were diluted in 0.2 μm-filtered DPBS (Lonza, BE17-512F) to achieve approximately 30-90 particles/ frame. A continuous flow protocol was used. Size mode and concentration data are from technical quadruplicates. For each vector stock, four 60-90 s videos were recorded and analyzed sequentially. The size modes reported in **Figure 2.1b**, per the standard operating procedure at the time, were derived from finite track length-adjusted (FTLA) plots fitted to size distribution data determined from 60 s measurements. Later during the course of the thesis,

distribution data were smoothed not through FTLA calculation, but by increasing measurement times to 90 s per replicate. Accordingly, size modes reported in FIGURES 3.1 and 3.6 were derived from raw data plots[1].

Western Blotting

AAV2 stocks were incubated in urea buffer (200 mM Tris/HCl [pH 8.0], 5% SDS, 8 M urea, 0.1 mM EDTA, 2.5% DTT, 0.03% bromophenol blue) at 95°C for 10 min and loaded on 10% SDS-PAGE gels. After electrophoretic separation, proteins were blotted on nitrocellulose membranes (Amersham, 10600004). Membranes were incubated with anti-AAV VP1/VP2/VP3 rabbit polyclonal antibody at a dilution of 1:50 (Progen, 65158) overnight at 4°C followed by an incubation with the polyclonal rabbit anti-mouse immunoglobulin HRP conjugate at a dilution 1:2,000 (Agilent, P0260) for 90 min at room temperature. After application of Chemiluminescent Peroxidase Substrate (Sigma-Aldrich, CPS160-1KT), luminescent signals were detected on the chemiluminescence reader MicroChemi (DNR Bio-Imaging Systems). All antibodies were diluted in TBS-T (50 mM Tris/HCl, 150 mM NaCl, 0.1% Tween-20 [pH 7.4]) containing 2% powdered milk.

5.3 Functional Experiments

Mice & *In Vivo* Gene Transfer

Mice were kept in individually ventilated cages under specific pathogen-free conditions. All animal experiments were performed and documented in accordance with the regulations of the German animal protection law and the respective European Union guidelines. Each animal experiment was pre-registered with and monitored by the Darmstadt regional administrative council (Regierungspräsidium).

Short-Term Biodistribution of GFP-Transferring LVs in BALB/ Mice

Twenty-two male BALB/cAnNCrl mice were purchased from Charles River (028BALB /c). One was sacrificed before the start of the experiment; splenocytes isolated

---

[1]It should be noted that raw data and FTLA plots from the same measurement yield slightly different size modes. In a direct comparison on three preparations of VSV-LV, differences in size modes between raw data and FTLA plots ranged from 0.7 to 2.9 nm. This is no reason for concern, as size modes of aliquots of the same VSV-LV stock were found to vary by up to 4 nm between measurements.

TABLE 5.1: Primers.

Primer	No.	Sequence (5' to 3')[a]
PGK fw	1	ctgcaggaattcCGAGCTCTTACGCGTGCTAGC
PGK rev	2	ctgcagggatccCCAAGCTTACTTAGATCGCAGATCCTGG
MCMV fw	3	ctgcaggaattcATTACTGGCACGTATACTGAGTCATTAGG
MCMV rev	4	ctgcagggatccGCAGCGAGGAGCTCTGCGTTCT
EF1a fw	5	ctgcaggaattcGGATCTGCGATCGCTCCGGT
EF1a rev	6	ctgcagggatccCTAGCCGTAGGCGCCGGTCAC
MSE10 fw	7	AAAAGGCCCAGCCGGCCAAG
MSE10 rev	8	ACTAGTCGCACCGCCACCGCCCGCTGCTGCCTTTTGCAGCAC
WPRE fw	9	CGCTTTCCCCCTCCCTATTG
WPRE in	10	6-FAM[b]-ACAGGGGCTCGGCTGTTGGGCACTGACA-BHQ[c]-1
WPRE rev	11	TGATTTCCCCGACAACACCA
Alb fw	12	GGATGACTTTGCACAGTTCCT
Alb rev	13	CCAGAGAGCTACACCTGACC
ITR fw	14	GGAACCCCTAGTGATGGAGTT
ITR rev	15	CGGCCTCAGTGAGCGA
ITR in	16	6-FAM-CACTCCCTCTCTGCGCGCTCG
Alb fw	17	CGGAGCAACTGAAGACTGTCA
Alb in	18	HEX[d]-TGTTGCAAGGCTGCTGACAAGGACACCTGC-BHQ1
Alb rev	19	ACCACGTGCACAGAAAATGG

[a] Capitals indicate template-complementary sequence, small capitals indicate non-complementary sequence (containing e.g. restriction sites);
[b] (6-FAM) 6-carboxyfluorescein;
[c] (BHQ-1) Black Hole Quencher 1;
[d] (HEX) Hexachlorofluorescein;

from it were used to assess functionality of the vector stocks meant for *in vivo* testing (FIGURES 3.1 & 3.2). One day prior to vector injection, the remaining 21 mice received 200 ng/ animal of human IL7 (Miltenyi Biotec, 130-095-361) in DPBS (Lonza, 17-512F) via tail vein injection at a total volume of 50 μL/ animal. Some intravenous injections were (partially) unsuccessful, with nine animals receiving some (4 animals) or all (5 animals) of the cytokine dose subcutaneously. Accordingly, equally sized groups (7 animals/ group) for vector injection were assigned based on the quality of IL7 injection, such that each group contained approximately the same number of subcutaneously and intravenously injected animals. Each animal received, via tail vein injection, 200 μL of PBS-based mix containing 200 ng/ animal of human IL7 and either 1.0E10 particles/ animal of mCD4-LV-PGK-GFP, 1.3E10 particles/ animal of mCD8-LV-PGK-GFP or no vector. Six days after vector injection, animals were sedated via isofluorane inhalation, bled from the retroorbital nexus and subsequently euthanized by cervical dislocation. Spleens, bones and liver were harvested for processing.

LV-Mediated CAR Transfer in BALB/c Mice

Four and one day before vector administration, fourteen male BALB/cAnNCrl mice (Charles River, 028BALB/c) were injected subcutaneously (i.e. into a skinfold at the neck) with 200 ng/ animal of human IL7 in DPBS (50 µL/ animal). Drops of peripheral blood were taken from the retroorbital nexus on doi -5, +2 +9, +16, +23, +30 and +44; nucleated cells were analyzed by flow cytometry. Animals were grouped for vector injection based on the levels of CD19+ cells observed on doi -5, such that each group contained a roughly similar distribution of peripheral blood CD19+ levels. Mice received either a mix of mCD4-LV-PGK-CAR (0.9E10 particles/ animal) and mCD8-LV-PGK-CAR (0.8E10 particles/ animal) in a volume of 200 µL/ animal or PBS via tailvein injection. On doi +50, mice were sedated via isofluorane inhalation, bled from the retroorbital nexus and subsequently euthanized by cervical dislocation. Spleens were harvested for processing.

AAV Biodistribution in Ai9 Reporter Mice

Female Ai9 mice (Jackson Laboratories, 007909) received tailvein injections of 1.7E11 vg/ animal of AAV2-cre or mCD8-AAV-cre in 130 µL/ animal of DPBS. Fourteen days later, mice were sedated via isofluorane inhalation, bled from the retroorbital nexus and subsequently euthanized by cervical dislocation. Liver, lung, heart, kidney, thymus, and spleen were removed, arranged on the back of a black-plastic 96-well plate and whole-organ fluorescence was measured using an IVIS Spectrum (Perkin Elmer) in epifluorescence mode (Ex 535 nm, Em 600 nm, 1-60 s exposure, subject height 1.5 cm). Nucleated cells were isolated from spleens, bones and blood.

Isolation of Primary Murine Cells

Splenocytes and Splenic Pan T Cells

After extraction, mouse spleens were transferred to 5 mL of TCM (consisting of RPMI 1640 (Sigma, R0883) supplemented with 10% FBS, 2 mM L-glutamine, 1× NEAA (Gibco, 11140-050), 1× sodium pyruvate (Gibco, 11360-070), 25 mM HEPES (Sigma, H3537), penicillin-streptomycin, and 50 µM β-mercaptoethanol). Next, cell suspensions were generated by grinding the spleens through 70 µm cell strainers (Thermo Fisher Scientific, 352350) using the back sides of syringe plungers. Strainers were rinsed several times with TCM from the respective well, using 1 mL per rinse. The cell

suspension was homogenized by pipetting with a 1 mL micropipette, then transferred to 15 or 50 mL Falcon tubes; optionally, 5-8 mL of TCM were added. Tubes were then centrifuged (3-400 x g, 4°C or RT[2], 5 min) and supernatant was removed. Red blood cell lysis was performed by resuspending cell pellets in 5 mL of 1x Pharm Lyse (from 10x, Becton Dickinson [BD], 555899) ammonium chloride-based lysis buffer and incubating for 6 min at room temperature. Lysis was stopped by two consecutive washes with 8 and 13 mL of TCM or DPBS, respectively. Cell pellets were then resuspended in 5 mL of TCM/PBS. Splenic Pan T cells were isolated from splenocytes via the Mouse Pan T Cell Isolation Kit II (Miltenyi Biotec, Ref 130-095-130), using MS Columns (Miltenyi Biotec, 130-042-201), following the manufacturer's protocol.

Peripheral Blood Nucleated Cells

From the lithium heparin tubes into which they were collected, blood samples were transferred to 15 mL tubes, centrifuged (3-400 x g, RT, 5 min) and the supernatant (i.e. the plasma) was discarded. Pellets were resuspended in 10 mL of lysis buffer and incubated for 10 min, then centrifuged (3-400 x g, RT, 5 min). Importantly, for blood, lysis was only stopped after centrifugation by removal of the supernatant and resuspension of pellets in 10-13 mL of PBS. Samples were then washed again with 10-13 mL of PBS. Subsequently, pellets were resuspended in 1 mL/ tube of PBS.

Bone Marrow Cells

Bones for marrow extraction usually comprised femur, tibia and ilium (one set or both). Using scalpels, remaining tissue was cleaned off the bones as completely as possible, and bone ends were clipped off. Clean, opened bones were transferred into 0.5 mL tubes, the bottom of which had previously been pierced with a needle. Bone-laden 0.5 mL tubes were then stuck into 1.5 mL tubes, 50 μL/ tube of PBS were added and tubes were centrifuged to remove the marrow from the bones (7E3 rpm, 3 min, RT). Empty bones and supernatants were discarded and cell pellets were resuspended in 1 mL of PBS. Cell material was passed through 70 μm strainers and pelleted (3-400 x g, RT, 5 min). Pellets were resuspended in 2 mL/ tube of lysis buffer. After 15 min of incubation at RT, PBS was added to a final volume of 13 mL/ tube to

---

[2]Often when few spleens were processed at a time for *ex vivo* purposes, spleens were collected into ice-cold TCM, centrifuged in pre-cooled centrifuges and kept on ice whenever not handled. For final analyses however, this was found to be impractical due to the number of samples requiring parallel processing. Instead of subjecting the samples to temperature fluctuations, all tissues were collected into room temperature medium and handled as well as centrifuged at room temperature. Samples were then only cooled once they had been distributed for staining.

stop the lysis. Cell material was then washed twice with 13 mL/ of PBS and finally resuspended in 10 mL of the same.

Liver Cells

Liver was dissociated using the Liver Dissociation Kit, mouse (Miltenyi Biotec, 130-105-807) and Gentle MACS Octo dissociator (Miltenyi Biotec) following the manufacturer's instructions. After completion of the dissociation program, material was passed through $100\,\mu$m strainers into 50 mL Falcons containing 5 mL of DMEM with L-glutamine (see p. 78). Tubes were centrifuged (400 x g, RT, 5 min), supernatant was discarded and pellets were resuspended in 2 mL of lysis buffer. After 15 min at RT, lysis was stopped by addition of 8 mL/ tube of DMEM with glutamine and the cell material was pelleted (3-400 x g, RT, 10 min). The pellets were then resuspended in 10 mL/ tube of DMEM with glutamine.

Cell Counting & Viability Determination

When cells were extracted from one or few spleens or blood samples for *ex vivo* experiments, cell count and viability were determined using the LUNA-FL Automated Fluorescence Cell Counter (Logos Biosystems, L20001), LUNA Cell Counting Slides (Logos Biosystems, L12001), and acridine orange/propidium iodide dye (Logos Biosystems, F23001). When many organs were processed in parallel, i.e. when they were processed during the final analysis of an *in vivo* setup, cell count and viability of samples in 96-well V-bottom plates were determined using the automated staining function of a MACSQuant Analyzer 10 (Miltenyi Biotec) and propidium iodide solution (Miltenyi Biotec, 130-093-233).

Freezing

Cells were frozen by pelleting (3-400 x g, 5 min) followed by resuspension in FBS (Sigma-Aldrich, F7524) containing 10% v/v DMSO (Sigma-Aldrich, D8418-100ML) to a final concentration of approximately 1E6 to 1E7 cells/mL and transferred to -80°C in isopropanol-filled freezing vessels. Cells were transferred to liquid nitrogen vapor phase storage 1 to 7 d later.

Transduction & Culture of (Primary) Cells

For the transductions described in Figures 2.2, 2.7, 2.8 and 3.2, mouse splenocytes or Pan T cells were activated and transduced on the day of thawing (or isolation). 4E4 cells/well (50 μL per well) were mixed in TCM with recombinant human (rh) IL7 (Miltenyi Biotec, 130-095-361), rhIL15 (Miltenyi Biotec, 130-095-764), and 4E4 αmCD3/αmCD28-beads/well (Invitrogen, 11456D) and seeded into wells of 96-well plates. Vector stocks were diluted in TCM, and 50 μL/well of vector-containing supernatant was added to the cells, resulting in final cytokine concentrations of 25 U/mL for rhIL7 and 50 U/mL for rhIL15. For LV transduction, cells were spin-fected (1.5 h, 800 x g, 32°C). AAV-transduced cells were incubated for 5–6 h at 37°C. Afterward, 100 μL/well of TCM containing 25 U/mL of rhIL7 and 50 U/mL of rhIL15 were added.

The transduction of Ai9 splenocyte with AAVs described in Figures 3.11 & 3.12 differed from the procedure recounted above in that cells were directly seeded in 100 μL/ 96-well of TCM with cytokines and dynabeads, to which in 100 μL/ 96-well of (vector-containing) plain TCM were added. After vector addition, cells were incubated at 37°C without manipulation until measurement.

Cells of the murine T cell 58m8ab line (kindly provided by Inan Edes and Wolfgang Uckert, Berlin) were kept in T25 flasks in 10 mL of TCM at 37°C, 5% CO_2, 90% relative humidity and subcultured twice a week at ratios between 1:8 and 1:15. 58m8ab cells were transduced in plain TCM (i.e. TCM w/o cytokines or dynabeads). For the detection trial described in Figure 3.7a, 5E4 cells/ 48-well were treated with the indicated amounts of LV, which were dispersed in the well volume by subsequent thorough pipetting. One day after vector addition, cells were washed: Well-content was taken up in 4.6 mL/ well of TCM, transferred to a 50 mL tube and spun (300 x g, 5 min). Supernatant was removed, pellets were resuspended in 400 μL/ pellet of TCM and transferred back to 48-wells. For the titration described in Figure 3.7bc, 1E4 58m8ab cells in 50 μL of TCM per 96-well were mixed with 50 μL/ well of vector dilution in TCM. One day after vector addition, cell material was pelleted in V-bottom plates (300 x g, 5 min), supernatant was removed, pellets were resuspended in 200 μL/ well of TCM and the cells were transferred back to flat-bottom plates.

In Situ Target Cell Ablation Assay

A20 cells (ATCC, Manassas, VA, USA; TIB-208) were cultured in T25 flasks in 10 mL of RPMI 1640 supplemented with 10% FBS, 2 mM L-glutamine, and 50 μM

β-mercaptoethanol at 37°C, 5% CO_2, 90% relative humidity subcultured thrice a week at ratios between 1:5 and 1:20. Three days before the assay, medium was changed to TCM.

A20 cells were stained using the CellTrace Violet Cell Proliferation Kit (Thermo, C34557) following manufacturer's instructions. Cultures supplemented with hIL7, either only containing 4E4 BALB/c splenocytes per 96-well or containing a mix of 4E4 BALB/c splenocytes and 4E3 CellTrace-stained A20 cells per well, were set up. Vector stocks were treated with DNase I (Ambion, AM2222) following the manufacturer's instructions. Vectors were then diluted in TCM and 50 μL/ well of vector-containing TCM or plain supernatant were added to the cells, resulting in a final IL7 concentration of 25 U/mL. Cultures were then spinfected (1.5 h, 800 x g, 32°C). Afterwards, 100 μL/well of TCM containing 25 U/mL of rhIL7 were added before cell material was transferred from flat- to U-bottom plates and incubated for two days.

Treatment of Whole Blood for *Ex Vivo* Assays

Whole Blood Transduction

Blood from CAC BALB/cAnNCrl mice was collected in lithium heparin tubes (BD, 365966), and 150 μL/ well were transferred into wells of 48-well plates. Recombinant human IL7 was added to each well to a final concentration of 25 U/ mL together with 2E10 LV particles per well (or an equivalent volume of Dulbecco's phosphate-buffered saline (DPBS, Lonza)). Blood was incubated on a horizontal shaker (INFORS HT, throw 25 mm) at 180 rpm at 37°C, 5% CO_2, 90% relative humidity for 6 h. Afterward, erythrocytes were eliminated by Histopaque centrifugation. Samples were diluted with 1 mL each of room-temperature DPBS and layered onto 1 mL of room temperature Histopaque 1083 (Sigma-Aldrich, 10831-100ML) in 15 mL tubes. Tubes were centrifuged at 400 x g, room temperature, for 30 min. After centrifugation, all material above the Histopaque plug was collected (as indicated in FIGURE 2.3). The material was washed once with 10 mL of PBS (300 x g, 10 min, room temperature). Pellets were resuspended in 1 mL of DPBS, and cell numbers were determined using the Luna Fl. Cells were activated using rhIL7+15 as well as αmCD3/αmCD28-beads (as described in the section above) and seeded into 96-well plates at approximately 3E4 cells/ well (200 μL per well). Cells were incubated at 37°C, 5% CO_2, 90% relative humidity for 5 days prior to analysis.

Whole Blood Binding

Blood from BALB/cAnNCrl mice was collected in lithium heparin tubes, and $100\,\mu$L/ well were transferred into wells of 48-well plates[3]. Lentiviral vector (or an equivalent volume of DPBS) was added to a dose of 1E10 particles/ well and dispersed in the blood by careful horizontal shaking. Blood was incubated on a horizontal shaker (TiMix 2, Edmund Bühler, 3 mm throw) at 400 rpm at 37°C, 5% CO_2, 90% relative humidity for 2 h. Afterward, erythrocytes were eliminated by Histopaque centrifugation. Samples were diluted with 1 mL each of room-temperature DPBS and layered onto 1 mL of room temperature Histopaque 1083 (Sigma-Aldrich, 10831-100ML) in 15 mL tubes. Tubes were centrifuged at 400 x g, room temperature, for 30 min. After centrifugation, the phase thought to contain mononuclear cells was collected. The material was washed with 5 mL of PBS/ tube (400 x g, 10 min, room temperature) and subsequently transferred to micronic tubes for staining.

Immunostaining and Flow Cytometry

Immunostaining for flow cytometry was performed in the 96-tube format in 1.4 mL round-bottom tubes (Micronic, MP32022). Wash buffers were used cold (4°C). For washes, cells were centrifuged at 300-400 x g, 4°C for 5 min. After centrifugation, supernatant was removed using a multichannel aspirator with a spacer, leaving 100–$200\,\mu$L of dead volume. After removal of supernatant, pellets were resuspended by 1–3 s of vortexing. To determine immune phenotype and transgene positivity, cell suspensions were washed two to three times with 400-500 μL of wash buffer (2% FBS, 0.1% sodium azide, 1 mM EDTA in PBS) per wash per tube. Subsequently, $1\,\mu$L of mouse FcR blocking reagent (Miltenyi Biotec, 130-092-575) in $20\,\mu$L of wash buffer was added to each tube to block unspecific FcR-mediated binding of antibodies. Cells were vortexed and incubated for 10 min at room temperature before antibody cocktails in wash buffer were added to the cells at $20\,\mu$L/ tube (**TABLE 5.2**). After 3–5 s of vortexing, cells were incubated at 4°C for 30–45 min. When use of a secondary antibody was necessary (**FIGURE** 3.7), cells were washed an additional three times after completion of the primary antibody incubation, and $20\,\mu$L/ tube of secondary staining mix were added before the samples were incubated for another 30 min at 4°C. Cells were then washed two to three times before cell pellets were resuspended by vortexing in $200\,\mu$L of 0.5% formaldehyde in PBS[4]. Samples were

---

[3]Notably, due to suboptimal sampling, the volume of whole blood obtained from mouse 1 was insufficient. Accordingly, blood from mouse 1 was diluted 2:5 with warm DPBS before distribution to wells.

[4]To avoid quenching of tdT by the fixative, samples from cre-transfer experiments were left unfixed and measured on the day of staining.

kept in the dark at 4°C until measurement. Flow cytometry was performed on a MACSQuant Analyzer 10 (Miltenyi Biotec), and data were analyzed using FCS Express 6 (De Novo Software). Where appropriate, isotype or full minus one controls were used to inform gating decisions. Single stain controls were prepared from UltraComp eBeads Plus (Thermo, 01-3333) to enable *post hoc* compensation.

LV Vector Copy Number qPCR

Genomic DNA (gDNA) was extracted in the 96-well format using DNeasy 96 Blood & Tissue Kit (QIAGEN, 69581) following the manufacturer's instructions. gDNA was eluted into AE buffer. To determine lentiviral VCNs, quantitative real-time PCR was performed on a LightCycler 480 II Real-Time PCR System (Roche, Basel, Switzerland) using primers against WPRE and murine albumin (*Alb*).

The VCNs displayed in FIGURES 2.2 and 2.3 were obtained using $0.5\,\mu$M primers 9, 11, 12 and 13 (TABLE 5.1) in twenty microliter reactions containing $8\,\mu$L of template and using QuantiTect SYBR Green PCR Mix (QIAGEN, 204143). A standard for WPRE was generated by serial dilution of pSEW-GFP lentiviral transfer plasmid [Demaison et al., 2002] in AE buffer. An *Alb* standard was generated by extracting gDNA from 1E6 to 1E2 58m8ab cells. The thermocycling program comprised initial activation (95°C, 15 min), followed by 45 cycles of denaturation (94°C, 15 sec), annealing (58°C, 30 sec) and extension (72°C, 30 sec) as well as a melt curve ramp starting at 50°C.

VCNs in FIGURES 3.4 & 3.10 and SUPPLEMENTARY FIGURES 6.1 & 6.2 were determined using primers 9, 11, 17, 19 and probes 10 and 18 (TABLE 5.1) at final concentrations of $0.5\,\mu$M and $0.2\,\mu$M, respectively, using LightCycler 480 Probes Master Mix (Roche, 04887301001). The thermocycling program comprised initial activation (95°C, 10 min), followed by 45 cycles of denaturation (95°C, 10 sec), annealing (60°C, 40 sec) and extension (72°C, 1 sec) and subsequent cooling to 40°C.

For FIGURE 3.4 and SUPPLEMENTARY FIGURE 6.1, $25\,\mu$L reactions containing $10\,\mu$L of template/ well were set up. An optimized standard for WPRE was made by serially diluting pPGK-GFP-W lentiviral transfer plasmid in AE buffer and supplementing 750 genomes/ reaction of gDNA from the human Nalm6 B cell line[5]. An *Alb* standard was generated by extracting gDNA from varying quantities of 58m8ab cells. To increase the WPRE content per reaction, gDNA as well as plasmid samples were concentrated approximately 1.3-fold by SpeedVac.

Quantitative PCR results shown in FIGURE 3.10 and SUPPLEMENTARY FIGURE 6.2

---

[5]Human gDNA was added as a carrier in the hope that an increased DNA content of the low-copy WPRE standard samples would improve their amplification curves, i.e. reduce curve flattening.

TABLE 5.2: Antibodies and viability dye used in flow cytometry.

Figure	Antibody/ dye	Manufacturer, ID	µL/ sample
2.2, 2.3, 2.7, 3.2	αCD3-BV421	Becton Dickinson, 564008	1
	αCD8a-PerCP-Cy5.5	Becton Dickinson, 561109	1
	αCD4-APC	Becton Dickinson, 561091	1
	eFluor 780	Thermo Fisher, 65-0865-14	0.12
2.8, 3.11, 3.12	αCD8a-PerCP-Cy5.5	see above	1
	eFluor 780	see above	0.12
2.4, 2.5	αCD19-VioBlue	Miltenyi Biotec, 130-118-463	1
	αNKp46-BV510	Becton Dickinson, 563455	1
	αCD11b-FITC	BioLegend, 101205	1
	αHis-PE	Miltenyi Biotec, 130-092-691	1
	αCD8a-PerCP-Cy5.5	see above	1
	αCD3-APC	Miltenyi Biotec, 130-122-943	1
	eFluor 780	see above	0.2
2.6	αCD19-VioBlue	see above	2
	αc-myc-FITC	Miltenyi Biotec, 130-116-485	1
	αCD8a-PerCP-Cy5.5	see above	1
	eFluor 780	see above	0.12
3.5	αCD19-VioBlue	see above	2
	αCD3-PE	Becton Dickinson, 555275	1
	αCD8a-PerCP-Cy5.5	see above	1
	αCD4-APC	see above	1
	eFluor 780	see above	0.2
3.7	1. recombinant mCD19-Fc	R&D, 9730-CD-050	1.14^a / 0.3^b
	2. αmIgG2ab-FITC	Miltenyi Biotec, 130-119-149	2^a / 1^b
	or αc-myc-FITC	see above	1
	eFluor780	see above	0.2
3.9, 3.10	αCD3-BV421	see above	1
	αc-myc-FITC	see above	2
	αCD19-PE	Miltenyi Biotec, 130-123-272	2
	αCD8a-PerCP-Cy5.5	see above	1
	αCD4-APC	see above	1
	eFluor 780	see above	0.2
3.15, 3.16	αCD19-VioBlue	see above	1.5
	αCD4-VioGreen	Miltenyi Biotec, 130-118-696	1.5
	αCD8a-PerCP-Cy5.5	see above	1.5
	αCD3-APC	see above	1.5
	eFluor 780	see above	0.2

[a] FIGURE 3.7A;

[b] FIGURE 3.7BC;

are based on $15\,\mu$L reactions containing $6\,\mu$L of template. Unspiked serial dilutions of pPGK-CAR-W served as WPRE standard material and gDNA isolated from 5E6-5E3 A20 mouse B cells was used to establish an *Alb* standard curve.

5.4 Analysis and Visualization

Illustrations

Cartoons (e.g. workflow/ literature summaries, approximations of genetic and particle structures) were generated using Adobe Illustrator version 25.4.1.

Protein Structure Visualizations

The structures of DARPin-modified MV envelope proteins in FIGURE 2.1 and a DARPin-decorated AAV particle in FIGURE 2.7 were approximated using the indicated PDB structures and UCSF Chimera 1.13.1. Spacing of unstructured domains was estimated using α-helical peptides of appropriate length. The structure of AAV VP with a DARPin insertion in the GH2/GH3 loop in FIGURE 1.2 was predicted using ColabFold [Mirdita et al., 2021] and visualized in UCSF Chimera.

Image Analysis

Mean gray values of organ surface fluorescence in fluorescence images generated during *in vivo* imaging (p. 60) were determined using (Fiji Is Just) ImageJ version 1.53c.

Statistics and Graphing

Statistical analyses were carried out in GraphPad Prism version 9.2.0. Tested flow cytometry signals were assumed to be normally distributed. Data generated from cells of the same mouse were handled as matched data.

Supplementary Materials

A

Alb copies/ reaction

spleen   blood   bone marrow   liver
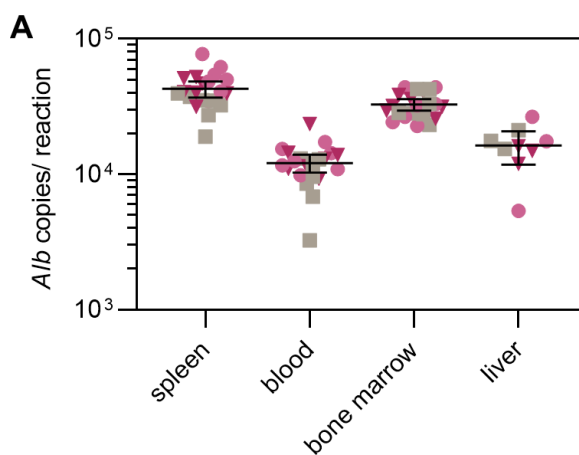
SUPPL. FIGURE 6.1: Uniformity of qPCR input (related to FIGURE 3.4C)
A Samples from mice treated with mCD4-LV-PGK-GFP (pink circles), mCD8-LV-PGK-GFP (red triangles) or PBS (grey squares) were analyzed by qPCR. As a measure for the uniformity of sample deposition and DNA extraction, *Alb* copies per qPCR reaction are plotted for four tissues. Symbols represent arithmetic means of technical triplicates from n = 7 mice/ group (total: 21 mice) for spleen, blood and bone marrow and n = 3 mice/ group (total: 9 mice) for liver. Solid lines are arithmetic means. Error bars represent 95% confidence intervals (CIs).
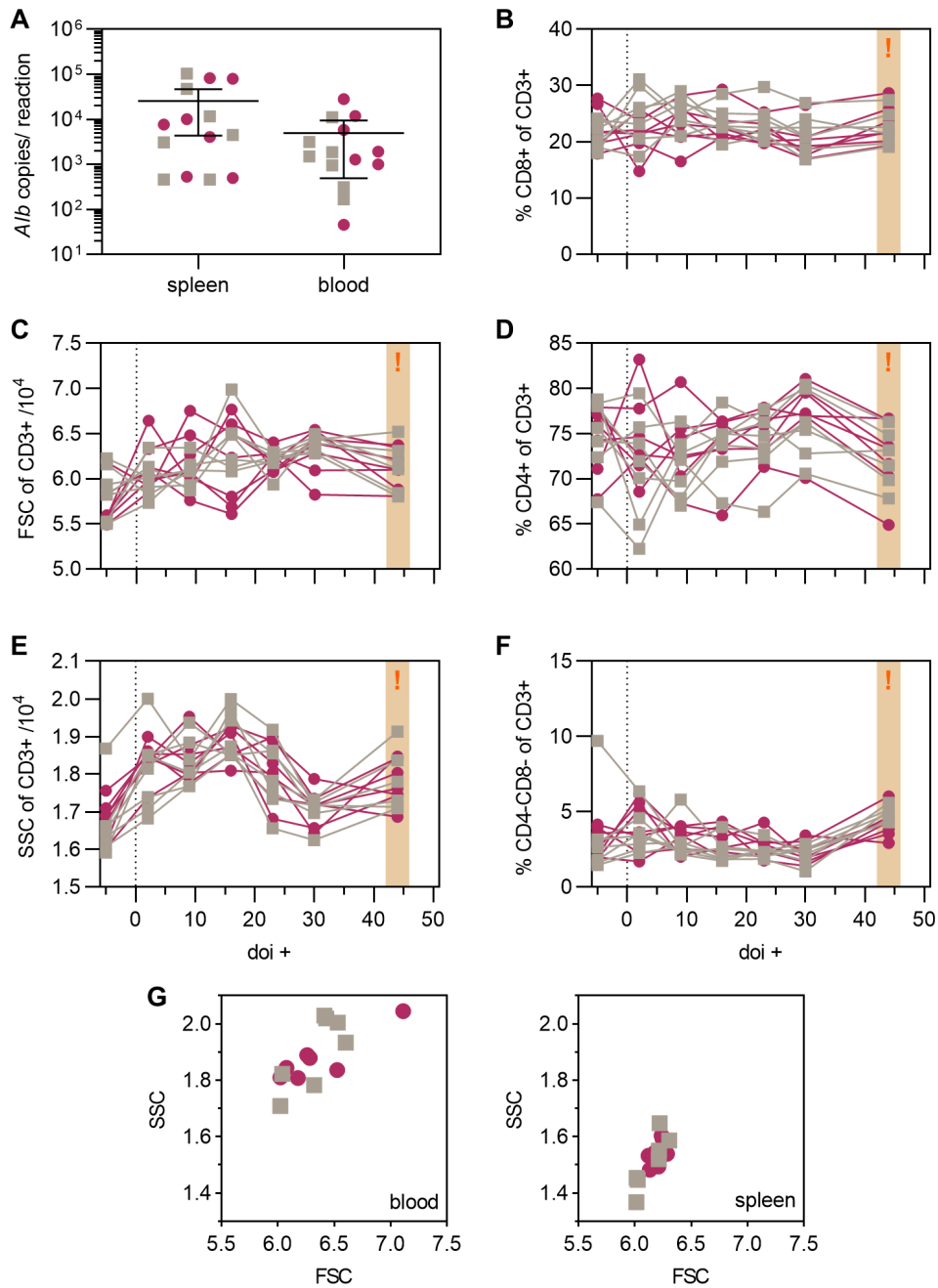
SUPPL. FIGURE 6.2: qPCR input and additional metrics (related to FIGURES 3.9 & 3.10)
A Samples from mice treated with MIX (red ●) or PBS (grey ■) were analyzed by qPCR. As a measure for the uniformity of sample deposition and DNA extraction, *Alb* copies per qPCR reaction are plotted for two tissues. Symbols represent arithmetic means of technical triplicates from n = 7 mice/ group (total: 14 mice). Solid lines are arithmetic means. Error bars represent 95% confidence intervals (CIs). **B-F** Additional flow cytometry metrics from peripheral blood. Symbols represent data from n = 7 mice/ group. **C** FSC and **E** SSC of CD3+ viable singlets from peripheral blood. Arithmetic means of viable T cells' scatter parameters are plotted. **BDF** Frequencies of **B** CD8+, **D** CD4+ and **F** CD4-CD8- cells among viable singlets. Cave: A mistimed vortex step during sample processing on doi +44 resulted in cross-contamination of unknown extent (ocre bars, orange exclamation marks). **G** FSC and SSC of CD3+ viable cells from blood and spleen at final analysis. Symbols represent arithmetic means of viable T cells' scatter parameters from n = 7 mice/ group.
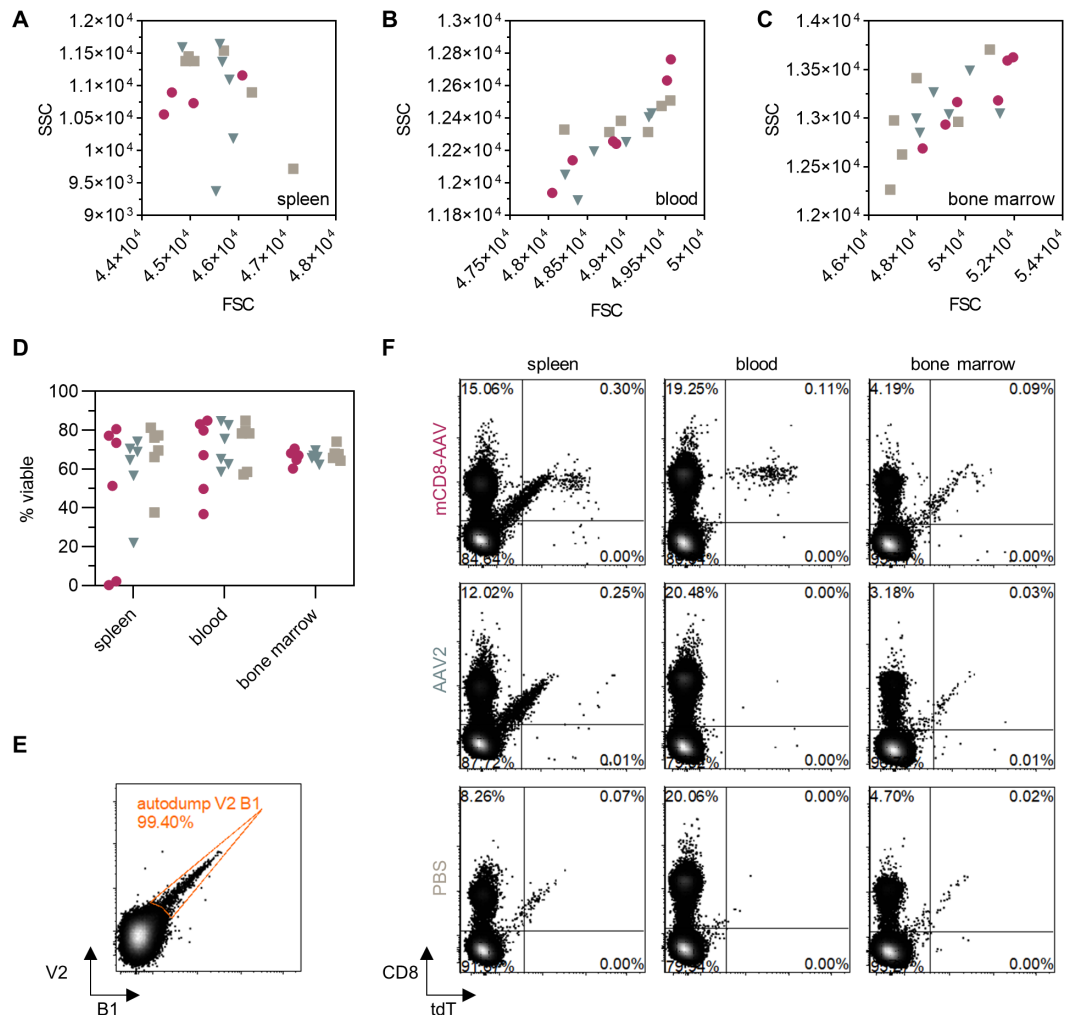
Suppl. Figure 6.3: **Additional metrics and gating information (related to Fig.s 3.15 & 3.16)** **A-D** Further characterization of cell material obtained from spleens, blood and bone marrow of mice treated with mCD8-AAV-cre (red ●), AAV2-cre (blue ▼) or PBS (grey ■). Symbols represent data from n = 6 mice/group (total: 18). **A-C** FSC and SSC of CD3+ viable singlets. Arithmetic means of viable T cells' scatter parameters are plotted. **D** Viability of singlet cells. **E** Autofluorescent events were removed from the plots shown in Figures 3.15 & 3.16 via an autofluorescence dump gate. The gate was set on a spleen-derived 'full minus V2'-control sample, not stained with αmCD4-VioGreen antibodies and utilizing the unused B1 (FITC) channel of the flow cytometer. **F** To illustrate the impact of the dump gate, flow cytometry plots were generated from the data underlying Figure 3.15 without dumping autofluorescent events. Plots show tdT vs. CD8 signal of viable singlet cells.

Bibliography

Abordo-Adesida, E., A. Follenzi, C. Barcia, S. Sciascia, M. G. Castro, L. Naldini, and P. R. Lowenstein (2005). Stability of lentiviral vector-mediated transgene expression in the brain in the presence of systemic antivector immune responses. Hum Gene Ther *16*, 741–751. DOI: `10.1089/hum.2005.16.741`.

Agarwal, S., J. D. Hanauer, A. M. Frank, V. Riechert, F. B. Thalheimer, and C. J. Buchholz (2020). In vivo generation of CAR T cells selectively in human CD4+ lymphocytes. Mol Ther *20*, 30239–2. DOI: `10.1016/j.ymthe.2020.05.005`.

Agarwal, S., T. Weidner, F. B. Thalheimer, and C. J. Buchholz (2019). In vivo generated human CAR T cells eradicate tumor cells. Oncoimmunology *8*, e1671761. DOI: `10.1080/2162402X.2019.1671761`.

Anastasov, N., I. Höfig, S. Mall, A. M. Krackhardt, and C. Thirion (2016). Optimized Lentiviral Transduction Protocols by Use of a Poloxamer Enhancer, Spinoculation, and scFv-Antibody Fusions to VSV-G. Methods Mol Biol *1448*, 49–61. DOI: `10.1007/978-1-4939-3753-0_4`.

Anliker, B., T. Abel, S. Kneissl, J. Hlavaty, A. Caputi, J. Brynza, I. C. Schneider, R. C. Münch, H. Petznek, R. E. Kontermann, U. Koehl, I. C. D. Johnston, K. Keinänen, U. C. Müller, C. Hohenadl, H. Monyer, K. Cichutek, and C. J. Buchholz (2010). Specific gene transfer to neurons, endothelial cells and hematopoietic progenitors with lentiviral vectors. Nat Methods *7*, 929–935. DOI: `10.1038/nmeth.1514`.

Axelrod, M. L., W. C. Meijers, E. M. Screever, J. Qin, M. G. Carroll, X. Sun, E. Tannous, Y. Zhang, A. Sugiura, B. C. Taylor, A. Hanna, S. Zhang, K. Amancherla, W. Tai, J. J. Wright, S. C. Wei, S. R. Opalenik, A. L. Toren, J. C. Rathmell, P. B. Ferrell, E. J. Phillips, S. Mallal, D. B. Johnson, J. P. Allison, J. J. Moslehi, and J. M. Balko (2022). T cells specific for a-myosin drive immunotherapy-related myocarditis. Nature *611*, 818–826. DOI: `10.1038/s41586-022-05432-3`.

Becker, J., J. Fakhiri, and D. Grimm (2022). Fantastic AAV Gene Therapy Vectors and How to Find Them-Random Diversification, Rational Design and Machine Learning. Pathogens *11*. DOI: `10.3390/pathogens11070756`.

Behrendt, R., T. Schumann, A. Gerbaulet, L. A. Nguyen, N. Schubert, D. Alexopoulou, U. Berka, S. Lienenklaus, K. Peschke, K. Gibbert, S. Wittmann, D. Lindemann, S. Weiss, A. Dahl, R. Naumann, U. Dittmer, B. Kim, W. Mueller, T. Gramberg, and A. Roers (2013). Mouse SAMHD1 has antiretroviral activity and suppresses a spontaneous cell-intrinsic antiviral response. Cell Rep *4*, 689–696. DOI: `10.1016/j.celrep.2013.07.037`.

Bender, R. R., A. Muth, I. C. Schneider, T. Friedel, J. Hartmann, A. Pluckthun, A. Maisner, and C. J. Buchholz (2016). Receptor-Targeted Nipah Virus Glycoproteins Improve Cell-Type Selective Gene Delivery and Reveal a Preference for Membrane-Proximal Cell Attachment. PLoS Pathog *12*, e1005641. DOI: `10.1371/journal.ppat.1005641`.

Bishop, D. C., L. E. Clancy, R. Simms, J. Burgess, G. Mathew, L. Moezzi, J. A. Street, G. Sutrave, E. Atkins, H. M. McGuire, B. S. Gloss, K. Lee, W. Jiang, K. Maddock, G. McCaughan, S. Avdic, V. Antonenas, T. A. O'Brien, P. J. Shaw, D. O. Irving, D. J. Gottlieb, E. Blyth, and K. P. Micklethwaite (2021). Development of CAR T-cell lymphoma in 2 of 10 patients effectively treated with piggyBac-modified CD19 CAR T cells. Blood *138*, 1504–1509. DOI: 10.1182/blood.2021010813.

Breuer, C. B., K. S. Hanlon, J.-S. Natasan, A. Volak, A. Meliani, F. Mingozzi, B. P. Kleinstiver, J. J. Moon, and C. A. Maguire (2020). In vivo engineering of lymphocytes after systemic exosome-associated AAV delivery. Sci Rep *10*, 4544. DOI: 10.1038/s41598-020-61518-w.

Brudno, J. N., N. Lam, D. Vanasse, Y.-w. Shen, J. J. Rose, J. Rossi, A. Xue, A. Bot, N. Scholler, L. Mikkilineni, M. Roschewski, R. Dean, R. Cachau, P. Youkharibache, R. Patel, B. Hansen, D. F. Stroncek, S. A. Rosenberg, R. E. Gress, and J. N. Kochenderfer (2020). Safety and feasibility of anti-CD19 CAR T cells with fully human binding domains in patients with B-cell lymphoma. Nat Med *26*, 270–280. DOI: 10.1038/s41591-019-0737-3.

Buchholz, C. J., T. Friedel, and H. Büning (2015). Surface-Engineered Viral Vectors for Selective and Cell Type-Specific Gene Delivery. Trends Biotechnol *33*, 777–790. DOI: 10.1016/j.tibtech.2015.09.008.

Buchholz, C. J., M. D. Mühlebach, and K. Cichutek (2009). Lentiviral vectors with measles virus glycoproteins - dream team for gene transfer? Trends Biotechnol *27*, 259–265. DOI: 10.1016/j.tibtech.2009.02.002.

Burwitz, B. J., J. S. Reed, K. B. Hammond, M. A. Ohme, S. L. Planer, A. W. Legasse, A. J. Ericsen, Y. Richter, G. Golomb, and J. B. Sacha (2014). Technical advance: liposomal alendronate depletes monocytes and macrophages in the nonhuman primate model of human disease. J Leukoc Biol *96*, 491–501. DOI: 10.1189/jlb.5TA0713-373R.

Canté-Barrett, K., R. D. Mendes, W. K. Smits, Y. M. van Helsdingen-van Wijk, R. Pieters, and J. P. P. Meijerink (2016). Lentiviral gene transfer into human and murine hematopoietic stem cells: size matters. BMC Res Notes *9*, 312. DOI: 10.1186/s13104-016-2118-z.

Cascalho, M., D. Huynh, A. R. Lefferts, L. Stein, T. Lanigan, J. Decker, L. D. Shea, and J. L. Platt (2018). Durable targeting of B-lymphocytes in living mice. Sci Rep *8*, 11143. DOI: 10.1038/s41598-018-29452-0.

Castle, M. J. (2019). *Adeno-associated virus vectors. Design and delivery*. Vol. volume 1950. Methods in molecular biology. New York, NY: Humana Press and Springer. 1 online resource (xii, 426.

Chan, K. Y., M. J. Jang, B. B. Yoo, A. Greenbaum, N. Ravi, W.-L. Wu, L. Sánchez-Guardado, C. Lois, S. K. Mazmanian, B. E. Deverman, and V. Gradinaru (2017). Engineered AAVs for efficient noninvasive gene delivery to the central and peripheral nervous systems. Nat Neurosci *20*, 1172–1179. DOI: 10.1038/nn.4593.

Charitidis, F. T., E. Adabi, F. B. Thalheimer, C. Clarke, and C. J. Buchholz (2021). Monitoring CAR T cell generation with a CD8-targeted lentiviral vector by single-cell transcriptomics. Mol Ther Methods Clin Dev *23*, 359–369. DOI: 10.1016/j.omtm.2021.09.019.

clinicaltrials.gov (2022). *ClinicalTrials.gov*. URL: https://clinicaltrials.gov/ (visited on Jan. 19, 2022).

Coiras, M., M. Bermejo, B. Descours, E. Mateos, J. García-Pérez, M.-R. López-Huertas, M. M. Lederman, M. Benkirane, and J. Alcamí (2016). IL-7 Induces SAMHD1 Phosphorylation in CD4+ T Lymphocytes, Improving Early Steps of HIV-1 Life Cycle. Cell Rep *14*, 2100–2107. DOI: 10.1016/j.celrep.2016.02.022.

Cordes, N., C. Kolbe, D. Lock, T. Holzer, D. Althoff, D. Schäfer, F. Blaeschke, B. Kotter, S. Karitzky, C. Rossig, T. Cathomen, T. Feuchtinger, I. Bürger, M. Assenmacher, T. Schaser, and A. D. Kaiser (2021). Anti-CD19 CARs displayed at the surface of lentiviral vector particles promote transduction of target-expressing cells. Mol Ther Methods Clin Dev *21*, 42–53. DOI: 10.1016/j.omtm.2021.02.013.

Cordes, N., N. Winter, C. Kolbe, B. Kotter, J. Mittelstaet, M. Assenmacher, T. Cathomen, A. Kaiser, and T. Schaser (2022). Adapter-Mediated Transduction with Lentiviral Vectors: A Novel Tool for Cell-Type-Specific Gene Transfer. Viruses *14*. DOI: 10.3390/v14102157.

Cunningham, J., S. Chandra, A. Emmanuel, A. Mazzarelli, C. Passaro, P. Baldwin, M. Nguyen-McCarty, C. Rocca, S. Joyce, J. Kim, V. Vagin, J. Kaczmarek, H. Chavan, H. Jewell, Y. Lipsitz, M. Shamashkin, K. Hlavaty, J. Rodriguez, C. Co, P. Cruite, H. Ennajdaoui, V. Duback, J. Elman, S. Amatya, C. Harding, S. Lyubinetsky, V. Patel, L. Pepper, A. Ruzo, S. Iovino, B. Varghese, A. E. Foster, B. Gorovits, K. Elpek, M. Laska, T. McGill, J. V. Shah, T. J. Fry, and D. Dambach (2021). In Vivo Delivery of a CD20 CAR Using a CD8-Targeted Fusosome in Southern Pig-Tail Macaques (M. nemestrina) Results in B Cell Depletion. Blood *138*, 2769. DOI: 10.1182/blood-2021-148709.

Dalwadi, D. A., A. Calabria, A. Tiyaboonchai, J. Posey, W. E. Naugler, E. Montini, and M. Grompe (2021). AAV integration in human hepatocytes. Molecular Therapy *29*, 2898–2909. DOI: 10.1016/j.ymthe.2021.08.031.

Danenberg, H. D., G. Golomb, A. Groothuis, J. Gao, H. Epstein, R. V. Swaminathan, P. Seifert, and E. R. Edelman (2003). Liposomal alendronate inhibits systemic innate immunity and reduces in-stent neointimal hyperplasia in rabbits. Circulation *108*, 2798–2804. DOI: 10.1161/01.CIR.0000097002.69209.CD.

Davila, M. L., C. C. Kloss, G. Gunset, and M. Sadelain (2013). CD19 CAR-targeted T cells induce long-term remission and B Cell Aplasia in an immunocompetent mouse model of B cell acute lymphoblastic leukemia. PLoS ONE *8*, e61338. DOI: 10.1371/journal.pone.0061338.

Demaison, C., K. Parsley, G. Brouns, M. Scherr, K. Battmer, C. Kinnon, M. Grez, and A. J. Thrasher (2002). High-level transduction and gene expression in hematopoietic repopulating cells using a human immunodeficiency virus type 1-based lentiviral vector containing an internal spleen focus forming virus promoter. Hum Gene Ther *13*, 803–813. DOI: `10.1089/10430340252898984`.

Deverman, B. E., P. L. Pravdo, B. P. Simpson, S. R. Kumar, K. Y. Chan, A. Banerjee, W.-L. Wu, B. Yang, N. Huber, S. P. Pasca, and V. Gradinaru (2016). Cre-dependent selection yields AAV variants for widespread gene transfer to the adult brain. Nat Biotechnol *34*, 204–209. DOI: `10.1038/nbt.3440`. (Visited on Mar. 14, 2016).

Eichhoff, A. M., K. Börner, B. Albrecht, W. Schäfer, N. Baum, F. Haag, J. Körbelin, M. Trepel, I. Braren, D. Grimm, S. Adriouch, and F. Koch-Nolte (2019). Nanobody-Enhanced Targeting of AAV Gene Therapy Vectors. Mol Ther Methods Clin Dev *15*, 211–220. DOI: `10.1016/j.omtm.2019.09.003`.

Elsallab, M., B. L. Levine, A. S. Wayne, and M. Abou-El-Enein (2020). CAR T-cell product performance in haematological malignancies before and after marketing authorisation. Lancet Oncol *21*, e104–e116. DOI: `10.1016/S1470-2045(19)30729-6`.

EMA (2023). *Hemgenix: EPAR - Product information*. URL: `https://www.ema.europa.eu/en/documents/product-information/hemgenix-epar-product-information_en.pdf` (visited on Mar. 6, 2023).

– (2021a). *Abecma: EPAR - Product information*. URL: `https://www.ema.europa.eu/en/documents/product-information/abecma-epar-product-information_en.pdf` (visited on Feb. 22, 2022).

– (2022a). *Breyanzi: EPAR - Product information*. URL: `https://www.ema.europa.eu/en/documents/product-information/breyanzi-epar-product-information_en.pdf` (visited on Oct. 6, 2022).

– (2022b). *Carvykti: EPAR - Product information*. URL: `https://www.ema.europa.eu/en/documents/product-information/carvykti-epar-product-information_en.pdf` (visited on Oct. 6, 2022).

– (2022d). *Imlygic: EPAR - Product information*. URL: `https://www.ema.europa.eu/en/documents/product-information/imlygic-epar-product-information_en.pdf` (visited on Feb. 22, 2022).

– (2021b). *Kymriah: EPAR - Product information*. URL: `https://www.ema.europa.eu/en/documents/product-information/kymriah-epar-product-information_en.pdf` (visited on Feb. 22, 2022).

– (2022e). *Libmeldy: EPAR - Product information*. URL: `https://www.ema.europa.eu/en/documents/product-information/libmeldy-epar-product-information_en.pdf` (visited on Oct. 6, 2022).

– (2021c). *Luxturna: EPAR - Product information*. URL: https://www.ema.europa.eu/en/documents/product-information/luxturna-epar-product-information_en.pdf (visited on Feb. 22, 2022).

– (2022g). *Roctavian: EPAR - Product information*. URL: https://www.ema.europa.eu/en/documents/product-information/roctavian-epar-product-information_en.pdf (visited on Feb. 22, 2022).

– (2022h). *Strimvelis: EPAR - Product information*. URL: https://www.ema.europa.eu/en/documents/product-information/strimvelis-epar-product-information_en.pdf (visited on Feb. 22, 2022).

– (2021f). *Tecartus: EPAR - Product information*. URL: https://www.ema.europa.eu/en/documents/product-information/tecartus-epar-product-information_en.pdf (visited on Feb. 22, 2022).

– (2022i). *Upstaza: EPAR - Product information*. URL: https://www.ema.europa.eu/en/documents/product-information/upstaza-epar-product-information_en.pdf (visited on Feb. 22, 2022).

– (2021g). *Yescarta: EPAR - Product information*. URL: https://www.ema.europa.eu/en/documents/product-information/yescarta-epar-product-information_en.pdf (visited on Feb. 22, 2022).

– (2021h). *Zolgensma: EPAR - Product information*. URL: https://www.ema.europa.eu/en/documents/product-information/zolgensma-epar-product-information_en.pdf (visited on Feb. 22, 2022).

Ertl, H. C. J. (2022). Immunogenicity and toxicity of AAV gene therapy. Front Immunol *13*, 975803. DOI: 10.3389/fimmu.2022.975803.

Finkelshtein, D., A. Werman, D. Novick, S. Barak, and M. Rubinstein (2013). LDL receptor and its family members serve as the cellular receptors for vesicular stomatitis virus. Proc Natl Acad Sci U S A *110*, 7306–7311. DOI: 10.1073/pnas.1214441110.

Food and Drug Administration (2021). *Briefing Document Food and Drug Administration (FDA) Cellular, Tissue, and Gene Therapies Advisory Committee (CTGTAC) Meeting #70 Toxicity Risks of Adeno-associated Virus (AAV) Vectors for Gene Therapy (GT) September 2-3, 2021*. URL: https://www.fda.gov/media/151599/download (visited on Feb. 21, 2022).

Frank, A. M., A. H. Braun, L. Scheib, S. Agarwal, I. C. Schneider, F. Fusil, S. Perian, U. Sahin, F. B. Thalheimer, E. Verhoeyen, and C. J. Buchholz (2020a). Combining T-cell-specific activation and in vivo gene delivery through CD3-targeted lentiviral vectors. Blood Adv *4*, 5702–5715. DOI: 10.1182/bloodadvances.2020002229.

Frank, A. M. and C. J. Buchholz (2018). Surface-engineered lentiviral vectors for selective gene transfer into subtypes of lymphocytes. Mol Ther Methods Clin Dev *12*, 19–31. DOI: 10.1016/j.omtm.2018.10.006.

Frank, A. M., T. Weidner, J. Brynza, W. Uckert, C. J. Buchholz, and J. Hartmann (2020b). CD8-specific DARPins improve selective gene delivery into human and primate T lymphocytes. Hum Gene Ther *31*, 679–691. DOI: 10.1089/hum.2019.248.

Friedmann, T. (1992). A brief history of gene therapy. Nat Genet *2*, 93–98. DOI: 10.1038/ng1092-93.

Funke, S., I. C. Schneider, S. Glaser, M. D. Mühlebach, T. Moritz, R. Cattaneo, K. Cichutek, and C. J. Buchholz (2009). Pseudotyping lentiviral vectors with the wild-type measles virus glycoproteins improves titer and selectivity. Gene Ther *16*, 700–705. DOI: 10.1038/gt.2009.11.

Funke, S., A. Maisner, M. D. Mühlebach, U. Koehl, M. Grez, R. Cattaneo, K. Cichutek, and C. J. Buchholz (2008). Targeted cell entry of lentiviral vectors. Mol Ther *16*, 1427–1436. DOI: 10.1038/mt.2008.128.

Gil-Farina, I. and M. Schmidt (2016). Interaction of vectors and parental viruses with the host genome. Curr Opin Virol *21*, 35–40. DOI: 10.1016/j.coviro.2016.07.004.

Gilham, D. E., M. Lie-A-Ling, N. Taylor, and R. E. Hawkins (2010). Cytokine stimulation and the choice of promoter are critical factors for the efficient transduction of mouse T cells with HIV-1 vectors. J Gene Med *12*, 129–136. DOI: 10.1002/jgm.1421.

Grieger, J. C. and R. J. Samulski (2005). Packaging capacity of adeno-associated virus serotypes: impact of larger genomes on infectivity and postentry steps. J Virol *79*, 9933–9944. DOI: 10.1128/JVI.79.15.9933-9944.2005.

Gutierrez-Guerrero, A., M. J. Abrey Recalde, P. E. Mangeot, C. Costa, O. Bernadin, S. Périan, F. Fusil, G. Froment, A. Martinez-Turtos, A. Krug, F. Martin, K. Benabdellah, E. P. Ricci, S. Giovannozzi, R. Gijsbers, E. Ayuso, F.-L. Cosset, and E. Verhoeyen (2021). Baboon Envelope Pseudotyped "Nanoblades" Carrying Cas9/gRNA Complexes Allow Efficient Genome Editing in Human T, B, and CD34+ Cells and Knock-in of AAV6-Encoded Donor DNA in CD34+ Cells. Front Genome Ed *3*, 604371. DOI: 10.3389/fgeed.2021.604371.

Haber, E., E. Afergan, H. Epstein, D. Gutman, N. Koroukhov, M. Ben-David, M. Schachter, and G. Golomb (2010). Route of administration-dependent anti-inflammatory effect of liposomal alendronate. J Control Release *148*, 226–233. DOI: 10.1016/j.jconrel.2010.08.030.

Hacein-Bey-Abina, S., C. von Kalle, M. Schmidt, M. P. McCormack, N. Wulffraat, P. Leboulch, A. Lim, C. S. Osborne, R. Pawliuk, E. Morillon, R. Sorensen, A. Forster, P. Fraser, J. I. Cohen, G. de Saint Basile, I. Alexander, U. Wintergerst, T. Frebourg, A. Aurias, D. Stoppa-Lyonnet, S. Romana, I. Radford-Weiss, F. Gross, F. Valensi, E. Delabesse, E. Macintyre, F. Sigaux, J. Soulier, L. E. Leiva, M. Wissler, C. Prinz, T. H. Rabbitts, F. Le Deist, A. Fischer, and M. Cavazzana-Calvo (2003). LMO2-associated clonal T cell proliferation in two patients after gene therapy for SCID-X1. Science *302*, 415–419. DOI: 10.1126/science.1088547.

Han, J., K. Tam, C. Tam, R. P. Hollis, and D. B. Kohn (2021). Improved lentiviral vector titers from a multi-gene knockout packaging line. Mol Ther Oncolytics *23*, 582–592. DOI: `10.1016/j.omto.2021.11.012`.

Hartmann, J., R. C. Münch, R.-T. Freiling, I. C. Schneider, B. Dreier, W. Samukange, J. Koch, M. A. Seeger, A. Plückthun, and C. J. Buchholz (2018). A Library-Based Screening Strategy for the Identification of DARPins as Ligands for Receptor-Targeted AAV and Lentiviral Vectors. Mol Ther Methods Clin Dev *10*, 128–143. DOI: `10.1016/j.omtm.2018.07.001`.

Hartmann, J., F. B. Thalheimer, F. Höpfner, T. Kerzel, K. Khodosevich, D. García-González, H. Monyer, I. Diester, H. Büning, J. E. Carette, P. Fries, and C. J. Buchholz (2019). GluA4-Targeted AAV Vectors Deliver Genes Selectively to Interneurons while Relying on the AAV Receptor for Entry. Mol Ther Methods Clin Dev *14,* 252–260. DOI: `10.1016/j.omtm.2019.07.004`.

Herbst, F., C. R. Ball, F. Tuorto, A. Nowrouzi, W. WANG, O. Zavidij, S. M. Dieter, S. Fessler, F. van der Hoeven, U. Kloz, F. Lyko, M. Schmidt, C. von Kalle, and H. Glimm (2012). Extensive methylation of promoter sequences silences lentiviral transgene expression during stem cell differentiation in vivo. Mol Ther *20*, 1014–1021. DOI: `10.1038/mt.2012.46`.

Herzog, R. W. (2020). Encouraging and Unsettling Findings in Long-Term Follow-up of AAV Gene Transfer. Mol Ther *28*, 341–342. DOI: `10.1016/j.ymthe.2020.01.007`.

Ho, N., S. Agarwal, M. Milani, A. Cantore, C. J. Buchholz, and F. B. Thalheimer (2022). In vivo generation of CAR T cells in the presence of human myeloid cells. Mol Ther Methods Clin Dev *26*, 144–156. DOI: `10.1016/j.omtm.2022.06.004`.

Hodgins, N. O., W. T. Al-Jamal, J. T.-W. Wang, A. C. Parente-Pereira, M. Liu, J. Maher, and K. T. Al-Jamal (2016). In vitro potency, in vitro and in vivo efficacy of liposomal alendronate in combination with gd T cell immunotherapy in mice. J Control Release *241*, 229–241. DOI: `10.1016/j.jconrel.2016.09.023`.

Hordeaux, J., Q. Wang, N. Katz, E. L. Buza, P. Bell, and J. M. Wilson (2018). The Neurotropic Properties of AAV-PHP.B Are Limited to C57BL/6J Mice. Mol Ther *26*, 664–668. DOI: `10.1016/j.ymthe.2018.01.018`.

Hordeaux, J., Y. Yuan, P. M. Clark, Q. Wang, R. A. Martino, J. J. Sims, P. Bell, A. Raymond, W. L. Stanford, and J. M. Wilson (2019). The GPI-Linked Protein LY6A Drives AAV-PHP.B Transport across the Blood-Brain Barrier. Mol Ther *27*, 912–921. DOI: `10.1016/j.ymthe.2019.02.013`.

Hörner, M., C. Jerez-Longres, A. Hudek, S. Hook, O. S. Yousefi, W. W. A. Schamel, C. Hörner, M. D. Zurbriggen, H. Ye, H. J. Wagner, and W. Weber (2021). Spatiotemporally confined red light-controlled gene delivery at single-cell resolution using adeno-associated viral vectors. Sci Adv *7*, eabf0797. DOI: `10.1126/sciadv.abf0797`.

Huang, Q., K. Y. Chan, I. G. Tobey, Y. A. Chan, T. Poterba, C. L. Boutros, A. B. Balazs, R. Daneman, J. M. Bloom, C. Seed, and B. E. Deverman (2019). Delivering genes across the blood-brain barrier: LY6A, a novel cellular receptor for AAV-PHP.B capsids. PLoS ONE *14*, e0225206. DOI: `10.1371/journal.pone.0225206`.

Huang, Q., A. T. Chen, K. Y. Chan, H. Sorensen, A. J. Barry, B. Azari, T. Beddow, Q. Zheng, B. Zhao, I. G. Tobey, F.-E. Eid, Y. A. Chan, and B. E. Deverman (2022). *Targeting AAV vectors to the CNS via de novo engineered capsid-receptor interactions*. DOI: `10.1101/2022.10.31.514553`.

Huckaby, J. T., E. Landoni, T. M. Jacobs, B. Savoldo, G. Dotti, and S. K. Lai (2021). Bispecific binder redirected lentiviral vector enables in vivo engineering of CAR-T cells. J Immunother Cancer *9*, e002737. DOI: `10.1136/jitc-2021-002737`.

Iliff, S. A. (2002). An additional "R": remembering the animals. ILAR J *43*, 38–47. DOI: `10.1093/ilar.43.1.38`.

Iwamoto, C., K. Takenaka, S. Urata, T. Yamauchi, T. Shima, T. Kuriyama, S. Daitoku, Y. Saito, T. Miyamoto, H. Iwasaki, I. Kitabayashi, K. Itoh, J. Kishimoto, D. Kohda, T. Matozaki, and K. Akashi (2014). The BALB/c-specific polymorphic SIRPA enhances its affinity for human CD47, inhibiting phagocytosis against human cells to promote xenogeneic engraftment. Exp Hematol *42*, 163–171.e1. DOI: `10.1016/j.exphem.2013.11.005`.

Judd, J., F. Wei, P. Q. Nguyen, L. J. Tartaglia, M. Agbandje-McKenna, J. J. Silberg, and J. Suh (2012). Random Insertion of mCherry Into VP3 Domain of Adeno-associated Virus Yields Fluorescent Capsids With no Loss of Infectivity. Mol Ther Nucleic Acids *1*, e54. DOI: `10.1038/mtna.2012.46`.

June, C. H. and M. Sadelain (2018). Chimeric Antigen Receptor Therapy. N Engl J Med *379*, 64–73. DOI: `10.1056/NEJMra1706169`. (Visited on July 9, 2018).

Kang, M., S. H. Lee, M. Kwon, J. Byun, D. Kim, C. Kim, S. Koo, S. P. Kwon, S. Moon, M. Jung, J. Hong, S. Go, S. Y. Song, J. H. Choi, T. Hyeon, Y.-K. Oh, H. H. Park, and B.-S. Kim (2021). Nanocomplex-Mediated In Vivo Programming to Chimeric Antigen Receptor-M1 Macrophages for Cancer Therapy. Adv Mater *33*, e2103258. DOI: `10.1002/adma.202103258`.

Keyes, D. (2004). *Flowers for Algernon*. Mariner Books.

Kochenderfer, J. N., S. A. Feldman, Y. Zhao, H. Xu, M. A. Black, R. A. Morgan, W. H. Wilson, and S. A. Rosenberg (2009). Construction and preclinical evaluation of an anti-CD19 chimeric antigen receptor. J Immunother *32*, 689–702. DOI: `10.1097/CJI.0b013e3181ac6138`. (Visited on Jan. 13, 2017).

Kochenderfer, J. N., Z. Yu, D. Frasheri, N. P. Restifo, and S. A. Rosenberg (2010). Adoptive transfer of syngeneic T cells transduced with a chimeric antigen receptor that recognizes murine CD19 can eradicate lymphoma and normal B cells. Blood *116*, 3875–3886. DOI: `10.1182/blood-2010-01-265041`.

Kohn, L. A. and D. B. Kohn (2021). Gene Therapies for Primary Immune Deficiencies. Front Immunol *12*, 648951. DOI: 10.3389/fimmu.2021.648951.

Kueberuwa, G., M. Kalaitsidou, E. Cheadle, R. E. Hawkins, and D. E. Gilham (2018). CD19 CAR T Cells Expressing IL-12 Eradicate Lymphoma in Fully Lymphoreplete Mice through Induction of Host Immunity. Mol Ther Oncolytics *8*, 41–51. DOI: 10.1016/j.omto.2017.12.003.

Kumar, M., B. Keller, N. Makalou, and R. E. Sutton (2001). Systematic determination of the packaging limit of lentiviral vectors. Hum Gene Ther *12*, 1893–1905. DOI: 10.1089/104303401753153947.

Lang, J. F., S. A. Toulmin, K. L. Brida, L. C. Eisenlohr, and B. L. Davidson (2019). Standard screening methods underreport AAV-mediated transduction and gene editing. Nat Commun *10*, 3415. DOI: 10.1038/s41467-019-11321-7.

Leborgne, C., E. Barbon, J. M. Alexander, H. Hanby, S. Delignat, D. M. Cohen, F. Collaud, S. Muraleetharan, D. Lupo, J. Silverberg, K. Huang, L. van Wittengerghe, B. Marolleau, A. Miranda, A. Fabiano, V. Daventure, H. Beck, X. M. Anguela, G. Ronzitti, S. M. Armour, S. Lacroix-Desmazes, and F. Mingozzi (2020). IgG-cleaving endopeptidase enables in vivo gene therapy in the presence of anti-AAV neutralizing antibodies. Nat Med *26*, 1096–1101. DOI: 10.1038/s41591-020-0911-7.

Li, C. and R. J. Samulski (2020). Engineering adeno-associated virus vectors for gene therapy. Nat Rev Genet *21*, 255–272. DOI: 10.1038/s41576-019-0205-4.

Liu, S., Q. Cheng, T. Wei, X. Yu, L. T. Johnson, L. Farbiak, and D. J. Siegwart (2021). Membrane-destabilizing ionizable phospholipids for organ-selective mRNA delivery and CRISPR-Cas gene editing. Nat Mater *20*, 701–710. DOI: 10.1038/s41563-020-00886-0.

Lock, D., N. Mockel-Tenbrinck, K. Drechsel, C. Barth, D. Mauer, T. Schaser, C. Kolbe, W. Al Rawashdeh, J. Brauner, O. Hardt, N. Pflug, U. Holtick, P. Borchmann, M. Assenmacher, and A. Kaiser (2017). Automated Manufacturing of Potent CD20-Directed Chimeric Antigen Receptor T Cells for Clinical Use. Hum Gene Ther *28*, 914–925. DOI: 10.1089/hum.2017.111.

Lockowandt, M., D. M. Günther, L. Quintino, L. S. Breger, C. Isaksson, and C. Lundberg (2020). Optimization of production and transgene expression of a retrogradely transported pseudotyped lentiviral vector. J Neurosci Methods *336*, 108542. DOI: 10.1016/j.jneumeth.2019.108542.

Mangeot, P.-E., S. Dollet, M. Girard, C. Ciancia, S. Joly, M. Peschanski, and V. Lotteau (2011). Protein transfer into human cells by VSV-G-induced nanovesicles. Mol Ther *19*, 1656–1666. DOI: 10.1038/mt.2011.138. (Visited on July 2, 2015).

Maude, S. L., T. W. Laetsch, J. Buechner, S. Rives, M. Boyer, H. Bittencourt, P. Bader, M. R. Verneris, H. E. Stefanski, G. D. Myers, M. Qayed, B. D. Moerloose, H. Hiramatsu, K. Schlis, K. L. Davis, P. L. Martin, E. R. Nemecek, G. A. Yanik, C. Peters, A. Baruchel, N. Boissel, F. Mechinaud, A. Balduzzi, J. Krueger, C. H. June, B. L. Levine, P. Wood, T. Taran, M. Leung, K. T. Mueller, Y. Zhang, K. Sen, D. Lebwohl, M. A. Pulsipher, and S. A. Grupp (2018). Tisagenlecleucel in Children and Young Adults with B-Cell Lymphoblastic Leukemia. N Engl J Med *378*, 439–448. DOI: 10.1056/NEJMoa1709866.

McCarty, D. M. (2008). Self-complementary AAV vectors; advances and applications. Mol Ther *16*, 1648–1656. DOI: 10.1038/mt.2008.171.

Meliani, A., F. Boisgerault, R. Hardet, S. Marmier, F. Collaud, G. Ronzitti, C. Leborgne, H. Costa Verdera, M. Simon Sola, S. Charles, A. Vignaud, L. van Wittenberghe, G. Manni, O. Christophe, F. Fallarino, C. Roy, A. Michaud, P. Ilyinskii, T. K. Kishimoto, and F. Mingozzi (2018). Antigen-selective modulation of AAV immunogenicity with tolerogenic rapamycin nanoparticles enables successful vector re-administration. Nat Commun *9*, 4098. DOI: 10.1038/s41467-018-06621-3.

Meyer, N. L. and M. S. Chapman (2021). Adeno-associated virus (AAV) cell entry: structural insights. Trends Microbiol *30*, 432–451. DOI: 10.1016/j.tim.2021.09.005.

Michels, A., A. M. Frank, D. M. Günther, M. Mataei, K. Börner, D. Grimm, J. Hartmann, and C. J. Buchholz (2021). Lentiviral and adeno-associated vectors efficiently transduce mouse T lymphocytes when targeted to murine CD8. Mol Ther Methods Clin Dev *23*, 334–347. DOI: 10.1016/j.omtm.2021.09.014.

Michels, A., N. Ho, and C. J. Buchholz (2022). Precision medicine: In vivo CAR therapy as a showcase for receptor-targeted vector platforms. Mol Ther *30*, 2401–2415. DOI: 10.1016/j.ymthe.2022.05.018.

Micklethwaite, K. P., K. Gowrishankar, B. S. Gloss, Z. Li, J. A. Street, L. Moezzi, M. A. Mach, G. Sutrave, L. E. Clancy, D. C. Bishop, R. H. Y. Louie, C. Cai, J. Foox, M. MacKay, F. J. Sedlazeck, P. Blombery, C. E. Mason, F. Luciani, D. J. Gottlieb, and E. Blyth (2021). Investigation of product-derived lymphoma following infusion of piggyBac-modified CD19 chimeric antigen receptor T cells. Blood *138*, 1391–1405. DOI: 10.1182/blood.2021010858.

Milani, M., A. Annoni, F. Moalli, T. Liu, D. Cesana, A. Calabria, S. Bartolaccini, M. Biffi, F. Russo, I. Visigalli, A. Raimondi, S. Patarroyo-White, D. Drager, P. Cristofori, E. Ayuso, E. Montini, R. Peters, M. Iannacone, A. Cantore, and L. Naldini (2019). Phagocytosis-shielded lentiviral vectors improve liver gene therapy in nonhuman primates. Sci Transl Med *11*, eaav7325. DOI: 10.1126/scitranslmed.aav7325.

Milone, M. C. and U. O'Doherty (2018). Clinical use of lentiviral vectors. Leukemia *32*, 1529–1541. DOI: 10.1038/s41375-018-0106-0. (Visited on June 13, 2018).

Mirdita, M., K. Schuetze, Y. Moriwaki, L. Heo, S. Ovchinnikov, and M. Steinegger (2021). *ColabFold - Making protein folding accessible to all*. DOI: 10.1101/2021.08.15.456425. URL: https://www.biorxiv.org/content/10.1101/2021.08.15.456425v1.

Muik, A., J. Reul, T. Friedel, A. Muth, K. P. Hartmann, I. C. Schneider, R. C. Münch, and C. J. Buchholz (2017). Covalent coupling of high-affinity ligands to the surface of viral vector particles by protein trans-splicing mediates cell type-specific gene transfer. Biomaterials *144*, 84–94. DOI: 10.1016/j.biomaterials.2017.07.032. (Visited on Aug. 21, 2017).

Münch, R. C., H. Janicki, I. Völker, A. Rasbach, M. Hallek, H. Büning, and C. J. Buchholz (2013). Displaying high-affinity ligands on adeno-associated viral vectors enables tumor cell-specific and safe gene transfer. Mol Ther *21*, 109–118. DOI: 10.1038/mt.2012.186.

Münch, R. C., A. Muth, A. Muik, T. Friedel, J. Schmatz, B. Dreier, A. Trkola, A. Plückthun, H. Büning, and C. J. Buchholz (2015). Off-target-free gene delivery by affinity-purified receptor-targeted viral vectors. Nat Commun *6*, 6246. DOI: 10.1038/ncomms7246.

Munis, A. M., G. Mattiuzzo, E. M. Bentley, M. K. Collins, J. E. Eyles, and Y. Takeuchi (2019). Use of Heterologous Vesiculovirus G Proteins Circumvents the Humoral Anti-envelope Immunity in Lentivector-Based In Vivo Gene Delivery. Mol Ther Nucleic Acids *17*, 126–137. DOI: 10.1016/j.omtn.2019.05.010.

Nair, S. and A. Rein (2014). Antiretroviral restriction factors in mice. Virus Res *193*, 130–134. DOI: 10.1016/j.virusres.2014.07.002. (Visited on Nov. 15, 2018).

Nakamura, T., K.-W. Peng, M. Harvey, S. Greiner, Lorimer, Ian A J, C. D. James, and S. J. Russell (2005). Rescue and propagation of fully retargeted oncolytic measles viruses. Nat Biotechnol *23*, 209–214. DOI: 10.1038/nbt1060.

Naldini, L., U. Blömer, P. Gallay, D. Ory, R. Mulligan, F. H. Gage, I. M. Verma, and D. Trono (1996). In vivo gene delivery and stable transduction of nondividing cells by a lentiviral vector. Science *272*, 263–267.

Nawaz, W., B. Huang, S. Xu, Y. Li, L. Zhu, H. Yiqiao, Z. Wu, and X. Wu (2021). AAV-mediated in vivo CAR gene therapy for targeting human T-cell leukemia. Blood Cancer J *11*, 119. DOI: 10.1038/s41408-021-00508-1.

Nikolic, J., L. Belot, H. Raux, P. Legrand, Y. Gaudin, and A. A Albertini (2018). Structural basis for the recognition of LDL-receptor family members by VSV glycoprotein. Nat Commun *9*, 1029. DOI: 10.1038/s41467-018-03432-4.

Nyberg, W. A., J. Ark, A. To, S. Clouden, G. Reeder, J. J. Muldoon, J.-Y. Chung, W. H. Xie, V. Allain, Z. Steinhart, C. Chang, A. Talbot, S. Kim, A. Rosales, L. P. Havlik, H. Pimentel, A. Asokan, and J. Eyquem (2023). An evolved AAV variant enables efficient genetic engineering of murine T cells. Cell. DOI: 10.1016/j.cell.2022.12.022.

Parayath, N. N., S. B. Stephan, A. L. Koehne, P. S. Nelson, and M. T. Stephan (2020). In vitro-transcribed antigen receptor mRNA nanocarriers for transient expression in circulating T cells in vivo. Nat Commun *11*, 6080. DOI: 10.1038/s41467-020-19486-2.

Parayath, N. N. and M. T. Stephan (2021). In Situ Programming of CAR T Cells. Annu Rev Biomed Eng *23*, 385–405. DOI: 10.1146/annurev-bioeng-070620-033348.

Paunovska, K., A. J. Da Silva Sanchez, C. D. Sago, Z. Gan, M. P. Lokugamage, F. Z. Islam, S. Kalathoor, B. R. Krupczak, and J. E. Dahlman (2019). Nanoparticles Containing Oxidized Cholesterol Deliver mRNA to the Liver Microenvironment at Clinically Relevant Doses. Adv Mater *31*, e1807748. DOI: 10.1002/adma.201807748.

Pfeiffer, A., F. B. Thalheimer, S. Hartmann, A. M. Frank, R. R. Bender, S. Danisch, C. Costa, W. S. Wels, U. Modlich, R. Stripecke, E. Verhoeyen, and C. J. Buchholz (2018). In vivo generation of human CD19-CAR T cells results in B-cell depletion and signs of cytokine release syndrome. EMBO Mol Med *10*, e9158. DOI: 10.15252/emmm.201809158.

Philippidis, A. (2020). After Third Death, Audentes' AT132 Remains on Clinical Hold. Hum Gene Ther *31*, 908–910. DOI: 10.1089/hum.2020.29133.bfs.

Plückthun, A. (2015). Designed ankyrin repeat proteins (DARPins): binding proteins for research, diagnostics, and therapy. Annu Rev Pharmacol Toxicol *55*, 489–511. DOI: 10.1146/annurev-pharmtox-010611-134654.

Qasim, W. (2019). Allogeneic CAR T cell therapies for leukemia. Am J Hematol *94*, S50–S54. DOI: 10.1002/ajh.25399.

Raper, S. E., N. Chirmule, F. S. Lee, N. A. Wivel, A. Bagg, G.-p. Gao, J. M. Wilson, and M. L. Batshaw (2003). Fatal systemic inflammatory response syndrome in a ornithine transcarbamylase deficient patient following adenoviral gene transfer. Mol Genet Metab *80*, 148–158. DOI: 10.1016/j.ymgme.2003.08.016.

Reul, J., A. Muik, and C. J. Buchholz (2019). Ligand Coupling to the AAV Capsid for Cell-Specific Gene Transfer. Methods Mol Biol *1950*, 35–50. DOI: 10.1007/978-1-4939-9139-6_3.

Rive, C. M., E. Yung, L. Dreolini, S. D. Brown, C. G. May, D. J. Woodsworth, and R. A. Holt (2022). Selective B cell depletion upon intravenous infusion of replication-incompetent anti-CD19 CAR lentivirus. Mol Ther Methods Clin Dev *26*, 4–14. DOI: 10.1016/j.omtm.2022.05.006.

Riyad, J. M. and T. Weber (2021). Intracellular trafficking of adeno-associated virus (AAV) vectors: challenges and future directions. Gene Ther *28*, 683–696. DOI: 10.1038/s41434-021-00243-z.

Ruella, M., J. Xu, D. M. Barrett, J. A. Fraietta, T. J. Reich, D. E. Ambrose, M. Klichinsky, O. Shestova, P. R. Patel, I. Kulikovskaya, F. Nazimuddin, V. G. Bhoj, E. J. Orlando, T. J. Fry, H. Bitter, S. L. Maude, B. L. Levine, C. L. Nobles, F. D. Bushman, R. M. Young, J. Scholler, S. I. Gill, C. H. June, S. A. Grupp, S. F. Lacey, and J. J. Melenhorst (2018). Induction of resistance to chimeric antigen receptor T cell therapy by transduction of a single leukemic B cell. Nat Med *24*, 1499–1503. DOI: 10.1038/s41591-018-0201-9.

Rurik, J. G., I. Tombácz, A. Yadegari, P. O. Méndez Fernández, S. V. Shewale, L. Li, T. Kimura, O. Y. Soliman, T. E. Papp, Y. K. Tam, B. L. Mui, S. M. Albelda, E. Puré, C. H. June, H. Aghajanian, D. Weissman, H. Parhiz, and J. A. Epstein (2022). CAR T cells produced in vivo to treat cardiac injury. Science *375*, 91–96. DOI: 10.1126/science.abm0594.

Sadelain, M. (2017). CD19 CAR T Cells. Cell *171*, 1471. DOI: 10.1016/j.cell.2017.12.002.

Schüßler-Lenz, M., J. Scherer, and J. Müller-Berghaus (2022). Arzneimittel für neuartige Therapien (ATMP): Ankunft in der Versorgung. Pharmakon *10*, 337–343. DOI: 10.1691/pn.20220034.

Shultz, L. D., J. Keck, L. Burzenski, S. Jangalwe, S. Vaidya, D. L. Greiner, and M. A. Brehm (2019). Humanized mouse models of immunological diseases and precision medicine. Mamm Genome *30*, 123–142. DOI: 10.1007/s00335-019-09796-2.

Skelton, D., N. Satake, and D. B. Kohn (2001). The enhanced green fluorescent protein (eGFP) is minimally immunogenic in C57BL/6 mice. Gene Ther *8*, 1813–1814. DOI: 10.1038/sj.gt.3301586.

Smirnov, S., A. Petukhov, K. Levchuk, S. Kulemzin, A. Staliarova, K. Lepik, O. Shuvalov, A. Zaritskey, A. Daks, and O. Fedorova (2021). Strategies to Circumvent the Side-Effects of Immunotherapy Using Allogeneic CAR-T Cells and Boost Its Efficacy: Results of Recent Clinical Trials. Front Immunol *12*, 780145. DOI: 10.3389/fimmu.2021.780145.

Smith, T. T., S. B. Stephan, H. F. Moffett, L. E. McKnight, W. Ji, D. Reiman, E. Bonagofski, M. E. Wohlfahrt, S. P. S. Pillai, and M. T. Stephan (2017). In situ programming of leukaemia-specific T cells using synthetic DNA nanocarriers. Nat Nanotechnol *12*, 813–820. DOI: 10.1038/nnano.2017.57.

Strech, D. and U. Dirnagl (2019). 3Rs missing: animal research without scientific value is unethical. BMJ Open Sci *3*. DOI: 10.1136/bmjos-2018-000048.

Stripecke, R., M. Carmen Villacres, D. Skelton, N. Satake, S. Halene, and D. Kohn (1999). Immune response to green fluorescent protein: implications for gene therapy. Gene Ther *6*, 1305–1312. DOI: 10.1038/sj.gt.3300951.

Theuerkauf, S. A., A. Michels, V. Riechert, T. J. Maier, E. Flory, K. Cichutek, and C. J. Buchholz (2021). Quantitative Assays Reveal Cell Fusion at Minimal Levels of SARS-CoV-2 Spike Protein and Fusion-from-Without. iScience, 102170. DOI: 10.1016/j.isci.2021.102170.

Thomsen, G., A. H. M. Burghes, C. Hsieh, J. Do, B. T. T. Chu, S. Perry, B. Barkho, P. Kaufmann, D. M. Sproule, D. E. Feltner, W. K. Chung, V. L. McGovern, R. F. Hevner, M. Conces, C. R. Pierson, M. Scoto, F. Muntoni, J. R. Mendell, and K. D. Foust (2021). Biodistribution of onasemnogene abeparvovec DNA, mRNA and SMN protein in human tissue. Nat Med *27*, 1701–1711. DOI: 10.1038/s41591-021-01483-7.

Tsurutani, N., J. Yasuda, N. Yamamoto, B.-I. Choi, M. Kadoki, and Y. Iwakura (2007). Nuclear import of the preintegration complex is blocked upon infection by human immunodeficiency virus type 1 in mouse cells. J Virol *81*, 677–688. DOI: 10.1128/JVI.00870-06.

Vormittag, P., R. Gunn, S. Ghorashian, and F. S. Veraitch (2018). A guide to manufacturing CAR T cell therapies. Curr Opin Biotechnol *53*, 164–181. DOI: 10.1016/j.copbio.2018.01.025. (Visited on June 13, 2018).

Weber, T. (2021). Anti-AAV Antibodies in AAV Gene Therapy: Current Challenges and Possible Solutions. Front Immunol *12*, 658399. DOI: 10.3389/fimmu.2021.658399.

Weidner, T., S. Agarwal, S. Perian, F. Fusil, G. Braun, J. Hartmann, E. Verhoeyen, and C. J. Buchholz (2021). Genetic in vivo engineering of human T lymphocytes in mouse models. Nat Protoc *16*, 3210–3240. DOI: 10.1038/s41596-021-00510-8.

Wilson, J. M. and T. R. Flotte (2020). Moving Forward After Two Deaths in a Gene Therapy Trial of Myotubular Myopathy. Hum Gene Ther *31*, 695–696. DOI: 10.1089/hum.2020.182.

Wittmann, S., R. Behrendt, K. Eissmann, B. Volkmann, D. Thomas, T. Ebert, A. Cribier, M. Benkirane, V. Hornung, N. F. Bouzas, and T. Gramberg (2015). Phosphorylation of murine SAMHD1 regulates its antiretroviral activity. Retrovirology *12*, 103. DOI: 10.1186/s12977-015-0229-6.

Wörner, T. P., A. Bennett, S. Habka, J. Snijder, O. Friese, T. Powers, M. Agbandje-McKenna, and A. J. R. Heck (2021). Adeno-associated virus capsid assembly is divergent and stochastic. Nat Commun *12*, 1642. DOI: 10.1038/s41467-021-21935-5.

Xiao, X., J. Li, and R. J. Samulski (1998). Production of high-titer recombinant adeno-associated virus vectors in the absence of helper adenovirus. J Virol *72*, 2224–2232.

Zhang, J.-x., G. E. Diehl, and D. R. Littman (2008). Relief of preintegration inhibition and characterization of additional blocks for HIV replication in primary mouse T cells. PLoS ONE *3*, e2035. DOI: 10.1371/journal.pone.0002035.

Zhou, J.-E., L. Sun, Y. Jia, Z. Wang, T. Luo, J. Tan, X. Fang, H. Zhu, J. Wang, L. Yu, and Z. Yan (2022). Lipid nanoparticles produce chimeric antigen receptor T cells with interleukin-6 knockdown in vivo. J Control Release *350*, 298–307. DOI: 10.1016/j.jconrel.2022.08.033.

Zhou, Q., I. C. Schneider, I. Edes, A. Honegger, P. Bach, K. Schönfeld, A. Schambach, W. S. Wels, S. Kneissl, W. Uckert, and C. J. Buchholz (2012). T-cell receptor gene transfer exclusively to human CD8(+) cells enhances tumor cell killing. Blood *120*, 4334–4342. DOI: 10.1182/blood-2012-02-412973.

Zhou, Q., K. M. Uhlig, A. Muth, J. Kimpel, C. Lévy, R. C. Münch, J. Seifried, A. Pfeiffer, A. Trkola, C. Coulibaly, D. von Laer, W. S. Wels, U. F. Hartwig, E. Verhoeyen, and C. J. Buchholz (2015). Exclusive Transduction of Human CD4+ T Cells upon Systemic Delivery of CD4-Targeted Lentiviral Vectors. J Immunol *195*, 2493–2501. DOI: 10.4049/jimmunol. 1500956.

List of Figures

List of Tables

List of Abbreviations

AA Amino acid; **AAV** Adeno-associated vector; **AAVR** AAV receptor; **ADA-SCID** Adenosine deaminase deficiency; **BCMA** B cell maturation antigen; **CAR** Chimeric antigen receptor; **CI** Confidence interval; **CTV** Cell Trace Violet; **DARPin** Designed ankyrin repeat protein; **DART-AAV** DARPin-targeted AAV; **doi** Day of (vector) injection; **dpt** Days post transduction; **EMA** European Medicines Agency; **F** Fusion protein; **FBS** Fetal bovine serum; **FMO** Full minus one; **FSC** Forward scatter; **GOI** Genomes of infection; **GP** (Viral) Glycoprotein; **GvHD** Graft-versus-Host-Disease; **H** Hemagglutinin; **HIV-1** Human immunodeficiency virus 1; **hpt** Hours post transduction; **HSPG** Heparan sulfate proteoglycan; **IMAC** Immobilized metal ion affinity chromatography; **ITAM** Immunoreceptor tyrosine-based activation motif; **ITR** Inverted terminal repeat; **IVIS** *In vivo* imaging system; **LDLR** Low-density lipoprotein receptor; **LNP** Lipid nanoparticles; **LTR** Long terminal repeat; **LV** Lentiviral vector; **MCMV** Murine cytomegalovirus; **MFI** Mean fluorescense intensity; **MLV** Murine leukemia virus; **MV** Measles virus; **NC** (Polymer) nanocarriers; **NiV** Nipah virus; **PBMCs** Peripheral blood mononuclear cells; **PGK** Phosphoglycerate kinase; **Psi,** ψ Packaging signal; **qPCR** Quantitative PCR; **SA** Splice acceptor; **sc** Self-complementary; **scFv** Single chain fragment, variable; **SEM** Standard error of the mean; **SFFV** Spleen focus-forming virus; **SPF** Specific pathogen-free; **ss** Single stranded; **SSC** Sideward scatter; **tdT** tdTomato; **TU** Transducing units; **UT** Untreated/untransduced; **VCN** Vector copy numer; **vg** Vector genome; **VP** Viral protein; **VSV** Vesicular stomatitis virus; **WPRE** Woodchuck hepatitis virus posttranscriptional regulatory element;

Acknowledgement

I like to think that my approximately fifty months of doctoral work were not only formative, but also reasonably productive. They were so not because of my talents as a researcher, but because of the extraordinary opportunities I was given and the support I enjoyed by members of the group now known as ForG1.

As my foremost facilitator, Christian enabled this thesis and my (co-)first author-ship of four publications, i.a. by assigning me to fruitful projects and review tasks at auspicious times and making sure that funding was never an object. This support also provided me with ample opportunity to improve my writing and public speaking skills, enabled crucial insights into the workings of the scientific ecosystem, and even saw me contributing to the understanding of the virus that dominated public and private life throughout most of my doctoral work. I am privileged to have enjoyed his multi-faceted patronship and the company of his group.

In the amazing agglutination of (grad) students, postdocs and staff that was the latter, the serendipity of my choice of host laboratory became apparent. In addition to their warmth, which made the group my second (and, at times, first) home, the natural ease with which they held each other to scientific standards they were collectively proud of left me deeply impressed, hoping that I helped carry over some of its spirit to the next generation. I am thankful to have worked with inspiring and supportive people such as Frederic, who always had time for me, even when he did not; Jessica, whose organizational talent and black spreadsheet magic I aspire to; Gundi, whose vector stocks and pragmatic optimism are unparalleled and who, together with Manuela, Julia and Marina, ran a tight, clean and well-stocked lab that I was fortunate to work in; Naphang, of whom I always thought as my senior, and from whom I learned most of what I know about mouse experiments; Samuel and Vanessa, who let me be part of their pandemic response team, and Annika and Doro, without whose foundational work and critical input this thesis (which I hope does their contributions justice) would have been very different.

I will not soon forget my time at PEI, especially not its people, and hope that they remember me for a while as well - even if just by my legacy of googly-eyed lab appliances.

Contributors

Figure or tables identical to or derived from previously published figures or tables are marked accordingly in their legends.

Naturally, I did not generate all data described in this thesis by myself and relied critically on reagents conceived, produced, and characterized by others, as well as on helping hands during crunch times:

Plasmid encoding the MSE10-modified MV HΔ18 depicted in Figure 2.1a was cloned by A.M. Frank. The promoter variants of LV transfer plasmid pSEW-GFP assessed in Figure 2.1e as well as the pPGK-CAR-W plasmid (p. 77) were cloned by M. Mataei. AAV targeting plasmid pRC-αmCD8 and the complementing plasmid pRC-VP1 KO described in Figure 2.7 were cloned by M. Mataei (at the direction of D.M. Günther) and D.M. Günther, respectively. The plasmid encoding GFP driven by an EF1αcore promoter which was used for the production of vectors characterized in Figure 2.8 was cloned by M. Mataei. AAV transfer plasmid pSC-cre was cloned by J. Brynza (p. 77).

VSV-LV-SFFV-GFP, mCD8-LV-SFFV-GFP, mCD4-LV-PGK-CAR and mCD8-LV-PGK-CAR stocks were produced by G. Braun. VSV-LV-SFFV-hCD19-CAR stock was provided my F. Charitidis. AAV2-SFFV-cre and mCD8-SFFV-cre were produced by G. Braun. AAV2-SFFV-GFP, mCD8-SFFV-GFP and mCD8-EF1α-GFP were produced by M. Mataei. AAV vector genome titers were determined by M. Gallet. An overview of the vectors used in this thesis is provided in Tables 2.1 & 2.2.

Immunostaining and flow cytometry for Figure 2.2abd as well as the the experiment underlying Figure 2.7ef were performed by M. Mataei. The Western blot shown in Figure 2.7d was prepared by M. Mataei under the supervision of S.A. Theuerkauf.

In the *in vivo* experiments described in Chapter 3, F. Thalheimer, N. Ho, S. Theuerkauf, L. Zinser, M. Guaza-Lasheras, J. Gorol, F. John, M.B. Demircan, L.R. Knapp, F. Charitidis, D.M. Günther and A. Braun helped with animal procedures and/or during final analysis.

Published Writings

The author of this thesis has previously contributed to four publications, which are briefly summarized below.

Michels, A., Ho, N., Buchholz C.J. (2022) Precision Medicine: *In Vivo* CAR Therapy as a Showcase for Receptor-Targeted Vector Platforms. Molecular Therapy *30*, 2401-2415.
We summarize the current state-of-the-art of in vivo CAR therapy with a focus on the role of receptor-targeted vector platforms. We further discuss present challenges and potential solutions.

Michels, A., Frank, A.M., Günther, D.M., Mataei, M., Börner, K., Grimm, D., Hartmann, J., and Buchholz, C.J. (2021). Lentiviral and adeno-associated vectors efficiently transduce mouse T lymphocytes when targeted to murine CD8. Molecular Therapy Methods and Clinical Development *23*, 334–347.
We describe the effective use of mouse-targeted lentiviral and adeno-associated vectors, highlight the crucial role of receptor-targeting in determining species-compatibility and introduce the DART-AAV platform.

Theuerkauf, S.A.*, **Michels, A.***, Riechert, V., Maier, T.J., Flory, E., Cichutek, K., and Buchholz, C.J. (2021). Quantitative Assays Reveal Cell Fusion at Minimal Levels of SARS-CoV-2 Spike Protein and Fusion-from-Without. iScience, 102170.
We introduce reporter complementation assays for the safe & sensitive assessment of membrane fusion events mediated by SARS-CoV-2 Spike protein and report that Spike-VLPs mediate fusion-from-without.

Michels, A., Hartmann, J., and Buchholz, C.J. (2020). Chimeric antigen receptors in oncology: clinical applications and new developments [German]. Bundesgesundheitsblatt Gesundheitsforschung Gesundheitsschutz *63*, 1331–1340.
We provide an introduction to CAR therapy, its molecular basis and clinical landscape and discuss logistical challenges as well as new developments.

---

*These authors contributed equally.

Memento Mures!

I agree with those who argue that the six central principles of laboratory animal research ethics, i.e. **R**eplacement, **R**eduction, **R**efinement, **R**obustness, **R**egistration & **R**eporting [Strech and Dirnagl, 2019] should be complemented by another: **R**emembrance. [Iliff, 2002]

Seventy-one mice were killed in my name over the course of this thesis, as part of three animal experiments and for tissue harvesting and training. Their irreplaceable contribution will be remembered.

> " *P.S. please if you get a chanse put some flowrs on Algernons grave in the bak yard.*

[Keyes, 2004]

Colophon

This thesis was typeset with $\LaTeX\,2_\varepsilon$. It is based on the framework of the excellent *Clean Thesis* style developed by Ricardo Langner and aims to emulate the look of a life science textbook.

Download the *Clean Thesis* style at `http://cleanthesis.der-ric.de/`.